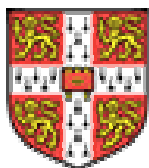


Filtered Multitone (FMT) Modulation for Broadband Fixed Wireless Systems

A dissertation submitted to the University of Cambridge
for the degree of Master of Philosophy

Ignacio Berenguer, Hughes Hall

August 2002



LABORATORY FOR COMMUNICATIONS ENGINEERING
Department of Engineering
University of Cambridge

Declaration

The research described in this dissertation was carried out by the author at Cambridge University between October 2001 and August 2002. Except as indicated, the contents are entirely original and are not the result of work done in collaboration. No part of this thesis has been submitted to any other university. The main body of the thesis contains no more than 15,000 words.

Ignacio Berenguer

Acknowledgments

I would like to express my gratitude to my supervisor, Dr. Ian Wassell, for giving me a very high degree of freedom in my research and for providing constant, guidance, proof reading and encouragement. I also wish to thank Dr. Malcolm Macleod, my advisor, for his valuable comments from time to time, not only about this thesis framework.

I also wish to thank all the members of the Laboratory for Communications Engineering who have been supportive, specially Kam Sanmugalingam.

I am also grateful to the British Council and La Caixa Scholarship who sponsored my research at the University of Cambridge.

Contents

Chapter 1. Introduction.....	1
Chapter 2. The Multipath Radio Channel.....	3
2.1. Exponentially decaying Rayleigh Fading Channel.....	3
Chapter 3. Introduction to Multi Carrier Modulation for Broadband Communication Systems	5
3.1. OFDM Modulation	6
3.1.1. Effects of multipath and Cyclic Prefix (CP) solution	8
3.1.2. OFDM generation	8
3.1.3. Virtual Carriers	9
3.1.4. Performance with Frequency and Timing Errors.....	10
3.1.5. The Peak to Average Power Problem	13
3.2. OFDM/DMT conclusion.....	13
Chapter 4. Filtered Multitone Modulation	15
4.1. FMT as a Multirate Filter Bank (General Principles).....	16
4.1.1. FMT Transmitter.....	16
4.1.2. FMT Receiver	20
4.1.3. Perfect reconstruction condition	22
4.1.4. Prototype design.....	23
4.2. OFDM as a filter bank	27
4.3. Virtual Carriers	28
4.4. Conclusion	30
Chapter 5. Equalization in FMT.....	31
5.1. Per subchannel DFE: Computation of the MMSE equalizer coefficients based on channel estimation	33
5.2. Efficient FMT equalization schemes	36
5.2.1. Frequency domain DFE	36
5.2.2. Time Domain DFE.....	38
5.2.3. Complexity.....	39
5.2.4. Achievable bit rate and loading algorithms	40
5.2.5. Simulation results.....	41
5.3. Precoding	44
5.4. Adaptive equalizers in FMT	45
5.4.1. Adaptive Decision Feedback Equalization	46
5.4.2. Simulation results.....	50
5.4.3. Proposed simplified adaptive algorithms.....	52
5.4.4. Further improvement in outdoor environments	53
5.4.5. Simulation results.....	55
5.4.6. Conclusions about the proposed scheme	56
Chapter 6. Conclusions, future improvements and usage.....	59
References.....	61

Appendix A: The Multipath Channel	63
Appendix B: Computation of the DFE coefficients	69
Appendix C: Precoding	75

Symbols/Acronyms

ADC	Analog to Digital Converter
ADSL	Asymmetric Digital Subscriber Line
AWGN	Additive White Gaussian Noise
BPSK	Binary Phase Shift Keying
BWA	Broadband Wireless Access
CP	Cyclic Prefix
DAB	Digital Audio Broadcasting
DAC	Digital to Analog Converter
DFE	Decision Feedback Equalizer
DFT	Discrete Fourier Transform
DMT	Discrete Multitone
DVB	Digital Video Broadcasting
DWMT	Discrete Wavelet Multitone Modulation
FDM	Frequency Division Multiplex
FFT	Fast Fourier Transform
FIR	Finite Impulse Response
FMT	Filtered Multitone
ICI	Inter Carrier Interference
ISI	Inter Symbol Interference
LMS	Least Mean Squares
LOS	Line of Sight
MCM	Multicarrier Modulation
OFDM	Orthogonal Frequency Division Multiplexing
P/S	Parallel to Serial
PAPR	Peak to Average Power Ratio
PDF	Probability Density Function
PR	Perfect Reconstruction
PSD	Power Spectral Density
QAM	Quadrature Amplitude Modulation
QPSK	Quadrature Phase Shift Keying
RC	Raised Cosine
RLS	Recursive Least Squares
RMS	Root Mean Square
RRC	Root Raised Cosine
S/P	Serial to Parallel
SNR	Signal to Noise Ratio
TDM	Time Division Multiplex
THP	Tomlinson Harashima Precoding
VC	Virtual Carrier
VDSL	Very High-speed Digital Subscriber Lines

Notation

M	Number of subchannels
T	FMT symbol period
k	Index for samples with sampling period equal to the FMT symbol period T

n	Index for samples with sampling period equal to T/M
$h_{(i)}(k)$	$=h(kM+i)$, i -th polyphase component of $h(n)$
$h^{(i)}(n)$	$=h(n)e^{j2\pi ni/M}$ transmitter filter of the i -th subchannel
$A^{(i)}(k)$	QAM or QPSK symbol of the i -th subchannel
\underline{x}	Column vector x
$\underline{\underline{x}}$	Matrix x
γ	Overlap

Publications

The following publications, appended at the end of the thesis, relate to the work in this thesis:

1. Inaki Berenguer, Ian J. Wassell, “FMT Modulation: Receiver Filter Bank definition for the Derivation of an Efficient Implementation”, Proc. IEEE 7th International OFDM Workshop, Hamburg, Germany, Sept. 2002
2. Inaki Berenguer, Ian J. Wassell, “Efficient FMT equalization in outdoor broadband wireless systems”, Proc. IEEE International Symposium on Advances in Wireless Communications, Victoria, Canada, Sept. 2002.

Chapter 1. Introduction

This thesis addresses Filtered Multitone (FMT) modulation, a multicarrier modulation technique initially introduced in 1999 for Very High Speed Digital Subscriber Line (VDSL) applications [1][2] that can also be used in Broadband Fixed Wireless Systems.

High data rate wireless communications are limited not only by additive noise but often more significantly by the Intersymbol Interference (ISI) owing to multipath propagation [3]. The effects of the ISI are negligible so long as the delay spread of the multipath channel is significantly shorter than the duration of one transmitted symbol. This implies that the symbol rate is limited by the channel memory. Multicarrier modulation is an approach to overcome this limitation [4][5][6]. Here, a set of subcarriers is used to transmit the information symbols in parallel in so-called subchannels. This allows a higher data rate to be transmitted by ensuring that the subchannel symbol duration exceeds that of the channel memory.

There are several approaches to multicarrier transmission. The spectral partitioning can generally be realized in the form of overlapping or non-overlapping subbands.

The multicarrier techniques used in today's standards (Digital Audio Broadcast, ADSL, HIPERLAN/2, Terrestrial Digital Video Broadcasting, etc [7]) are based on $\text{sinc}(f)$ overlapping methods in which adjacent carriers are at the nulls of the $\text{sinc}(f)$ function (see Fig. 1 (a)). A guard interval is added to each transmitted symbol to avoid ISI which occurs in multipath channels and destroys orthogonality. At the receiver, the guard interval is removed. If the guard interval length is longer than the maximum delay in the radio channel, zero ISI occurs and the orthogonality between subcarriers is maintained. In this case, the multipath channel only changes the amplitude and the phase of the subcarrier signals which can be easily equalized with a set of complex gain coefficients. However, the longer the delay spread of the channel, the higher the transmission inefficiency. These methods are known as Discrete Multitone Modulation (DMT) or Orthogonal Frequency Division Multiplexing (OFDM) when used in wireless systems [7].

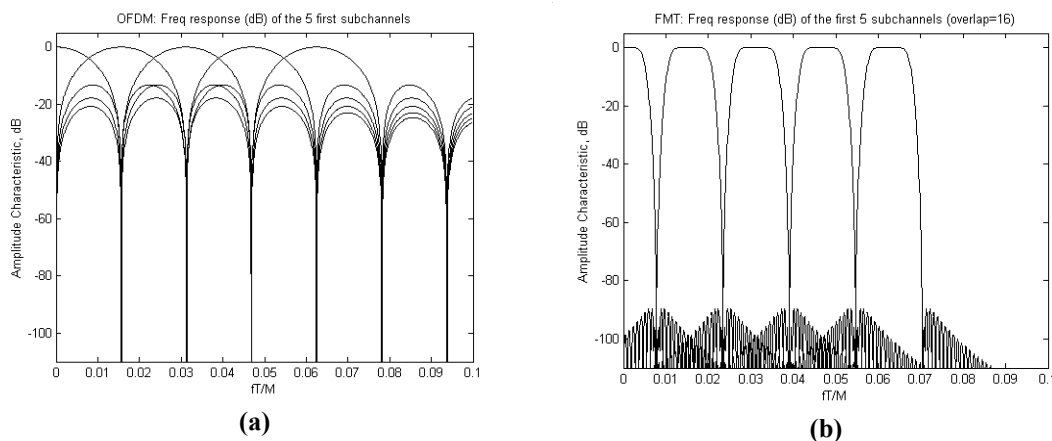


Fig. 1 Subchannel frequency response of the first 5 subchannels ($M=64$) (a) OFDM and (b) FMT with overlap=16

In contrast, in FMT modulation, the spectral partitioning is based on non-overlapping methods. This filter bank modulation technique is based on M -branch filters that are frequency shifted versions of a low pass prototype (uniform filter bank). The prototype filter, achieves a high level of spectral containment such that the Interchannel Interference (ICI) is negligible compared to the other noise signals in the system and the subcarriers can be considered close to orthogonal, whatever the length of the multipath channel (see Fig.1 (b)). In this way, FMT does not need the use of the cyclic prefix used in DMT/OFDM to maintain subcarrier orthogonality in the presence of multipath, thereby, improving the total throughput. However, per subchannel equalization is needed in order to reduce the remaining intersymbol interference [1].

These improvements are at the expense of higher complexity owing to filter bank implementation and equalization requirements.

The remainder of the thesis is organized as follows:

Chapter 2 gives an overview of the wireless radio channel characteristics.

Chapter 3 gives an overview of conventional multicarrier modulations used to combat the effects of multipath propagation, highlighting the main problems that FMT is trying to solve.

Chapter 4 describes the FMT modulation from the point of view of filter bank theory. It presents the low pass prototype filter that is the basic element of the filter bank and proposes methods and parameters for its design. An efficient FMT implementation using the M polyphase components of the prototype filter and the Fast Fourier Transform (FFT) will be introduced. Reasons for the introduction of equalization will also be presented.

Chapter 5 will present and also propose different equalization architectures based on channel estimation or adaptive algorithms. The performance of the various equalization architectures proposed will be investigated via the use of computer simulations.

Chapter 6 draws conclusions and discusses areas for future research.

Chapter 2. The Multipath Radio Channel

Multicarrier Modulation techniques were originally conceived to transmit data in time dispersive or frequency selective channels without the need for the use of complex channel equalization [5][8]. To understand how this can be achieved, the multipath wireless channel is described in Appendix A and some parameters that are useful to describe the severity of different multipath environments are presented.

The systems under consideration will operate in the range from 2.5 to 17GHz. Measurements confirm that these channels have similar characteristics and may be modelled in a similar way [10].

2.1. Exponentially decaying Rayleigh Fading Channel

We now present the exponentially decaying Rayleigh Fading Channel Model [15] used in the simulations conducted in this thesis. This channel was agreed by the IEEE 802.11 WLAN specification to be a baseline model for comparison of modulation methods. The multipath model is selected to be a Rayleigh fading model with an exponentially decaying power profile.

In this channel, the RMS delay spread τ_{RMS} completely characterizes the path delay profile. The model is simple to analyze and simulate. With a proper choice of the delay spread values it represents realistic conditions.

The channel is assumed static throughout the transmitted packet and is generated independently for each packet.

The impulse response of the channel is composed of complex samples with random uniformly distributed phase and Rayleigh distributed magnitude with average power decaying exponentially with equidistant delays, i.e.

$$c(k) = \sum_{k=0}^{K_{\max}-1} \alpha(k) \delta(t - kT_s) \quad (1)$$

where $c(k)$ is the channel impulse response and T_s is the sampling period.

Each of the equi-spaced coefficients of the impulse response $\alpha(k)$ are defined as:

$$\alpha(k) = N(0, \frac{1}{2}\sigma_k^2) + jN(0, \frac{1}{2}\sigma_k^2) \quad (2)$$

$$\sigma_k^2 = \sigma_0^2 e^{-kT_s/T_{RMS}} \quad (3)$$

$$\sigma_0^2 = 1 - e^{-T_s/T_{RMS}} \quad (4)$$

where $N(0, \sigma_k^2/2)$ is a zero mean Gaussian random variable with variance $\sigma_k^2/2$ (produced by generating a $N(0,1)$ random variable and multiplying it by $\sigma_k/\sqrt{2}$) and $\sigma_0^2 = 1 - e^{-T_s/T_{RMS}}$ is chosen so that the condition $\sum \sigma_k^2 = 1$ is satisfied to ensure same average received power:

$$\sum_{k=0}^{\infty} \sigma_k^2 = \sigma_0^2 \sum_{k=0}^{\infty} e^{-kT_s/T_{RMS}} = (1 - e^{-T_s/T_{RMS}}) \sum_{k=0}^{\infty} e^{-kT_s/T_{RMS}} = (1 - e^{-T_s/T_{RMS}}) \frac{1}{(1 - e^{-T_s/T_{RMS}})} = 1 \quad (5)$$

The number of samples to be taken in the impulse response should ensure sufficient decay of the impulse response tail, e.g. $K_{max} = 10T_{RMS}/T_s$.

For example, in HIPERLAN/2, the sampling rate is $1/T_s = 20\text{MHz}$, and for an indoor channel at 5GHz, the NLOS delay spread σ_{RMS} is 40ns. If we consider taps with a dynamic range of 30dB, K_{max} in Eq. (1) will be equal to 5. In Fig. 2 we show a single realization of this channel and the power profile with these parameters.

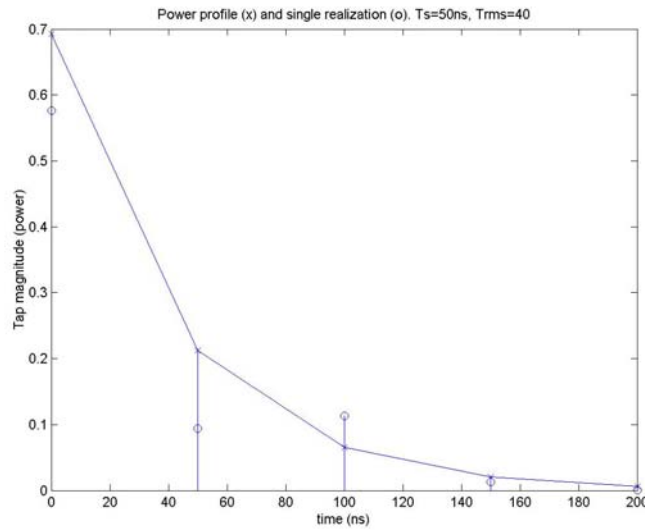


Fig. 2 Power profile (x) and a single realization (o)

Chapter 3. Introduction to Multi Carrier Modulation for Broadband Communication Systems

High data rate communications are limited not only by noise but often more significantly by the intersymbol interference (ISI) due to the memory of the dispersive wireless communications channel. Explicitly, this channel memory is caused by the dispersive Channel Impulse Response due to the different length propagation paths between the transmitting and the receiving antennas. The multipath propagation of the channel manifests itself by different transmitted symbols overlapping at the receiver, which leads to error rate degradation.

As a general rule, the effects of ISI on the transmission-error statistics are negligible as long as the delay spread is significantly shorter than the duration of one transmitted symbol. This implies that the symbol rate of communications systems is practically limited by the channel's memory. If symbol rates exceeding this limit are to be transmitted over the channel, mechanisms must be implemented in order to combat the effects of ISI. Channel equalization techniques can be used to suppress the echoes caused by the channel. To do this, the impulse response must be estimated or adaptive algorithms need to be used.

There is however an alternative approach to transmitting data over a multipath channel. Instead of attempting to cancel the effects of the channel's echoes, multicarrier modulation employs a set of subcarriers in order to transmit information symbols in parallel in so called subchannels over the channel. Since the system's data throughput is the sum of all the parallel channel's throughputs, **the data rate per subchannel is only a fraction of the data rate of a conventional single carrier system** having the same throughput. This allows us to design a system supporting high data rates while maintaining symbol durations much longer than the channel's memory without the need for channel equalization.

Among such proposed solutions, Multi-Carrier (MC) modulation is both elegant and efficient. It is based on a well-established history [4][5][6][18]. Various manifestations include, Orthogonal Frequency Division Multiplexing (OFDM) [7], Filtered Multitone (FMT) [2], Discrete Multitone (DMT) [8] and Discrete Wavelet Multitone (DWTM) [19].

3.1. OFDM Modulation

There are many approaches to multicarrier transmission. The spectral partitioning can generally be realized in the form of overlapping or non-overlapping subbands.

The multicarrier techniques that are used in today's standards (Digital Audio Broadcast, Wireless LAN, ADSL, Terrestrial Digital Video Broadcasting, etc) are based on sinc(f) overlapping methods. These methods are known as Discrete Multitone Modulation (DMT) or Orthogonal Frequency Division Multiplexing (OFDM) when it is used in a wireless environments and a cyclic prefix is added [7].

The baseband representation of the OFDM signal consisting of M subcarriers is given by [20]:

$$s(t) = \sum_{k=-\infty}^{\infty} \sum_{i=0}^{M-1} A^{(i)}(k) g(t - kT) \cdot e^{j i \frac{2\pi}{T} t} \quad (6)$$

where $g(t)$ is a rectangular pulse of duration T , $A^{(i)}(k)$ are QAM or QPSK symbols and T is the OFDM symbol duration. In the previous representation, each of the M subcarriers is centered at frequency $f_i = i/T$ Hz with $i=0,1,\dots,M-1$.

A single DMT symbol in the time domain can be described as:

$$u(t) = \left[\sum_{i=0}^{M-1} A^{(i)} e^{j \frac{2\pi}{T} i t} \right] \cdot g(t) \quad (7)$$

where:

$$g(t) = \begin{cases} 1 & 0 \leq t \leq T \\ 0 & \text{otherwise} \end{cases} \quad (8)$$

Here we are multiplying M perfect exponentials $e^{j2\pi f_i t}$ at frequency $f_i = i/T$ of infinite duration by a rectangular window $g(t)$ having a duration of one OFDM symbol (T). Those exponentials are modulated by a QAM symbol $A^{(i)}$. Since we are operating with Fourier transforms, multiplication in one domain is equivalent to convolution in the other domain. The Fourier transform of this rectangular window $g(t)$ is:

$$G(f) = \int_{-\infty}^{\infty} g(t) e^{-j2\pi f t} dt = \frac{j}{2\pi f} (e^{-j2\pi f T} - 1) = e^{-j\pi f T} \cdot T \cdot \frac{\sin(\pi f T)}{\pi f T} \quad (9)$$

which is convolved with the dirac delta subcarriers and determines the spectrum of each of the windowed complex exponential functions. This leads to the spectrum of the i -th single subcarrier in the form:

$$B_i(\omega) = e^{-j\pi f T} \cdot T \cdot \frac{\sin(\pi f T)}{\pi f T} * \delta(f - f_i) \quad (10)$$

and using the relationship $T=1/\Delta f$, the spectrum of the i -th subcarrier can be expressed as

$$B_i(f) = e^{-j\pi \frac{f-f_i}{\Delta f}} \cdot T \cdot \frac{\sin(\pi \frac{f-f_i}{\Delta f})}{\pi \frac{f-f_i}{\Delta f}}$$

Then, the absolute value of the frequency response is:

$$|B_i(f)| = T \cdot \left| \operatorname{sinc} \left(\frac{f - f_i}{\Delta f} \right) \right| \quad (11)$$

In this way, **the magnitude spectrum of each of the subcarriers will be a sinc function centered at frequencies $f_i = i/T$, with $i=0,1,\dots,M-1$** . Although **these subcarriers have overlapping (sinc(f)-shaped) spectra**, the signal waveforms are orthogonal. The resulting sinc(f) type spectral shaping for each subchannel yields some desirable signal orthogonality properties, namely zero intersymbol interference as well as zero intersubchannel interference provided the adjacent carriers are at the nulls of the sinc(f) function (see Fig. 3). The main lobe of the Fourier Transform of the rectangular window has a width equal to $2/T$ and the side lobes are quite high. The height of the sidelobes is not dependent of the length of the rectangular window and the ratio between the main lobe and the first side lobe is always -13dB (independent of how many subchannels M we consider). In Fig. 3 we show the OFDM/DMT spectrum with $M=8$.

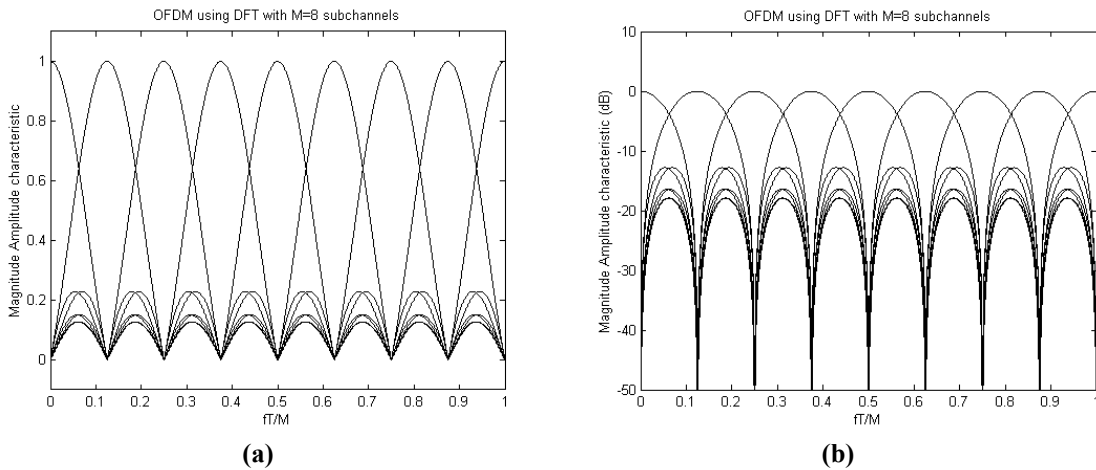


Fig. 3 OFDM frequency response with $M=8$ subchannels
(a) absolute value of the amplitude (b) amplitude in dB

In the representation, given by Eq. (6), the real and imaginary parts correspond to the in-phase and quadrature parts of the OFDM signal, which have to be multiplied by cosine and sine signals at the desired carrier frequency to produce the final OFDM signal [7].

Looking at Eq. (6), we can see the analogy with the IDFT. In this way, **the inverse DFT may be used to put QPSK (or QAM) data onto each of the M subcarriers**, spaced by $1/T$ Hz, where T is the IFFT block period. Each carrier is an IFFT basis function. In this way, the carriers are orthogonal to each other and may be demodulated by an equivalent FFT process without mutual interference at the receiver.

Basically, the OFDM/DMT spectrum fulfills Nyquist's criterion for an intersymbol interference free pulse shape. Notice that the pulse shape is present in the frequency domain and not in the time domain, for which the Nyquist criterion is usually applied. Therefore, instead of intersymbol interference (ISI), it is intercarrier interference (ICI)

that is avoided by having the maximum of one subcarrier spectrum corresponding to the zero crossings of all the others.

3.1.1. Effects of multipath and Cyclic Prefix (CP) solution

One of the most important properties of OFDM transmission is its robustness against multipath delay spread. This is achieved by having a long symbol period (M times longer than an equivalent single carrier transmission), which minimises the inter-symbol interference. The level of robustness can in fact be increased even more by the addition of a guard period between transmitted symbols as proposed in [18]. The guard period allows time for multipath signals from the previous symbol to decay before the information from the current symbol is gathered. The most effective guard period to use is a cyclic extension of the symbol. If a mirror in time, of the end of the symbol waveform is put at the start of the symbol as the guard period, this effectively extends the length of the symbol, while maintaining the orthogonality of the waveform. The guard time is chosen to be larger than the expected delay spread, such that multipath components from one symbol cannot interfere with the next symbol. This guard interval, ν , is usually chosen as 5 times the delay spread:

$$\nu = 5 \cdot \frac{\sigma_{RMS}}{T/M} \quad (12)$$

The guard interval consists of the repetition of the last ν samples of the OFDM symbol at the beginning of the symbol. This can be seen as repeating the last $\nu-1$ rows of the matrix that defines the IDFT at the beginning of the IDFT matrix [21].

In this way, multipath delays varying from 0 to ΔT ($\Delta T = \nu T/M$) can be tolerated. As long as the multipath delay echoes stay within the guard period duration, there is strictly no limitation regarding the power of the echoes: they may even exceed the power of the shortest path. The signal energy from all paths just combines at the input to the receiver, and since the FFT is energy conservative, the whole available power feeds the decoder. If the delay spread is longer than the guard interval then ISI results. However, provided the echoes are sufficiently small they do not cause significant problems. This is true most of the time since multipath echoes delayed longer than the guard period will have been reflected of very distant objects.

The cyclic extension, although an elegant solution, leads to a loss in transmission efficiency. For example, the current VDSL proposal suggest a total length of 640 samples for the cyclic extensions when $M=8192$. This results in a loss in spectral efficiency of 7.8%. For a total transmission bandwidth of 17.664 MHz, this loss can be interpreted as 1.38MHz of unused spectrum. In ADSL, $M=512$ and the cyclic extension is 32 samples so the loss of efficiency is 6.25% [22]. In a DAB system, this loss is 25% [26] and in HIPERLAN/2, 16 cyclic samples are added to the 64 data samples or equivalently, a loss in efficiency of 20% [23].

3.1.2. OFDM generation

Fig. 4 shows a typical OFDM based communication system. To generate the OFDM signal, the incoming serial data is first converted from serial to parallel and grouped into x bits each to form a complex symbol (e.g. QAM). The complex symbols are

modulated in a baseband fashion by the IDFT and converted back to serial data for transmission. A guard interval is inserted between symbols to avoid intersymbol interference (ISI). The discrete symbols are converted to analog and lowpass filtered before RF up-conversion. Then the data stream is fed into the channel. The receiver performs the inverse process of the transmitter. A one tap equalizer is used on each subchannel to correct channel distortion. The tap coefficients of the filter $q^{(i)}$ are calculated based on channel information [24].

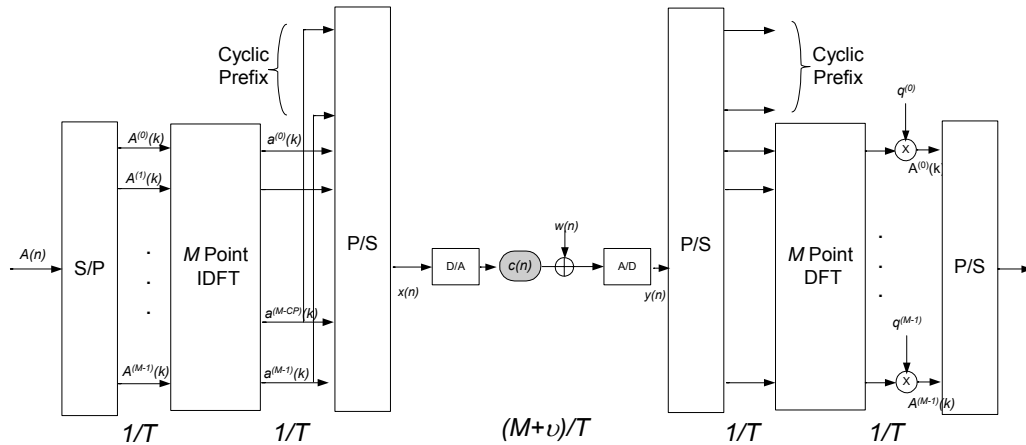


Fig. 4 OFDM communication system

Finally the data from the M QAM decoders is multiplexed back into a single serial data stream which is passed on to the error correction decoder. This can correct errors which typically occur when multipath causes selective fading of some carriers.

3.1.3. Virtual Carriers

Apart from the inefficiency of the cyclic prefix, another problem with OFDM is that it needs Virtual Carriers (VC). Looking at the frequency response for one of the subchannels, we see that it has high side lobes in adjacent channels that will be distorted by the DAC filter. Thus, VCs are inserted into the roll off region of the DAC interpolation filter, i.e. null symbols are transmitted to limit distortion, which further reduces transmission efficiency [25]. As we will see, FMT needs fewer virtual carriers so it improves the total throughput. In HIPERLAN/2, 12 out of 64 subcarriers are used as VCs which leads to an inefficiency of 18.75% [23]. In Fig. 5 we show an OFDM spectrum without VCs (a) and one with 12 VCs (b).

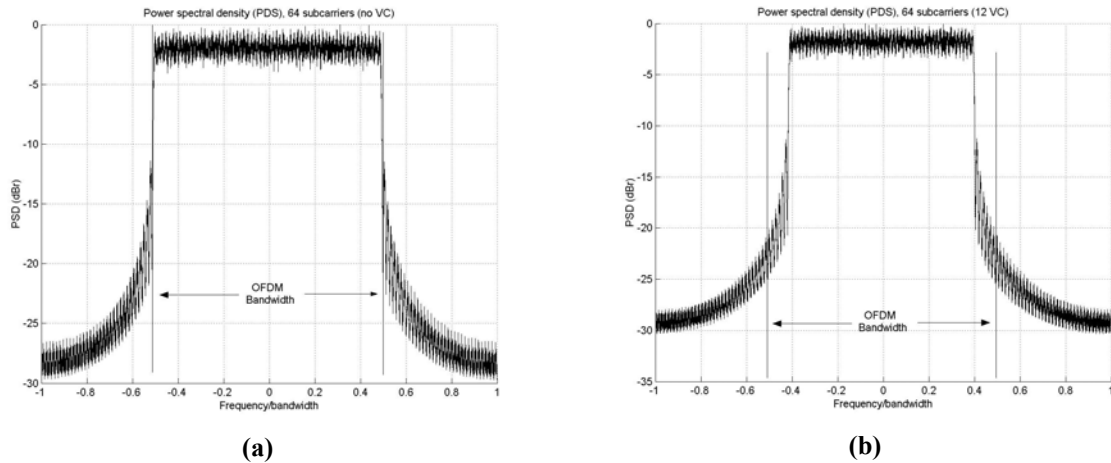


Fig. 5 Power spectral density (PSD) (a) without Virtual Carriers and (b) with 12 Virtual Carriers

3.1.4. Performance with Frequency and Timing Errors

The performance of the synchronization subsystem, in particular, the accuracy of frequency and timing estimation, is a major influence on the overall OFDM system performance due to the overlapping subchannel spectra. For a single carrier system, these inaccuracies only give degradation in the received SNR, rather than introducing interference.

Effects of Frequency Shift on OFDM

Carrier frequency errors which are caused by the mismatch between the oscillator in the transmitter and in the receiver, result in a shift of the received signal's spectrum in the frequency domain. If the frequency error is an integer multiple I of the subcarrier spacing Δf , then the received frequency domain subcarriers are shifted by $I \cdot \Delta f$. The subcarriers are still mutually orthogonal, but the received data symbols, which were mapped to the OFDM spectrum, are in the wrong position in the demodulated spectrum, resulting in a BER of 0.5.

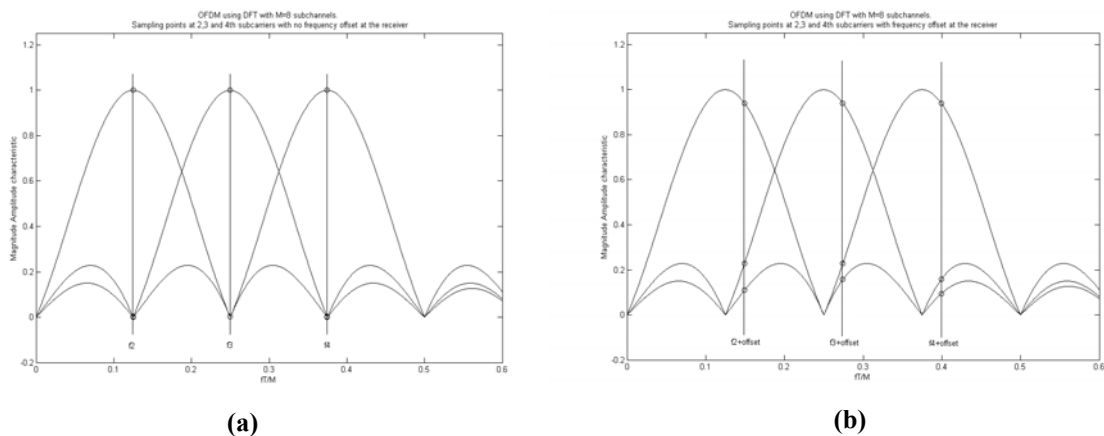


Fig. 6 OFDM symbol spectrum with sampling points for three subcarriers. (a) no frequency offset between tx and rx (b) frequency offset present

If the carrier frequency error is not an integer multiple of the subcarrier spacing, then energy spills over between the subcarriers, resulting in loss of their mutual orthogonality. In other words, interference is observed between the subcarriers, which degrades the BER of the system. This ICI can be quantified by observing the spectrum of the OFDM symbol as shown in Fig. 6.

The spectrum shape (absolute value) of the i -th subcarrier can be expressed as:

$$|B_i(f)| = \left| \frac{\text{sinc}\left(\pi \frac{f - f_i}{\Delta f}\right)}{\pi \frac{f - f_i}{\Delta f}} \right| = \left| \text{sinc}\left(\frac{f - f_i}{\Delta f}\right) \right| \quad (13)$$

The OFDM receiver samples the received time-domain signal and demodulates it by invoking the FFT. However, in the case of a carrier frequency shift, it generates the subchannel signals in the frequency domain at the sampling points $f_i + \delta f$. These sampling points are spaced from each other by the subcarrier spacing Δf and are misaligned by the frequency offset δf . Fig. 6(a) shows the sampling of the subcarrier at frequency f_i at the correct frequency, resulting in a maximum signal amplitude and no ICI. If the frequency reference of the receiver is offset with respect to that of the transmitter by a frequency error of δf , then the received symbols suffer from ICI as depicted in Fig. 6(b).

The total amount of ICI experienced by subcarrier i is the sum of the interference amplitude contributions of all the other subcarriers in the OFDM symbol

$$I_i = \sum_{j, j \neq i} A_j \cdot B_j(f_i + \delta f) \quad (14)$$

Since the QAM symbols A_j are random variables, the interference amplitude in subcarrier i , I_i , is also a random variable which cannot be calculated directly. If the number of interferers is high, however, then, according to the central limit theorem, the power spectral density of I_n can be approximated by that of a Gaussian process. Therefore, the effects of the ICI can be modeled by additional white Gaussian noise superimposed on the frequency domain data symbols.

The variance of this Gaussian process is the sum of the variances of the interference contributions

$$\sigma^2 = \sum_{j, j \neq i} \sigma_{A_j}^2 \cdot |B_j(f_i + \delta f)|^2 \quad (15)$$

The quantities $\sigma_{A_j}^2$ are the variances of the data symbols, which are the same for all j in a system that does not vary the average symbol power across different subcarriers. Additionally, because of the constant subcarrier spacing Δf , the interference amplitude contributions can be expressed more conveniently as:

$$|B_j(f_i + \delta f)| = \left| \text{sinc}\left((i - j) + \frac{\delta f}{\Delta f}\right) \right| \quad (16)$$

The sum of the interference power leads to the ICI variance expression

$$\sigma^2 = \sigma_a^2 \cdot \sum_{i=-N/2-1}^{N/2} \left| \text{sinc}\left(i + \frac{\delta f}{\Delta f}\right) \right|^2 \quad (17)$$

The frequency mismatch between the transmitter and receiver of a OFDM system not only results in ICI but also reduces the useful signal amplitude at the frequency domain sampling point by a factor of $f(\delta f) = \text{sinc}(\delta f / \Delta f)$. Using this and σ^2 , the theoretical influence of the ICI, approximated by a Gaussian process, can be calculated for a given modulation scheme in a AWGN channel. In the case of coherently detected QPSK, the closed-form expression for the BER $P_e(SNR)$ at a channel signal to noise ratio SNR is given by [3]

$$P_e(SNR) = Q(\sqrt{SNR}) \quad (18)$$

where the Gaussian Q() function is defined as:

$$Q(y) = \frac{1}{\sqrt{2\pi}} \int_y^\infty e^{-x^2/2} dx = \frac{1}{2} \text{erfc}\left(\frac{y}{\sqrt{2}}\right) \quad (19)$$

Assuming that the effects of the frequency error can be approximated by white Gaussian noise of variance σ^2 and taking into account the attenuated signal magnitude $f(\delta f) = \text{sinc}(\delta f / \Delta f)$, we can adjust the equivalent SNR to

$$SNR' = \frac{f(\delta f) \cdot \sigma_a^2}{\sigma^2 + \sigma_a^2 / SNR} \quad (20)$$

where σ_a^2 is the average symbol power and SNR is the real channel SNR .

The effects of Oscillator Phase Noise

A practical oscillator does not produce a carrier at exactly one frequency, but rather a carrier that is phase modulated by random phase jitter [33]. As a result, the instantaneous frequency, which is the time derivative of the phase, is never perfectly constant causing ICI in the OFDM receiver. This becomes a particularly grave problem for systems operating above 25GHz since at these frequencies it is difficult to find accurate and stable yet inexpensive oscillators.

Solutions for the synchronization problem

In OFDM, algorithms to deal with these problems are an active area of research. The synchronization process is normally split into a coarse acquisition phase and a fine tracking phase, if the characteristics of the random frequency and timing error are known. In the acquisition phase, an initial estimate of the errors is acquired, using more complex algorithms and possibly a higher amount of synchronization information in the data signal, whereas later the tracking algorithms only have to correct for small short-term deviations.

At the commencement of the synchronization process, neither the frequency error nor the timing misalignment are known; hence synchronization algorithms must be found that are sufficiently robust to cope with initial frequency errors.

Frequency offsets are usually compensated before the receiver because it affects all the subchannels in the same way. However, compensation in the time domain is not applicable for OFDMA, since the single subcarriers are allocated by different subscribers and therefore are subject to different distortions from the channel and

radio frequency processing. On the other hand, phase shifts are compensated on each subcarrier.

3.1.5. The Peak to Average Power Problem

An OFDM signal is the sum of many subcarrier signals that are modulated independently by different modulation symbols. Therefore, they can give a large peak to average power ratio (PAPR) when added coherently. When M signals are added with the same phase, they produce a peak power that is M times the average power. Therefore, RF power amplifiers should be operated in a large linear operating region, otherwise, the signal peaks get into the non linear region of the power amplifier causing signal distortion. This distortion introduces intermodulation among the subcarriers and also out of band radiation [20].

3.2. OFDM/DMT conclusion

As we have seen in the previous section, OFDM/DMT provides a $\text{sinc}(f)$ type subchannel spectral shaping that has some desirable signal orthogonality properties, namely zero intersymbol interference (ISI) as well as zero intersubchannel interference (ICI). However, in a non ideal channel situation, the large amount of spectral overlap between the sinc shaped subchannels necessitates the use of cyclic prefixing techniques and frequency offset correction algorithms.

Cyclic prefixing is employed in order to mitigate the effects of the loss of orthogonality caused by amplitude and phase distortion introduced by the transmission channel. Although the CP is an elegant and easy solution, it leads to a loss of efficiency in the data throughput. This gives us a reason to introduce other multicarrier modulation techniques such as FMT that do not need the use of the CP.

Also owing to the high sidelobes of the $\text{sinc}(f)$ functions, Virtual Carriers are needed to reduce the out of band power causing a further loss of efficiency. As we will see, due the high spectral containment in FMT we will not need to use VCs.

Unfortunately, the PAPR will affect FMT in the same way since it is a characteristic of all multicarrier modulation schemes.

Chapter 4. Filtered Multitone Modulation

We have seen that conventional multicarrier modulations such as OFDM use subchannels with overlapping spectra and use a CP to ensure that successive symbols do not overlap, thus ensuring zero intersymbol interference. Unfortunately, this method leads to a loss of efficiency owing to the CP. Other problems and inefficiencies that arise from the overlapping OFDM subcarriers have also been outlined.

In Filtered Multitone, we do not use a prefix between symbols. Instead, the bandwidth of each of the subcarriers are chosen to be quasi orthogonal in the frequency domain. This is achieved by the use of steep roll-off bandpass filters. The time domain response of these filters may overlap several successive transmitted symbol periods, but are close to being orthogonal in the frequency domain at both channel input and output. Per subchannel equalization is necessary to reduce any remaining intersymbol interference.

High levels of subchannel spectral containment is a desirable property for many applications. For example, because leakage of signal energy between subchannels may be considered negligible, echo cancellation is not needed in frequency division duplexing (FDD) transmission systems where the subchannels are closely spaced. In addition, synchronization among different users is not needed.

Tight subchannel spectral containment is good for spectrum management when different users share the same channel.

4.1. FMT as a Multirate Filter Bank (General Principles)

4.1.1. FMT Transmitter

With FMT, we choose a particular case of a uniform filter bank consisting of frequency shifted versions of a low pass prototype filter. This filter is selected to achieve a high degree of spectral containment, thus giving negligible ICI compared to the level of other noise signals in the system. In [2], it is proposed that the prototype filter is not required to satisfy the perfect reconstruction (PR) condition [34][35] because this constraint is only assured when the transmission channel does not introduce signal distortion. So when a channel introduces amplitude and phase distortion, the objective of high spectral containment (the main purpose of FMT) is more easily achieved if the perfect reconstruction constraint is relaxed although we will need to use equalization to remove ISI.

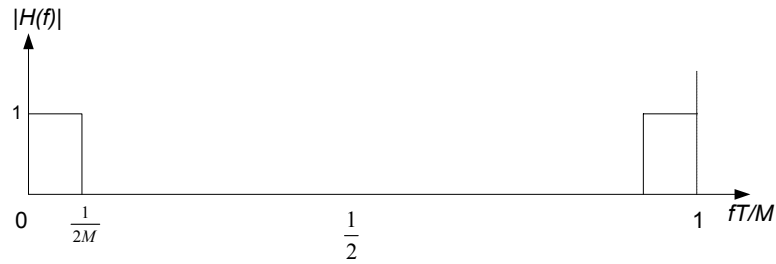


Fig. 7 Ideal Frequency Response of the low pass prototype

We can use any of the well known methods (eg. Window, Remez, etc [37]) to design the low pass prototype filter $h(n)$ with the objective of obtaining a symmetric Finite Impulse Response (FIR) filter with real coefficients that would approximate the ideal frequency response $H(f)$ shown in Fig. 7.

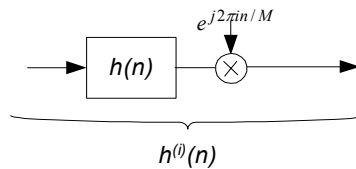


Fig. 8 Frequency shifted version of the prototype

With FMT, orthogonality between subchannels is ensured by using non-overlapping spectral characteristics as compared with the overlapping $\text{sinc}(f)$ type spectra employed in OFDM. Since the linear transmission medium does not destroy orthogonality achieved in this manner, cyclic prefixing is not needed. Clearly, the required amount of spectral containment must be achieved with acceptable filtering complexity. In a critically sampled filter bank [35], the frequency separation of the pass bands will be $1/T$ with a total of M bands. In this way, each of the transmitter pass band filters will be frequency-shifted versions of the low pass filter as shown in Fig. 9:

$$h^{(i)}(n) = \frac{1}{\sqrt{M}} h(n) \cdot e^{j2\pi \frac{i}{M} n}, \quad n = 0, 1, \dots, M\gamma - 1, \text{ and } i = 0, 1, \dots, M - 1 \quad (21)$$

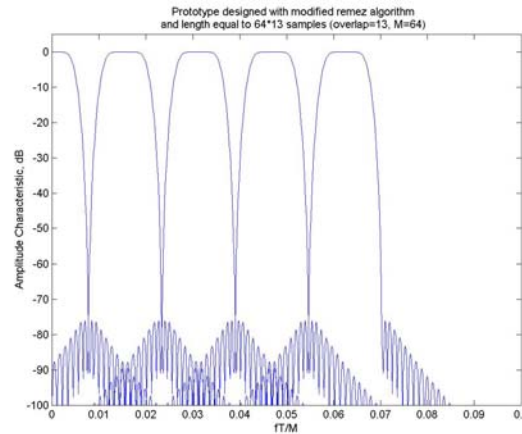


Fig. 9 FMT spectrum with 64 subchannels: 5 first subchannels

The length of the prototype filter $M\gamma$ is a multiple of the number of subchannels M . Parameter γ is called the overlap [35][2] since it is the number of blocks (each of M samples) to which the prototype is expanded. Usual values for γ in FMT are between 8 and 20. In Fig. 9 we show the frequency response of the first 5 subchannels of a 64 subchannel system using a prototype with overlap $\gamma=13$. Since the out of band power is lower than 76dB in adjacent bands and even less for other bands, we can consider that the ICI is zero compared with other noise signals in the system such as AWGN.

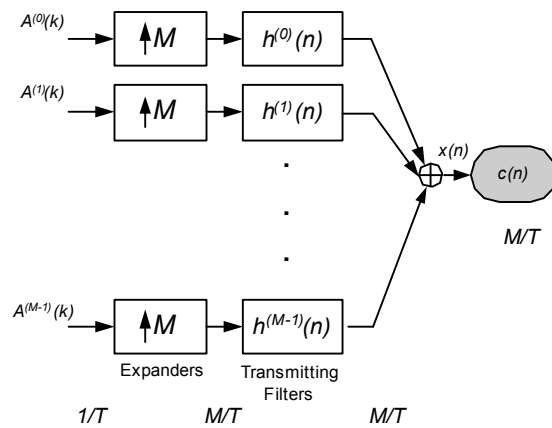


Fig. 10 FMT Transmitter: direct implementation

The direct implementation of the FMT filter bank is shown in Fig 10. The inputs $A^{(i)}(k)$ are QAM or QPSK symbols not necessarily from the same constellation. After upsampling by a factor of M (see [37]), each modulation symbol $A^{(i)}(k)$ is filtered at a rate M/T (where T is the FMT symbol period) by the subchannel filter defined in Eq. (21) centred at frequency $f_i=i/T$. The transmit signal $x(n)$ is obtained at the transmission rate M/T by adding together the M filter output signals that have been appropriately frequency shifted.

In the notation and figures, we have denoted k as the index for samples with a sampling period equal to T and n for the samples with a sampling period equal to T/M .

The system shown in Fig. 10 would not be practical if we could not derive an efficient implementation since all the filtering operations are performed in parallel and at a rate M/T .

We will now see how to derive from Fig. 10, an efficient implementation that makes use of the Inverse Discrete Fourier Transform (IDFT).

When analysing multirate signal processing systems we usually arrive at the situation where filter responses are better described in terms of their polyphase components [35].

If we take the prototype $h(n)$ with Z transform

$$H(z) = \sum_{n=-\infty}^{\infty} h(n)z^{-n} \quad (22)$$

we can always partition the index n into M phases, where each phase is characterized by choosing indices which are identical modulo M . Then for any integer M , we can decompose $H(z)$ as:

$$H(z) = \sum_{n=-\infty}^{\infty} h(nM)z^{-nM} + z^{-1} \sum_{n=-\infty}^{\infty} h(nM+1)z^{-nM} + \dots + z^{-(M-1)} \sum_{n=-\infty}^{\infty} h(nM+M-1)z^{-nM} \quad (23)$$

Thus, the k th phase of $h(n)$ is defined by:

$$h_{(k)}(m) = h(mM+k) \quad (24)$$

We now apply the polyphase representation to show how the computationally efficient implementation can be applied to the structure of Fig. 10.

Using the filter definition from Eq. (21), the signal at the channel input in Fig. 10 is given by:

$$x(n) = \frac{1}{\sqrt{M}} \sum_{i=0}^{M-1} \sum_{k=-\infty}^{\infty} A^{(i)}(k)h(n-kM)e^{j2\pi i(n-kM)/M} \quad (25)$$

$$x(n) = \sum_{k=-\infty}^{\infty} h(n-kM) \frac{1}{\sqrt{M}} \sum_{i=0}^{M-1} A^{(i)}(k)e^{j2\pi i n/M} \quad (26)$$

A change of notation $n=lM+m$ allows us to introduce the polyphase components of $h(n)$. With the notations $x(lM+m) = x_{(m)}(l)$ and $h(lM+m) = h_{(m)}(l)$ for $m=0, 1, \dots, M-1$, we obtain:

$$x_{(m)}(l) = \sum_{k=-\infty}^{\infty} h_{(m)}(l-k) \left\{ \frac{1}{\sqrt{M}} \sum_{i=0}^{M-1} A^{(i)}(k)e^{j2\pi i m/M} \right\} \quad (27)$$

$$x_{(m)}(l) = \sum_{k=-\infty}^{\infty} h_{(m)}(l-k)a^{(m)}(k) \quad (28)$$

where $a^{(m)}(k)$, $0 \leq m \leq M-1$, is the IDFT of $A^{(i)}(k)$ that may be efficiently implemented with the Inverse Fast Fourier Transform (IFFT). The m -th output of the IFFT is filtered by the m -th polyphase component of $h(n)$ and this filtering operation is

performed at rate $1/T$ and not M/T . From Eq. (27) we can derive the efficient implementation shown in Fig. 11.

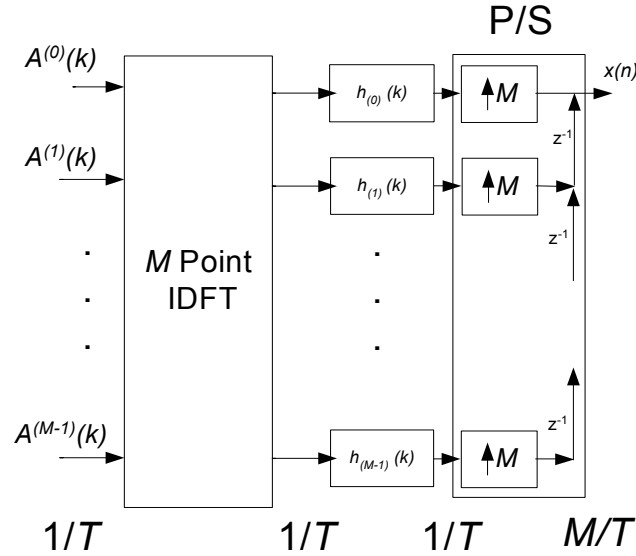


Fig. 11 FMT transmitter: Efficient Implementation

We can see in Fig. 11 that the filtering operation is performed at rate $1/T$ instead of M/T . At each instant, only the output of one polyphase filter needs to be computed due to the Parallel to Serial converter (P/S) and not the entire M samples as required in Fig. 10.

In Table 1 we show the number of operations to compute each output of $x(n)$ for both the direct and the efficient implementation. We will consider that the inputs are complex numbers. We note that in the direct implementation shown in Fig. 10, due to the introduction of zeros in the upsampler, only γ taps of each of the filters $h^{(i)}(n)$ are involved in the computation of each sample $x(n)$. These taps are complex numbers although the filtering operation will be implemented as shown in Fig. 8 in which the complex exponential multiplies only the output of the filters. In the efficient implementation, the IDFT implemented using the IFFT has a complexity of $(M/2)\log_2 M$ complex multiplications [37]. The coefficients of the polyphase components of the prototype filter are real numbers. Therefore, the number of complex multiplications (equivalent to four real multiplications) per output sample is:

Direct: $M \cdot [(\gamma/2) + 1]$

Efficient: $\{(M/2)\log_2 M / M\} + \gamma/2$

		Direct	Efficient
$M=64$	$\gamma=10$	384	8
	$\gamma=16$	576	11
$M=128$	$\gamma=10$	768	8.5
	$\gamma=16$	1152	11.5
$M=256$	$\gamma=10$	1536	9
	$\gamma=16$	2304	12

Table 1 Number of complex multiplications per output sample in FMT systems with 64, 128 and 256 subchannels and different values of the overlap parameter

4.1.2. FMT Receiver

In the receiver filter bank architecture (shown in Fig. 12) the receiving filters $\{g^{(i)}(n)\}$ are designed to be matched to the corresponding ones in the transmitter, i.e. from Eq. (21) $G^{(i)}(f) = (H^{(i)}(f))^*$.

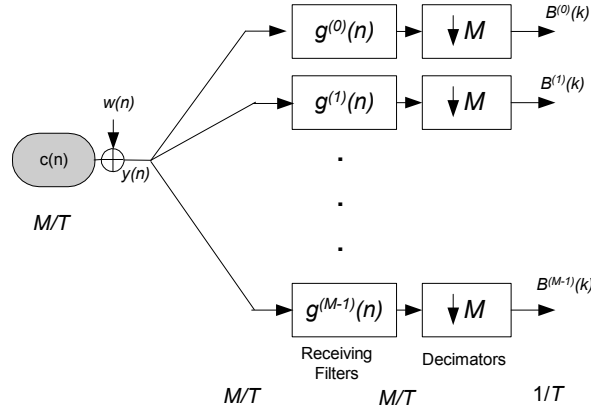


Fig. 12 FMT Receiver: direct implementation

Using the result that the inverse Fourier Transform of $(H^{(i)}(f))^*$ is $h^{(i)}(-n)$ we obtain:

$$g^{(i)}(n) = (h^{(i)}(-n))^* \quad (29)$$

therefore:

$$g^{(i)}(n) = \frac{1}{\sqrt{M}} h(-n) e^{-j\frac{2\pi}{M}(-n)i}, n = -M\gamma + 1, \dots, 0 \quad (30)$$

However, this filter is not causal. Since $g'(n)$ is defined for $n = -M\gamma + 1, \dots, -1, 0$ we need to apply a minimum delay of $M\gamma - 1$ samples to make it causal. However, differently to some other publications eg [38], we will apply a delay which is a multiple of the block size M . Specifically, we delay it $M\gamma$ samples and we call this response $g^{(i)}(n)$. This sample delay difference compared with other publications is what will allow us to define the efficient implementation. We should note that since we are using multirate blocks, this difference of one sample makes a change to the overall response of the filter. In the efficient implementation, it will also allow us to take blocks of M samples in a different way, otherwise, there will be an offset in the way we take the blocks of samples in the transmitter and in the receiver.

Applying a delay of $M\gamma$ samples to Eq. (30), the matched filter will maximize the SNR at that specific instant [3]. Therefore, the system will have an overall delay of γ blocks. However, since the prototype was not design with the perfect reconstruction constraint, we cannot say that the output of the filter bank is $A(k-\gamma)$.

Applying the delay to the receiver filters in Eq. (30) we obtain:

$$g^{(i)}(n) = g^{(i)}(n - M\gamma) \quad (31)$$

$$g^{(i)}(n) = \frac{1}{\sqrt{M}} h(-(n - M\gamma)) \cdot e^{j\frac{2\pi}{M}(n - M\gamma)i}, \quad n = 1, 2, \dots, M\gamma \quad (32)$$

which simplifies to:

$$g^{(i)}(n) = \frac{1}{\sqrt{M}} h(M\gamma - n) \cdot e^{j\frac{2\pi}{M}ni}, \quad n = 1, 2, \dots, M\gamma \quad (33)$$

and since $h(n)$ is symmetric, then the receiver filter at the i -th subchannel is:

$$g^{(i)}(n) = \frac{1}{\sqrt{M}} h(n - 1) \cdot e^{j\frac{2\pi}{M}ni}, \quad n = 1, 2, \dots, M\gamma \quad (34)$$

Applying Eq. (32), at the output of the i -th subchannel in Fig. 12 we get:

$$B^{(i)}(k) = \sum_{n=1}^{M\gamma} y(kM - n) g^{(i)}(n) = \frac{1}{\sqrt{M}} \sum_{n=1}^{M\gamma} y(kM - n) h(n - 1) e^{j\frac{2\pi}{M}ni} \quad (35)$$

To introduce the polyphase components of $h(n)$ defined in Eq. (24) we decompose n as $n = lM + t$, $l = 0, 1, \dots, \gamma - 1$ and $t = 1, 2, \dots, M$ to yield,

$$B^{(i)}(k) = \frac{1}{\sqrt{M}} \sum_{l=0}^{M-1} \sum_{t=0}^{\gamma-1} y(kM - lM - t) h(lM + t - 1) e^{j\frac{2\pi}{M}(lM + t)i} \quad (36)$$

$$= \frac{1}{\sqrt{M}} \sum_{l=0}^{M-1} \sum_{t=0}^{\gamma-1} y((k - l)M - t) h(lM + t - 1) e^{j\frac{2\pi}{M}ti} \quad (37)$$

If we make a change of variable $p = t - 1$:

$$B^{(i)}(k) = \frac{1}{\sqrt{M}} \sum_{p=0}^{M-1} \sum_{l=0}^{\gamma-1} y_{(k-l)M - (p+1)} h(lM + p) e^{j\frac{2\pi}{M}(p+1)i} \quad (38)$$

and applying:

$$e^{j\frac{2\pi}{M}(p+1)i} = e^{-j\frac{2\pi}{M}(M-p-1)i} \quad (39)$$

we obtain:

$$B^{(i)}(k) = \frac{1}{\sqrt{M}} \sum_{p=0}^{M-1} \left\{ \sum_{l=0}^{\gamma-1} y_{(k-l)M - p - 1} \cdot h(lM + p) \right\} \cdot e^{-j\frac{2\pi}{M}(M-p-1)i} \quad (40)$$

From Eq. (40) we are able to derive the efficient implementation shown in Fig. 13 where we apply the DFT operation (efficiently implemented with the FFT) to the M outputs of the M polyphase filters.

We can make some comments about Eq. (40) to see how the efficient implementation is derived.

(a) Since the receiving filters are as defined as in Eq. (34), and due to the downsampler in Fig. 13, the first output in the receiver filter bank will be at $k=1$ (M samples at rate M/T) and not at $k=0$.

(b) If we look inside Eq. (40), we will see that for $k=1$, we need the inputs $[y(0), y(1), \dots, y(M-1)]$. This is consistent with what we do in the efficient implementation shown in Fig. 13.

(c) The polyphase components of $h(n)$ are in reverse order with respect the DFT. That is why the first polyphase component in Fig. 13 is in the last branch of the filter bank.

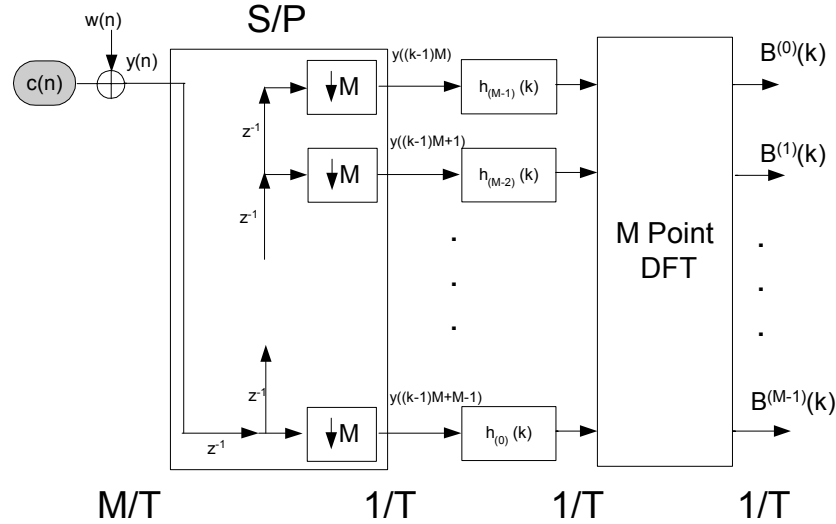


Fig. 13 FMT Receiver: Efficient implementation

We can also see from Eq. (40) that the implementation in Fig. 13 is mirrored (matched) to the implementation in Fig. 11. Since the prototype is symmetric and has $M\gamma$ samples, for each of the polyphase components $h_{(i)}(n)=h(nM+i)$, the matched filter is actually $h_{(M-i-1)}(n)$. That is why they are in reverse order to the ones in Fig. 11, since the whole implementation is matched to that of Fig. 11.

4.1.3. Perfect reconstruction condition

In conventional multicarrier communications systems based on filter banks, such as DWMT [19] or OFDM, to ensure that the transmission is free of ISI within a subchannel as well as free of ICI, the filter bank is required to satisfy the perfect reconstruction (PR) condition [35][34].

A filter bank is said to satisfy the PR condition if the reconstructed signal is identical to the input signal up to a specified delay. Therefore, from the transmitter and receiver filters shown in the Fig. 14 the PR constraint is [36]:

$$\sum_k h^{(i)}(k)g^{(i)}(nM-k) = \delta(n-\Delta) \quad , \forall i \quad (41)$$

$$\sum_k h^{(i)}(k)g^{(j)}(Mn-k) = 0 \quad , \quad \forall n, \quad i \neq j \quad (42)$$

Where Δ is a delay between the input and the output, $h^{(i)}(k)$ and $g^{(i)}(k)$ have been defined in Eq.(21) and Eq. (34) and δ is the Kronecker delta. We note that we refer to these filter banks as wavelet M -band transforms and to the analysis and synthesis filter banks as the direct and inverse transforms respectively.

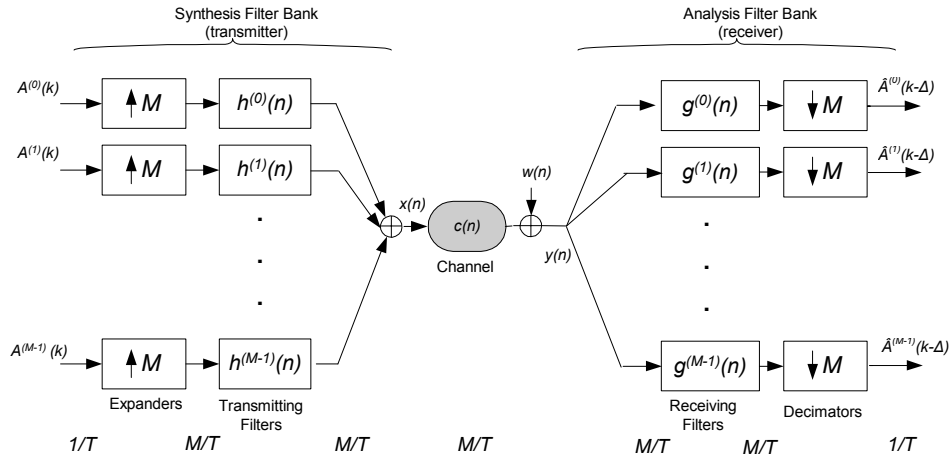


Fig. 14 Analysis and Synthesis Filter Bank

The PR reconstruction condition could be considered as a generalization of the Nyquist criterion for ISI free communications. We note that PR requires substantial overlap between subcarriers that is in contradiction with the desire for high spectral containment. References [35][34] provide a detailed treatment of PR filter banks and their extensions.

However, the previously applied PR condition does not take the channel distortion and noise into account, which are always present in a data communication systems. Consequently, the desirable properties of zero ISI and ICI are destroyed.

The approach followed in FMT is to remove ICI almost completely irrespective of the channel and then to remove the remaining ISI per subchannel using equalization. Therefore, by relaxing the PR constraints and introducing signal equalization at the receiver, filters that achieve high spectral containment can be found.

In the FMT filter bank, the design criterion will be high spectral containment. High spectral containment will avoid ICI but ISI will now exist in each subchannel and it will need to be removed.

We note that only a perfect brick wall filter would achieve PR and also satisfy the previously outlined FMT principles. Unfortunately this filter is not practical since it would require an infinitely long prototype filter.

4.1.4. Prototype design

In FMT modulation, the prototype filter completely defines the system. The choice of the prototype filter for the realization of the polyphase filter bank allows various tradeoffs between the number of subchannels, the level of spectral containment, the complexity of implementation and signal latency to be made. These tradeoffs are possible because the number of subchannels can be reduced without incurring a transmission efficiency loss, whereas in OFDM the minimum number of subchannels is constrained by efficiency requirements owing to the use of the cyclic prefix.

Since we are not required to design a prototype based on the PR constraint, we will focus on prototypes that accomplish high levels of spectral containment with the minimum complexity.

This prototype filter approximates an ideal filter which has a frequency response equal to zero outside the interval $|f| \leq 1/(2T)$ Hz as shown in the Fig. 15. In the design of the low pass filter $h(n)$, the sampling rate will be the highest system rate i.e., M/T . Therefore, the digital frequency (**at sampling rate M/T**) limit will be $1/(2M)$ (see Fig. 15). We will approximate this response with a linear phase FIR prototype filter with γM real coefficients. In this way, each of the polyphase filters will be a filter with real coefficients and length γ . We also note that the prototype is symmetric but that the polyphase components are not.

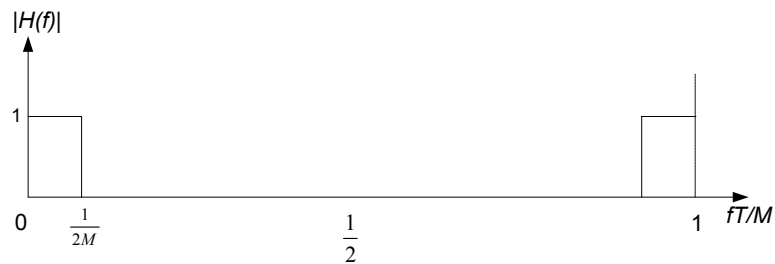


Fig. 15 Ideal Frequency Response of the low pass prototype

Since the desire is to design a low pass prototype filter, we propose to do it using standard filter design techniques.

In this section, we propose/discuss some of the parameters/constraints that are needed for the design. We will investigate two design techniques that give good results and also a third one proposed in [2].

We expect that as the FMT system becomes more mature, new optimization techniques will be proposed based on other constraints.

In classical low pass filter FIR design [37], the cutoff frequency is chosen to be the frequency at which the frequency response of the filter decays by 3dB. In our case, $1/(2T)$ is not the cutoff frequency because we want the frequency response to be zero at that frequency. Therefore, a lower frequency will be selected as the cutoff frequency. Depending on the value of the overlap γ , we will choose different values for the cutoff frequency.

We have found that there are two important values in the design of the prototype:

- f_{-3dB} : This value will be related to the flatness of the channel response in the subchannel. The closer to $f=1/(2T)$, the easier will be the equalization at the receiver and noise enhancement by the equalizer will be less of a problem. This value will be important in determining the ISI per subchannel and consequently the equalization requirements.

- The magnitude response at $f=1/(2T)$ or equivalently the spectral cross over with adjacent channels. Due to the uniform filter bank implementation, this value will be the crossing point between two adjacent subchannels. This value should be as low as possible since it will determine the ICI introduced by adjacent channels. If this value is sufficiently low we can assume independence of the subchannels at the output of the filter bank.

Obviously, for a fixed value of the overlap γ , there will be a tradeoff between these last two parameters.

We now present 3 design methods that give good results:

Low pass filter design using the window method

In classical FIR filter design [37], the cutoff frequency is chosen as the frequency at which the frequency response of the filter decays by 3dB. In our case, $1/(2T)$ is not the required cutoff frequency since we want the frequency response to be zero at that frequency. Therefore, a lower frequency than $1/(2T)$ will have to be selected as the cutoff frequency. For higher values of the overlap γ , we can choose a cutoff frequency closer to $1/(2T)$.

Several windows have been considered in the literature which offer different tradeoffs between transition width, sidelobe level, maximum stopband attenuation and passband ripple. We have seen that Hamming and Gaussian windows give good results. Reference [37] gives a complete analysis of how to apply the method. In Fig. 16, we show the first 5 channels of the FMT with Gaussian and Hamming windows, for $\gamma=14$ and different values of f_{cutoff} .

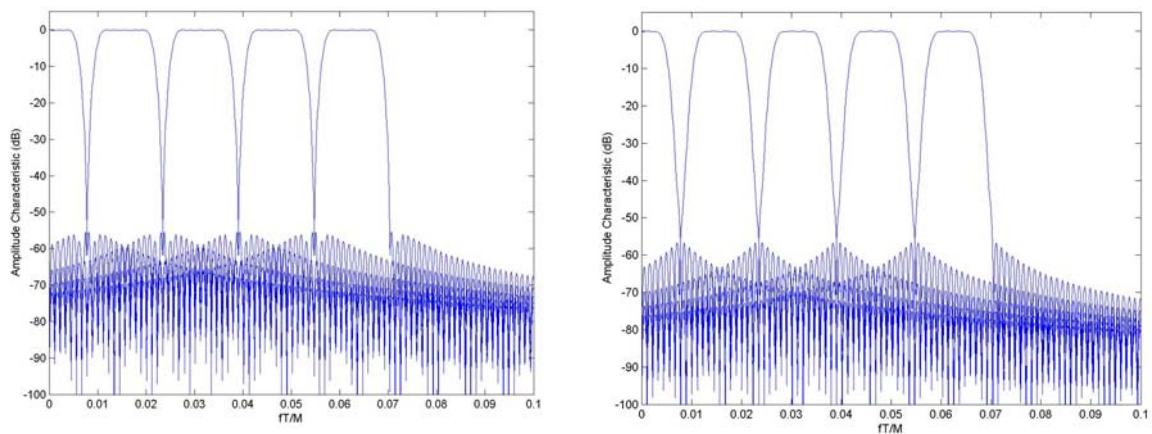


Fig. 16 First 4 subchannels with $\gamma=14$ (a) Hamming Window, $f_{\text{cutoff}}=0.38/T$ (b) Gaussian Window, $f_{\text{cutoff}}=0.315/T$

Modified Parks-McClellan Algorithm

We can also use a modification of the Parks-McClellan Algorithm [39]. The principle will be the same as the standard Parks-McClellan algorithm but without the

equi-ripple constraint doing that the filter response decays continuously at frequencies higher than $1/(2T)$. We got this characteristic by computing the filter with 2 more coefficients and then removing the first and last coefficients. In our design, we obtained good results providing the algorithm with four frequencies $[0, f_i, 0.5/T, 0.5]$ with amplitudes of $[1, 1, 0, 0]$ respectively. In Fig. 17 we show two designs with $\gamma=10$ and $\gamma=16$ with $f_i=0.13/T$ and $f_i=0.15/T$ respectively.

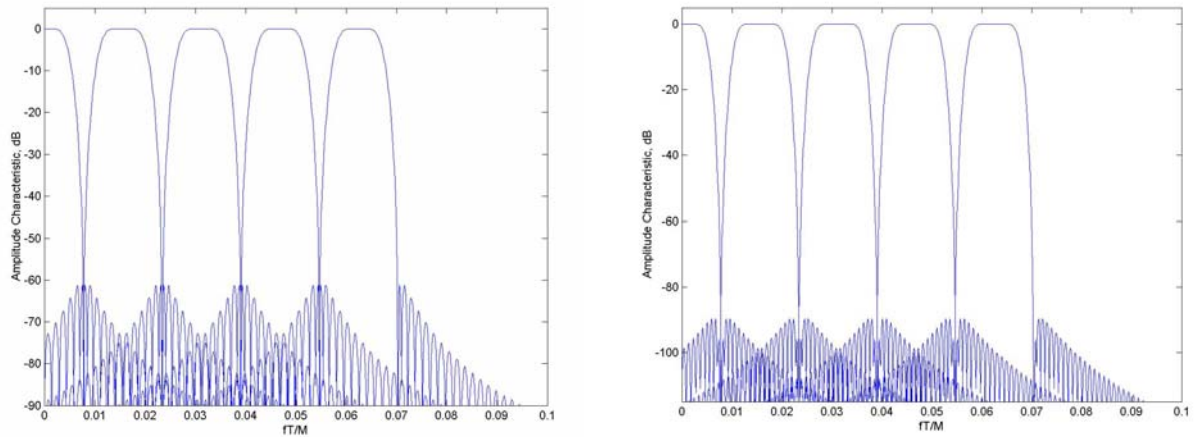


Fig. 17 First 5 subchannels with (a) $\gamma=10$ and frequency cut $0.13/T$ (b) $\gamma=16$ and first frequency cut $0.15/T$

IIR approximation by a FIR

In [1][2] the frequency response is considered to be given by

$$H(f) = \begin{cases} \left| \frac{1 + e^{-j2\pi fT}}{1 + \alpha e^{-j2\pi fT}} \right| & \text{if } -1/2T \leq f \leq 1/2T \\ 0 & \text{otherwise} \end{cases} \quad (43)$$

which defines the absolute value of the frequency response of a filter with a zero at $z=-1$ and a pole at $z=-\alpha$ as shown in Fig. 18

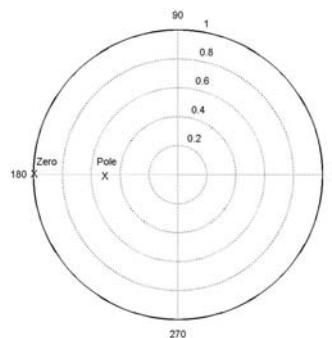


Fig. 18 z diagram for the Prototype design with $\alpha=0.5$

The parameter α ($0 \leq \alpha \leq 1$) controls the spectral roll off of the filter. For $\alpha \rightarrow 1$, the frequency characteristic of each subchannel is characterized by steep roll off towards the band edge frequencies.

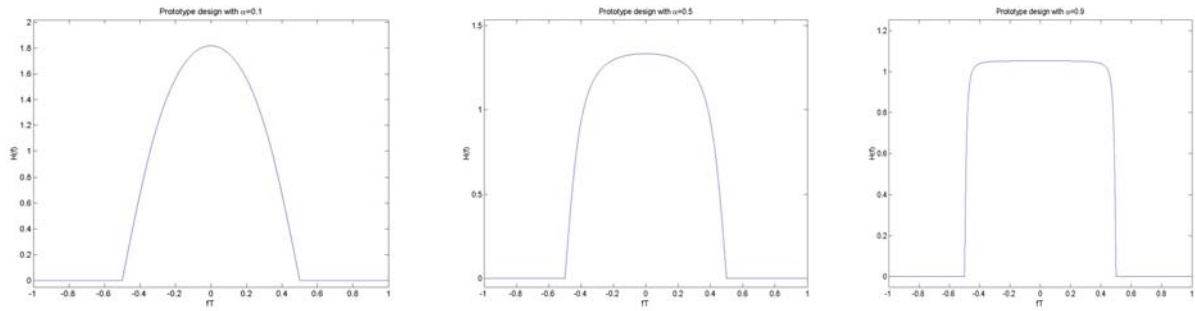


Fig. 19 Prototype design $H(f)$ for different α (a) $\alpha=0.1$ (b) $\alpha=0.5$ (c) $\alpha=0.9$

The frequency responses shown in Fig. 19 are effectively for an infinite number of coefficients. What we wish to do is to approximate the required prototype filter using a FIR structure with a finite number of coefficients. In doing so sidelobes will appear at frequencies higher than $1/(2T)$ and some ripple in the pass band will become evident. The higher the value of α , the higher the roll off making it more difficult to approximate with a finite number of samples. Consequently, the error (leakage in frequencies higher than $1/(2T)$ and ripple) will become higher.

Other methods

We note here that depending on the equalization and implementation method that we use, we could use iterative algorithms with different constraints.

4.2. OFDM as a filter bank

We can view conventional OFDM modulation from the same point of view as FMT. In this situation, the low pass prototype is a rectangular pulse in the time domain (see Fig. 20), i.e. a sinc function in the frequency domain.

The length of the overlap in this case will be $\gamma=1$. As we have seen in the previous section, the higher the overlap, the higher the spectral containment. This is the reason that we do not accomplish high spectral containment in OFDM. However, in this case the prototype accomplishes perfect reconstruction.

Although all subchannels overlap in frequency, the system exhibits neither ISI nor ICI (PR condition) as long as the channel is non dispersive, at the expense of high spectral overlap.

Fig. 21 shows the block diagram of a OFDM/DMT modulator. All the filters depicted at the output branches of the IDFT block have the trivial impulse response

$$h_{(i)}(k) = \delta(k), \quad \text{for } i = 0, 1, \dots, M - 1 \quad (44)$$

where $h_{(i)}(k)$ represents the i th polyphase components of a prototype filter $h(n)$ with impulse response:

$$h(n) = 1, \quad \text{for } n = 0, 1, \dots, M - 1 \quad (45)$$

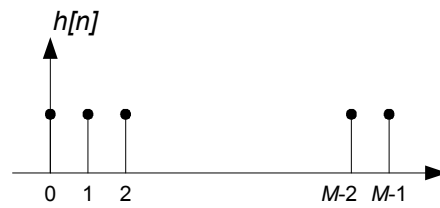


Fig. 20 DMT/OFDM Prototype

hence, each of the polyphase components have 1 sample.

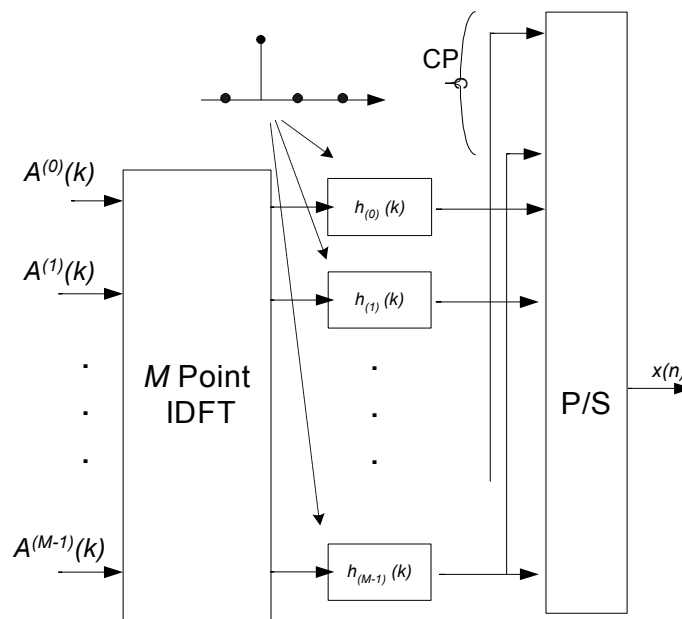


Fig. 21 OFDM/DMT Modulator

Following this explanation, we can view both FMT and DMT/OFDM as uniform filter banks based on a prototype. When the prototype $h(n)$ is an ideal rectangular pulse in time, the system will be called OFDM/DMT. Alternatively, when $h(n)$ is designed to minimize the overlap between the frequency response of two adjacent subchannels (i.e., an ideal rectangular pulse in the frequency domain) the corresponding system is called FMT.

4.3. Virtual Carriers

Due to the high spectral containment achieved by the prototype filter in FMT, negligible power leaks into adjacent bands. Consequently fewer Virtual Carriers (VC) are needed in order to be compliant with the regulatory power spectrum mask compared with OFDM, see section 3.1.3. In Fig. 22 we show the 20MHz spectrum occupied by OFDM HIPERLAN/2 with 12 VCs and FMT with 4 VC using a

prototype with $\gamma=16$. In fact, we can see that no VCs are required for FMT since the out of subband power is attenuated by more than 70dB.

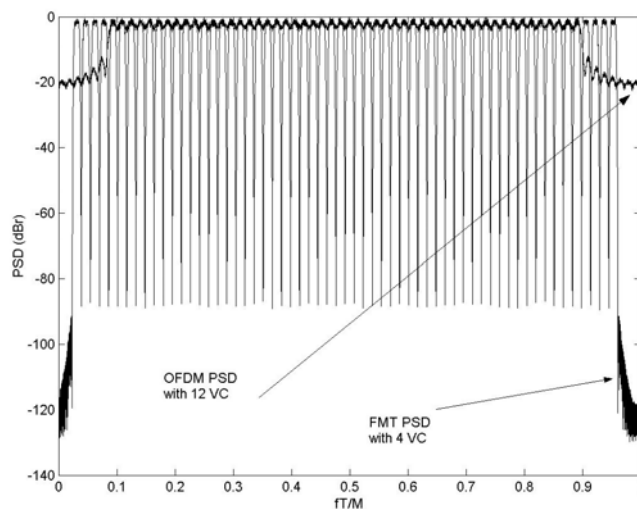


Fig. 22 20 MHz Power Spectral Density with 64 subcarriers and (a) OFDM with 12 VC (b) FMT (overlap $\gamma=16$) with 4 VC

In Fig. 23 we show the spectrum of the analog FMT signal centered at the transmitted frequency. We see that the out of band power of FMT can be considered negligible in comparison with that of OFDM.

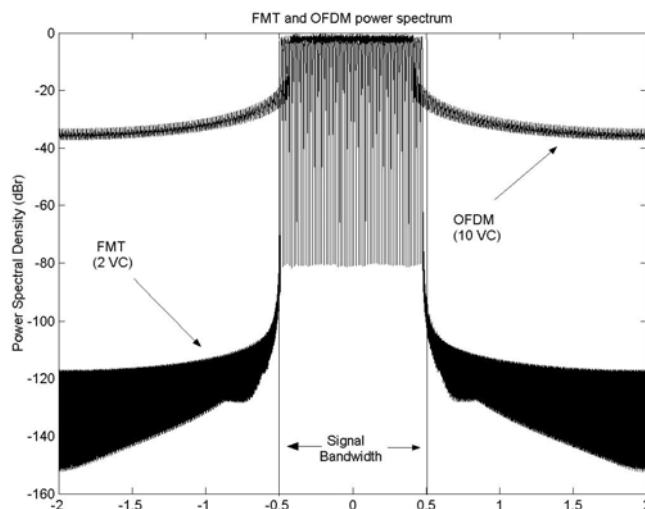


Fig. 23 Composite OFDM and FMT (overlap $\gamma=10$) out of band power spectrum

Another situation in which VCs are needed are in multi user systems. In this access system, each of the users is assigned a group of subcarriers from the total number M . Since it is not possible to ensure that all the users are perfectly synchronized (frame synchronization), we need to use VCs between users in a conventional OFDM to reduce the overlap in the frequency response.

As we see, in FMT we do not need to use either VCs or frame synchronization between different users because the out of band power is negligible.

In Fig. 24 we show an FMT system using a prototype with overlap $\gamma=16$ in which the 30th subcarrier has not been used. We see how the power of the adjacent subchannels does not leak into the subband corresponding to the 30th subchannel:

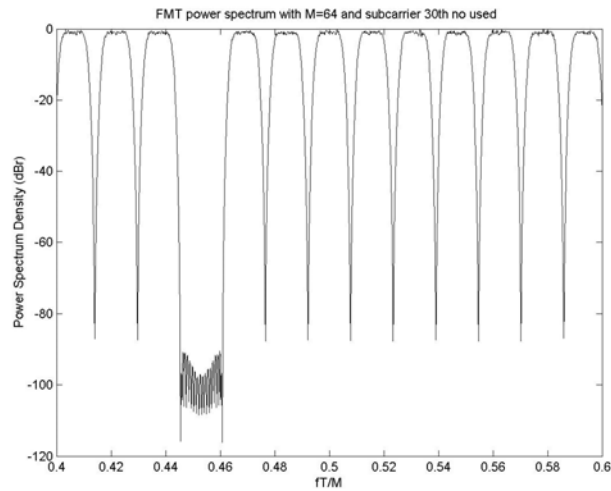


Fig. 24 Composite FMT power spectrum in which the 30th subcarrier has not been used

4.4. Conclusion

In this Chapter we have presented the basic theory and advantages of FMT Modulation, as a multicarrier modulation technique based on M -branch filters that are frequency shifted versions of a low pass prototype filter. We have provided the filter bank definition that leads us to derive an efficient implementation based on the FFT and a network of polyphase filters and we have proposed methods to design the low pass prototype. We have also presented reasons based on the PR violation to introduce per subchannel equalization and we have shown the reason to use less VCs in FMT than in OFDM.

Chapter 5. Equalization in FMT

We have shown that ICI can be neglected in an FMT system owing to the high spectral containment of the subchannels. However, since the filters have not been defined to satisfy the perfect reconstruction condition, ISI will be introduced into each of the subchannels. This can be easily understood from Fig. 1(b) and from the Nyquist criterion for ISI free modulation [3]. We see that the Nyquist frequency (the inverse of the symbol period) is exactly the same value as the frequency separation of the subchannels. Since in the prototype filter design we try to have all the spectra contained in $1/(2T)$, the Nyquist criterion will not be accomplished owing to the rapid decay of the frequency response before $f=1/(2T)$. The longer the overlap γ , the flatter can be the filter passband out to frequencies close to $f=1/(2T)$ and so less ISI will be introduced.

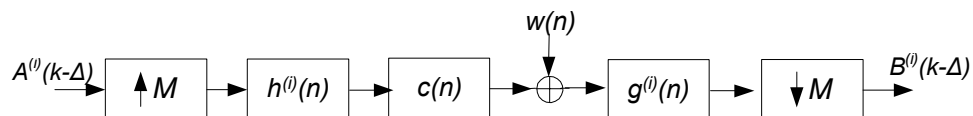


Fig. 25 Equivalent subchannel

Therefore, for a constant overlap γ , prototypes with good orthogonality in the frequency domain (i.e. they do not overlap significantly in frequency) will necessarily exhibit strong curvature toward the band edge of the prototype frequency response, necessarily leading to ISI on that subchannel. Therefore, an equalizer will be needed with FMT filter banks.

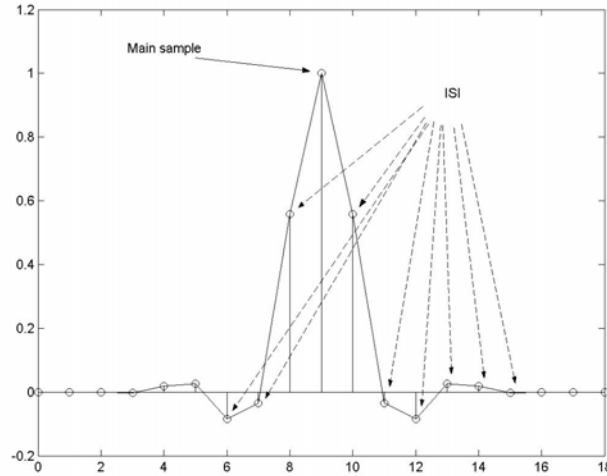


Fig. 26 Equivalent time response of the i -th subchannel

Assuming that the subchannels are well separated in frequency (as is arranged in FMT, see Fig. 9), the overall response for each of the subchannels will be independent of the adjacent channels (no ICI) and it can be considered equivalent to the cascade of the i -th transmitter filter, the multipath channel, $c(n)$, and the i -th receiver filter as shown in Fig. 25. This response will need to be equalized by a per subchannel equalizer.

It is important to note that even without the effect of the channel and the additive noise, we would still have ISI due to violation of the PR reconstruction condition. In Fig. 26, we show the impulse response of the i -th subchannel without the effect of the multipath channel. The prototype was computed with an overlap γ equal to 10, therefore, the length of the equivalent channel has 19 samples.

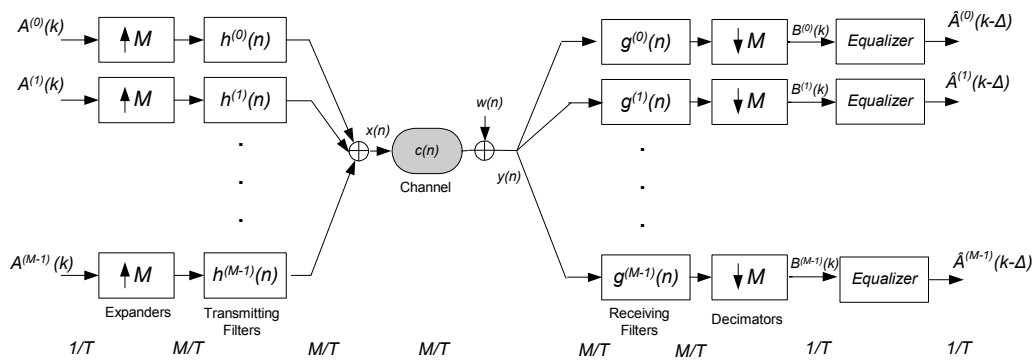


Fig. 27 Per subchannel equalization

The decision feedback equalizer

The Decision Feedback Equalizer (DFE) is a well established and effective approach for the mitigation of the ISI effects. It consists of a Feedforward Filter, a

Feedback Filter and a Decision Device (see Fig. 28). Both the Feedforward and the Feedback Filters are usually realized as transversal finite impulse response (FIR) filters. The feedback filters remove the postcursor of the intersymbol interference, i.e. the influence of the past symbols about which decisions have been made, while the feedforward filters minimize the effect of the precursor ISI, i.e. the effect of future symbols.

It has been seen that the DFE provides improved performance compared to the linear transversal equalizer and reduced complexity (with almost the same performance) compared to maximum likelihood sequence estimation (MLSE) [3].

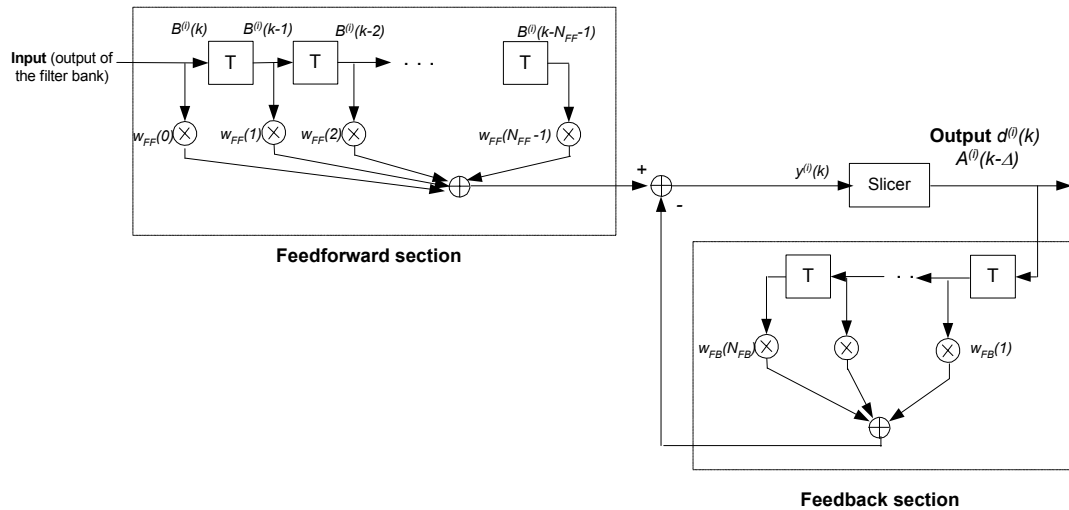


Fig. 28 Decision Feedback Equalizer (DFE)

Two optimality criteria have been used to optimize the coefficients of DFE filters, namely the Zero Forcing (ZF) criterion and the Minimum Mean Square Error (MMSE) criterion. The ZF tries to invert the channel impulse response without taking noise into account. Notches will therefore be compensated by high gain, which leads to intolerable noise enhancement. The ZF equalizer can therefore only be used on relatively flat channels with high SNRs ratios, that are not common on multipath wireless channels. Here, we consider a DFE that minimizes the mean square error criterion (MMSE-DFE), i.e. it minimizes the power of the error at the decision device (slicer). The MMSE-DFE has been identified as the best among the suboptimal (compared to MLSE) receivers for wireless applications and has been the subject of extensive theoretical studies [40][41].

5.1. Per subchannel DFE: Computation of the MMSE equalizer coefficients based on channel estimation

Let's consider a multipath channel $c(l)$ as defined in section 2.1 with L taps spaced at the sampling rate.

In this case, the overall response of the i -th subchannel (see Fig. 25) will be considered as the cascade of the i -th transmitter filter as defined in Eq. (21), the channel response $c(l)$ and the i -th receiver filter as defined in Eq.(34) decimated by a factor of M . Thus, the overall response of the i -th subchannel becomes:

$$h_{overall}^{(i)}(k) = \left(g^{(i)}(n) \otimes \sum_{p=0}^{L-1} c(p)h^{(i)}(n-p) \right) \downarrow_M \quad (46)$$

$$h_{overall}^{(i)}(k) = \sum_{n=1}^{M\gamma} g^{(i)}(n) \sum_{p=0}^{L-1} c(p)h^{(i)}(kM - n - p) \quad (47)$$

And using definitions from Eq. (21) and Eq. (34) we get:

$$h_{overall}^{(i)}(k) = \frac{1}{M} \sum_{n=1}^{M\gamma} h(n-1) e^{j\frac{2\pi}{M}ni} \sum_{p=0}^{L-1} c(p)h(kM - n - p) e^{j\frac{2\pi}{M}(nM-n-p)i} \quad (48)$$

$$h_{overall}^{(i)}(k) = \frac{1}{M} \sum_{n=1}^{M\gamma} h(n-1) \sum_{p=0}^{L-1} c(p)h(kM - n - p) e^{-j\frac{2\pi}{M}pi} \quad (49)$$

which is channel dependent and consequently we will need a different equalizer (i.e. different coefficients) for each of the subchannels. To remove the ISI introduced by the overall response in Eq. (49), the coefficients of a DFE equalizer can be computed based on the MMSE criterion.

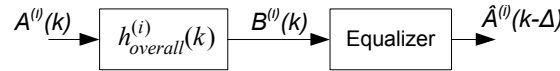


Fig. 29 Equivalent subchannel + Equalizer

We note that the additive noise at the output of the Filter Bank is no longer white since it has been filtered by $g^{(i)}(n)$. The coloured noise at the output of the filter bank is given by:

$$n_r^{(i)}(k) = \sum_{n_1=1}^{M\gamma-1} g^{(i)}(n_1) \cdot n(kM - n_1) = \sum_{n_1=1}^{M\gamma-1} h(n_1-1) e^{j\frac{2\pi}{M}n_1i} \cdot n(kM - n_1) \quad (50)$$

In each of the subchannels, we will use a DFE equalizer of the form shown in Fig. 28. In the equalizer, the input $B^{(i)}(k)$, the desired output, $A^{(i)}(k)$ and the filter tap weights are all assumed to be complex variables. The estimated error $e^{(i)}(k)$ at the decision device is also complex and we may write:

$$e^{(i)}(k) = d^{(i)}(k) - y^{(i)}(k) \quad (51)$$

where $d^{(i)}(k)$ is the output of the slicer and $y^{(i)}(k)$ the output of the DFE filtering operation.

The MMSE criterion to compute the DFE coefficients will minimize:

$$E\{|e^{(i)}(k)|^2\} = E\{|d^{(i)}(k) - y^{(i)}(k)|^2\} \quad (52)$$

We consider a DFE with N_{FF} and N_{FB} coefficients. Let $\{w_{FF,i}(k)\}$, $k=0,1,\dots,N_{FF}-1$, indicate the feedforward taps of the i -th subchannel and $\{w_{FB,i}(k)\}$, $k=1,2,\dots,N_{FB}$, the

corresponding feedback filter. Then we define two vectors containing the feedforward and feedback filters coefficients, respectively:

$$\underline{w}_{FF,i} = [w_{FF,i}(0), w_{FF,i}(1), w_{FF,i}(2), \dots, w_{FF,i}(N_{FF} - 1)] \quad (53)$$

$$\underline{w}_{FB,i} = [w_{FB,i}(1), w_{FB,i}(2), w_{FB,i}(3), \dots, w_{FB,i}(N_{FB})] \quad (54)$$

It is mathematically convenient to define an augmented response vector for the DFE as:

$$\underline{w}_i = [w_{FF,i}^*(0), w_{FF,i}^*(1), \dots, w_{FF,i}^*(N_{FF} - 1), -w_{FB,i}^*(1), -w_{FB,i}^*(2), \dots, -w_{FB,i}^*(N_{FB})]^T \quad (55)$$

and the corresponding augmented DFE input vector $\underline{x}^{(i)}(k)$ (data in the tapped delay line)

$$\underline{x}^{(i)}(k) = [B^{(i)}(k), B^{(i)}(k-1), \dots, B^{(i)}(k - N_{FF} + 1), d^{(i)}(k-1), d^{(i)}(k-2), \dots, d^{(i)}(k - N_{FB})]^T \quad (56)$$

where $B^{(i)}(k)$ is the output of multirate filter bank:

$$B^{(i)}(k) = \sum_{n=0}^{N_{eq}-1} h_{overall}^{(i)}(n) A^{(i)}(k-n) + n_r^{(i)}(k) \quad (57)$$

Therefore we will have

$$y^{(i)}(k) = \underline{w}_i^T \underline{x}^{(i)}(k) \quad (58)$$

We now suppose that the decisions are correct, $d^{(i)}(k) = A^{(i)}(k-\Delta)$ where Δ is a suitable delay between the FMT transmitter input and the DFE output. Thus, the data in the tapped delay line becomes:

$$\underline{x}^{(i)}(k) = [B^{(i)}(k), B^{(i)}(k-1), \dots, B^{(i)}(k - N_{FF} + 1), A^{(i)}(k - \Delta - 1), \dots, A^{(i)}(k - \Delta - N_{FB})]^T \quad (59)$$

The MMSE for the MMSE-DFE is [42]:

$$\sigma_{MMSE-DFE,i}^2 = \min_{w_{FB,i}, w_{FF,i}} E \left\{ \left| d^{(i)}(k) - y^{(i)}(k) \right|^2 \right\} \quad (60)$$

In Appendix B we show how to find the coefficients $w_{FB,i}$ and $w_{FF,i}$ that minimize Eq. (60) based on the correlation matrix of the input data and the crosscorrelation between the input data and the training symbols. We highlight here that we need to compute the inverse of a matrix of dimension $N_{FF} \times N_{FF}$.

Therefore, for each of the subchannels, we compute the DFE coefficients that minimize Eq.(60) based on the overall channel response defined in Eq. (49).

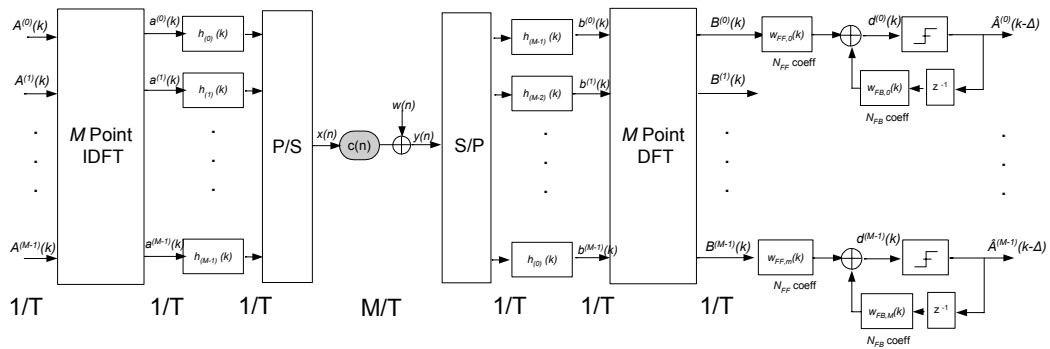


Fig. 30 FMT with per subchannel equalization

Although this scheme gives good results, it is computationally highly expensive because for every channel estimate $c(l)$, we need to compute the equivalent channel in Eq. (49) and invert M different correlation matrices of dimension $N_{FF} \times N_{FF}$. Nevertheless, there are some efficient algorithms for matrix inversion since they exhibit a specific structure although they still result in a high computational complexity since we require a different equalizer for each of the subchannels.

As we have shown in Chapter 2, wireless channels are time varying in nature hence, more efficient implementations need to be found. In theory, computation of the coefficients should be performed every time the channel changes.

5.2. Efficient FMT equalization schemes

Let's first consider the M point DFT of the channel impulse response:

$$\psi^{(i)} = \sum_{l=0}^{L-1} e^{-j2\pi \frac{i}{M} l} c(l) \quad , i = 0, 1, \dots, M-1 \quad (61)$$

5.2.1. Frequency domain DFE

If we are in the situation where the channel coherence bandwidth (as defined in Appendix A) is much larger than the subchannel separation $1/T$, we can consider that frequency flat fading applies to each of the subchannels and consequently, the effect of the multipath channel in each sub-channel can be equalized using a complex gain factor that compensates the phase and amplitude distortion introduced by the multipath channel. The condition of channel flatness is related to the RMS delay spread of the channel and the subchannel spacing. Therefore, for a constant RMS delay spread, if we have more subchannels in the same bandwidth (M higher), the flatness condition will be more easily achieved.

Under this assumption the convolution between the i -th transmit filter and the transmission channel is:

$$\sum_{n_1=0}^{M\gamma-1} c(n-n_1) \cdot h^{(i)}(n_1) \approx \psi^{(i)} \cdot h^{(i)}(n) = \psi^{(i)} \cdot e^{j2\pi \frac{i}{M} n} h(n) \quad , n = 0, 1, \dots, M\gamma-1 \quad (62)$$

$$i=0, 1, \dots, M-1$$

Hence, as proposed in [38] the effect of the multipath channel can be adaptively equalized by a one tap per subchannel, and using the M point DFT of the channel as defined in Eq. (61), the tap value is computed using:

$$q^{(i)} = \frac{1}{\psi^{(i)}} \quad i=0,1,\dots,M-1 \quad (63)$$

Which is identical to that used for OFDM systems employing a cyclic prefix.

Once the distortion introduced by the multipath channel has been compensated, we will still have the ISI introduced by the prototype filter as shown in Fig. 26. This ISI can be compensated by a fixed DFE equalizer whose coefficients are computed offline since they only depend on the prototype filter. Ignoring the effect of the multipath channel (that will be compensated with the gain factor given in Eq. (63)), the overall response of the i -th subchannel is:

$$h_{overall}^{(i)}(k) = \sum_{n=0}^{M\gamma-1} h^{(i)}(n)g^{(i)}(kM-n) \quad (64)$$

$$h_{overall}^{(i)}(k) = \frac{1}{M} \sum_{n=0}^{M\gamma-1} h(n)e^{j\frac{2\pi}{M}ki} h(kM-n-1)e^{j\frac{2\pi}{M}(kM-n)i} \quad (65)$$

$$h_{overall}^{(i)}(k) = \frac{1}{M} \sum_{n=0}^{M\gamma-1} h(n)h(kM-n-1) \quad (66)$$

which is independent of the subchannel index i . Therefore, we can use the same equalizer coefficients to equalize each of the subchannels. We note that for a prototype of length $M\gamma$, the length of the overall response in Eq. (66) will be $2\gamma-1$.

The coefficients of the fixed feedforward and feedback sections of the DFE equalizer can be computed using the MMSE criterion as described in section 5.1 substituting $h_{overall}^{(i)}(k)$ by the one defined in Eq.(66).

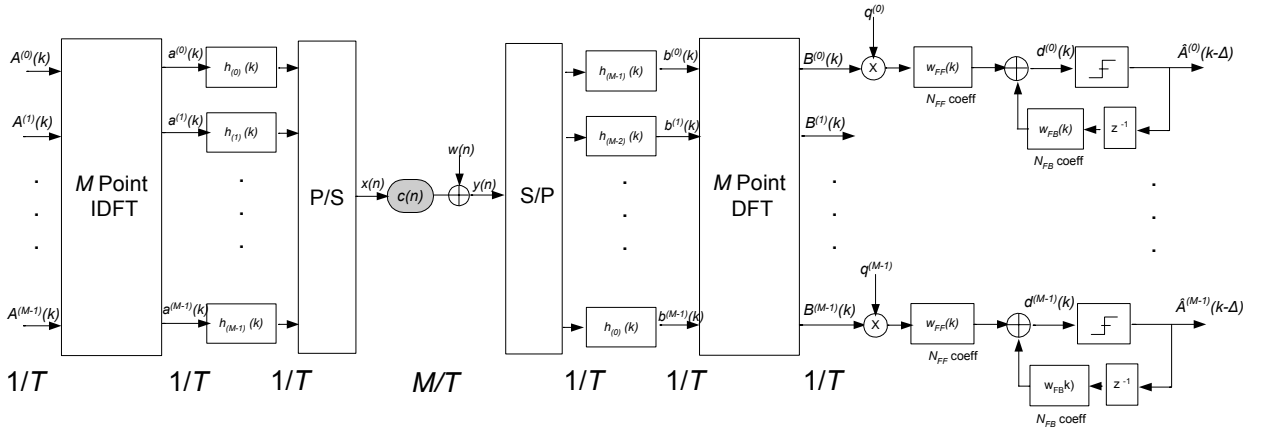


Fig. 31 Efficient per subchannel equalization based on a fixed DFE to compensate the prototype and a one tap equalizer to compensate the effect of the channel

Fig. 31 shows the block diagram for the proposed scheme. Note that the feedforward and feedback filters are common for all the subchannels and the coefficients are real since the response $h_{overall}^{(i)}(k)$ in Eq. (66) is also real.

5.2.2. Time Domain DFE

As proposed in [38], instead of using frequency domain equalization, to remove the ISI introduced by the prototype, we can apply a fixed time domain DFE just after the Serial to Parallel converter. In this way, instead of using the network of polyphase filters, we can directly apply the DFE equalizer. After the DFT, we again apply (as in the previous section), a one tap equalizer (per channel) as defined in Eq. (63) to compensate for the gain and phase rotation introduced into the subchannel. This scheme is shown in Fig. 32.

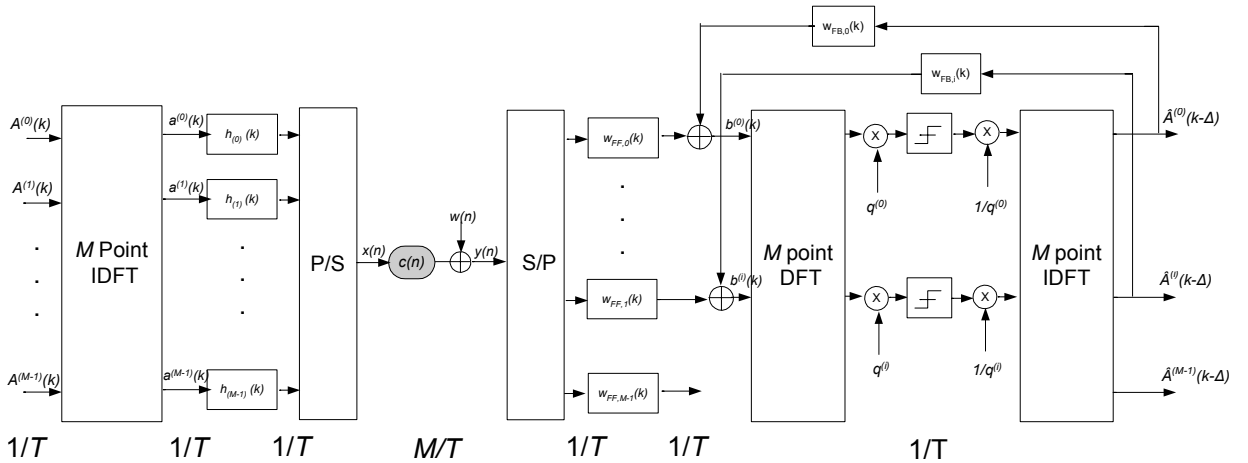


Fig. 32 FMT equalization with a fixed time domain DFE and one tap equalizer to compensate the channel

In this implementation, the DFE equalizers will try to minimize the difference between $b^{(i)}(k)$ and $a^{(i)}(k)$ as defined in Fig. 32 where $a^{(i)}(k)$ is the i -th output of the IDFT in the transmitter and $b^{(i)}(k)$ is the output of the DFE equalizer in the i -th subbranch. Therefore, without taking into account the effect of the channel, the i -th DFE equalizer is computed to compensate the effect of the i -th polyphase component of the transmitter $h_{(i)}(k)$.

Hence, the MMSE criterion will minimise:

$$\sigma_{MMSE-DFE}^2 = \min_{w_{FB}w_{FF}} E \left\{ \left| b^{(i)}(k) - a^{(i)}(k - \Delta) \right|^2 \right\} \quad (67)$$

The coefficients of the fixed feedforward and feedback sections of the DFE equalizer can be computed using the MMSE criterion as described in section 5.1 by using the polyphase components of the low pass prototype $h_{(i)}(k)$ in place of $h_{overall}^{(i)}(k)$. We note that in this case, the noise is white since it is applied directly to the DFE equalizer and it has not been filtered by the receiver filter $g^{(i)}(n)$.

The main advantage of this implementation in comparison with the one proposed in section 5.2.1 is that the response that the DFE is trying to equalize is shorter. In the previous section, the cascade of transmitter and receiver has a length equal to $2\gamma-1$. In this implementation, the response has a length equal to γ , therefore, we could expect a similar performance but with a shorter DFE.

The disadvantage is that we need a different equalizer for each of the subchannels since each of the polyphase components is different.

5.2.3. Complexity

As presented in [52], we give the computational complexity in terms of complex multiplications per subchannel and per output symbol for each of the **receiver** schemes presented considering that the channel has already been estimated. The computational complexity of the FFT block in terms of complex multiplications is $(M/2)\log_2 M$ [37].

In conventional OFDM receivers we use a complex gain to compensate the amplitude and phase distortion introduced into each of the subchannels, therefore we need $(1/2)\log_2 M + 1$ complex multiplications.

We now consider the calculations in terms of complex multiplications per output sample and per subchannel of the three FMT receiver schemes presented previously:

- Frequency domain DFE equalization based on the channel estimate and prototype: we need $(1/2)\log_2 M + \gamma + N_{FF} + N_{FB}$ complex multiplications per subchannel and output symbol.
- Fixed frequency domain DFE to compensate the prototype and one tap to compensate the channel: $(1/2)\log_2 M + \gamma + N_{FF} + N_{FB} + 1$ complex multiplications.
- Fixed time domain DFE to compensate the prototype and one tap to compensate the channel (applied twice as in Fig. 32): $(1/2)\log_2 M + N_{FF} + N_{FB} + \log_2 M + 2$ complex multiplications.

We remember that although the complexity of the fixed time domain and frequency domain DFE is similar (assuming $\log_2 M \approx \gamma$), we could obtain optimal results with shorter DFE equalizers in the time domain DFE scheme.

In the simplified FMT schemes, the initialisation cost of the fixed DFE equalizers is zero since they are computed offline based on the prototype. However, the initialization of the DFE equalizer depending on the channel estimate and the

prototype filter response requires the inversion of large matrices and is consequently a large overhead per received burst assuming a quasi-static channel.

5.2.4. Achievable bit rate and loading algorithms

One of the main reasons to introduce multicarrier based modulation schemes in wireless communications is to divide the channels into subbands so that each of these subbands will be affected differently by the multipath channel. At the receiver, the performance (SNR) in each of the subcarriers depends on the frequency domain channel transfer function. The occurrence of bit errors is normally concentrated in a set of severely faded subcarriers while in the rest of the multicarrier spectrum often no bit errors are observed. Therefore, a good approach is to make the transmitter aware of the low SNR subcarriers (i.e. via a reverse channel) and exclude them from transmission. On the other hand, some other subcarriers achieve a better SNR at the receiver and the potential loss of throughput due to the exclusion of faded subcarriers can be mitigated by employing higher-order constellations on the subcarriers exhibiting high SNR values. Therefore, loading the different subcarriers appears to be an interesting approach for increasing the capacity usage of the channel.

The theoretical channel capacity can be achieved by distributing the energy according to the waterpouring distribution [28]. However, this distribution is difficult to compute since it assumes infinite granularity in both subchannel bandwidth and constellation size. Different practical (sub-optimal) loading algorithms have been proposed in the multicarrier context. In general, these can be classified into margin-adaptive and rate-adaptive loading algorithms [29]. The margin adaptive ones maximize the margin (or equivalently minimize the bit error rate) for a fixed bit rate and given power constraint. Rate-adaptive loading algorithms maximize the bit rate for a fixed bit error rate and given power constraint.

To compute upper bounds on the achievable bit rate performance in a multicarrier modulation system, we choose to implement a rate-adaptive loading algorithm based on the one proposed in [30]. In this algorithm, the bits per subchannel are assigned according to the capacity of the subchannels:

$$b_i = \log_2 \left(1 + 10^{\frac{SNR_i - \Gamma}{10}} \right) \quad (68)$$

where SNR_i (dB) is the signal to noise ratio at the decision device in the i th subchannel and Γ (dB) is the SNR gap, representing the difference between the channel capacity and the actual capacity usage of the transmission scheme. The SNR gap depends on the bit error rate being aimed at and the modulation and coding scheme used in the transmission.

The distribution of bits obtained is still continuous in nature. In order to derive a discrete bit distribution from the continuous one, the number of bits b_i associated at the subchannel i is quantized in such a way so as to round it to the nearest number of bits per symbol according to the possible constellations. For example, in the case of 4/16/64-QAM constellations, the possible numbers of bits are 2, 4 and 6 respectively.

In Fig. 33 we show a sample simulated impulse response (time response and frequency response) of an exponentially decaying Rayleigh Fading Channel as described in section 2.1 with an RMS delay spread equal to 130ns and a sampling rate equal to 50ns.

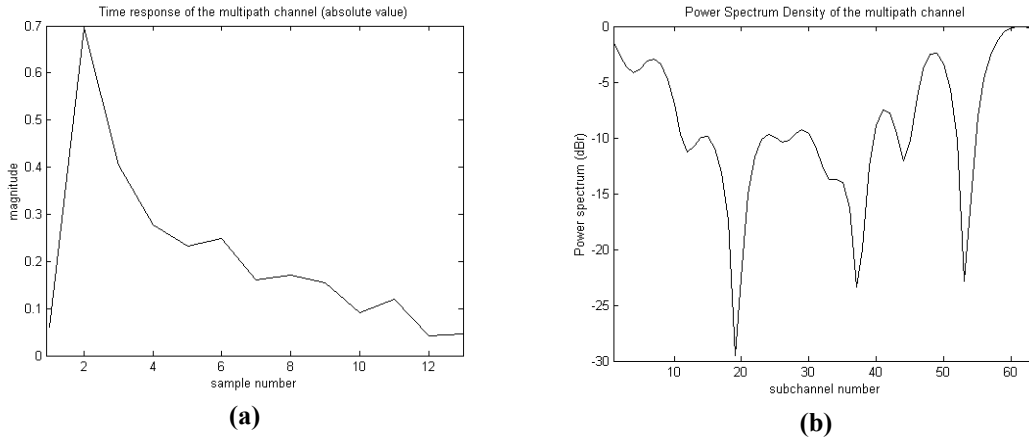


Fig. 33 Multipath Channel Impulse Response with RMS delay spread=130ns and sampling time=50ns (a) time domain response (b) frequency domain response (power spectrum density)

In Fig. 34, we show that the per subchannel SNR at the decision device in an FMT system with 64 subchannels equalized with a DFE of the type described section 5.1 operating in the multipath channel shown in Fig. 33 with SNR due to the AWGN equal to 28dB. We can see that the SNR in each subchannel follows the power spectrum shown in Fig. 33. Therefore, the achievable bit rate will be computed on a per subchannel basis, based on the SNR of each of the subchannels and loading algorithms.

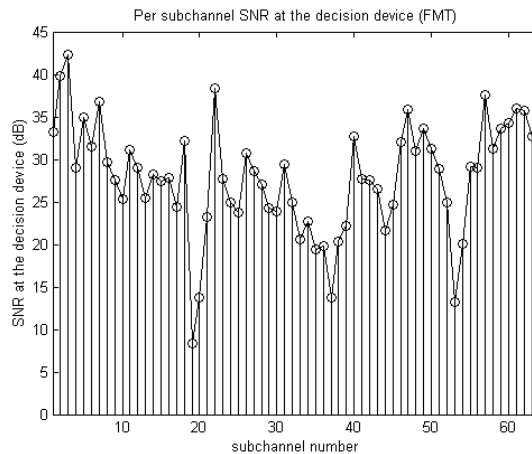


Fig. 34 Per subchannel SNR at the decision device in an FMT system with DFE as in section 5.1 with $M=64$ subcarriers operating in the multipath channel of Fig. 33(b)

5.2.5. Simulation results

We now consider multicarrier systems operating at a frequency of 5.2GHz eg, HIPERLAN/2 [23]. Each of the environments under consideration are characterized by their RMS delay spread and we generate the multipath fading as described in section 2.1:

$$c(t) = \sum_{m=0}^{L-1} \alpha(m) e^{j\phi(m)} \delta(t - \tau_m) \quad (69)$$

As in section 2.1, we assume that the amplitudes of the individual paths, $\alpha(m)$ are Rayleigh distributed and the phases, $\phi(m)$ are uniformly distributed over $[0, 2\pi]$ and L is the number of resolvable paths. We will only consider paths with an amplitude no greater than 30dB down from the strongest path. In the simulations, the time delays $\tau(m)$ are assumed to be uniformly spaced. We also assume a stationary multipath channel with an exponentially decaying power delay profile with RMS delay spreads in the range from 25ns (indoor) to 225ns (low range outdoor). The additive white Gaussian noise (AWGN) $w(n)$ is set to give a SNR equal to 25dB.

In the simulations, we consider OFDM and FMT systems with $M=64$ subcarriers. As in HIPERLAN/2, we assume a sampling rate $M/T=20$ MHz. Monte-Carlo simulations are performed with 100 independent channel realizations for each of the RMS delay spreads considered. In each of these channel realizations, 12800 QPSK symbols are transmitted.

The number of bits assigned to tone i per modulation interval is computed using:

$$b_i = \log_2 \left(1 + 10^{\frac{SNR_i - \Gamma}{10}} \right) \quad (70)$$

where SNR_i (dB) is the signal to noise ratio at the decision device in the i th subchannel. Following [38], we will take the SNR gap Γ_{dB} equal to 6dB. The achievable bit rate is computed as:

$$rate = \left(\sum_{i=used \ tone} b_i \right) \frac{M}{(M + \nu)T} \quad (71)$$

where ν denotes the length of the CP which is set to $3 \cdot \sigma_{RMS} \cdot M/T + 5$ for OFDM and to 0 in FMT. The number of subchannels used in Eq. (71) will be $M=64$ minus the total number of Virtual Carriers (VC). We used 2 VCs for the FMT system and 12 VCs for the OFDM system.

For the FMT prototype filter, the overlap factor of the prototype γ is 10 and the length of the feedforward and feedback filters in the DFE is 15 and 11 respectively. To compute the coefficients of the feedforward and feedback filters or the one tap equalizer (where used) we assume perfect channel estimation.

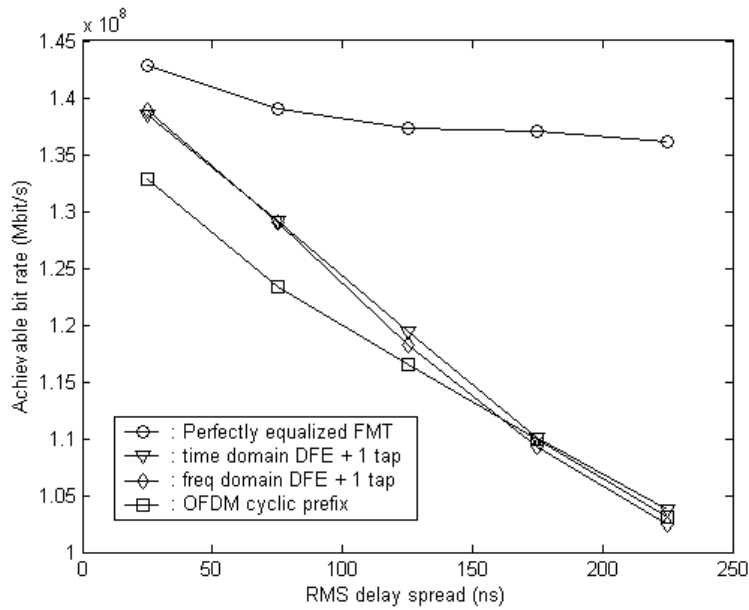


Fig. 35 Achievable bit rates (Mbit/s) for different FMT architectures in a multipath channel with rms in the range [25ns-225ns]

In Fig. 35 we compare 4 different schemes:

- OFDM with cyclic prefix adjusted to suit the RMS delay spread.
- FMT system perfectly equalized.
- FMT system with a fixed frequency domain DFE equalizer and 1 tap equalizer given by the inverse of the channel estimate.
- FMT system with a fixed time domain DFE equalizer and 1 tap equalizer given by the inverse of the channel estimate.

From the results presented in Fig. 35, it can be seen that for low values of channel delay spread, the subchannel response can be considered flat and so the one tap equalizer with a fixed DFE performs well. We can also see that the performance of the FMT system with DFE coefficients calculated as in section 5.1 does not experience a dramatic fall in performance with increasing RMS delay spread since it does not assume subchannel flatness. The improvement relative to that of OFDM is marked since the CP required by OFDM rises with the expected delay spread.

We remember that we have been very conservative and the OFDM system used for the simulations was implemented with a CP length adjusted to suit the specific RMS delay spread of the channel. In real systems, the delay spread cannot be known in advance and so the system is designed for the longest rms delay that will be encountered in its working environment. Therefore, FMT will give better performance compared to OFDM in a more realistic scenario.

5.3. Precoding

Receiver architectures based on a DFE suffer from the following two problems:

- Error propagation as a result of an incorrect decision in the feedback section of the DFE producing additional errors that would not have occurred if the first decision had been correct.
- Coded modulation cannot be applied in a straightforward manner since DFE needs zero delay decisions for the feedback section which is irreconcilable with the basic idea of channel coding.

The second problem can be solved at the expense of receiver complexity, such as using parallel decision feedback decoding (PDFD) which puts the DFE function inside a Viterbi decoder. Due to its complexity, this approach is in conflict with desirable characteristics of wireless devices.

To overcome these problems, precoding at the transmitter using a Tomlinson Harashima Precoder (THP) [43][44] is a practical solution.

This technique is possible only when the transmitter knows the channel response. The idea of the precoding is to move the cancellation of the postcursor ISI to the transmitter, where the past transmitted symbols are known without the possibility of errors. This means that the postcursor ISI impulse response must be known precisely at the transmitter.

In the FMT implementation proposed in section 5.1, precoding can be used [2] although the transmitter needs to know the wireless channel response. This implementation was proposed for VDSL systems where the channel response stays quasi constant for a long period of time and the channel estimate performed at the receiver can be passed to the transmitter to preequalize the signal. However, in wireless communications, the expense of passing this information to the transmitter may not always be practical since the channel can be highly variable in nature. Time Domain Duplex (TDD) is an option for duplexing in wireless systems in place of FDD. In TDD, the forward and reverse channels can be considered almost reciprocal during the time of two consecutive data frames. As a result, the channel information estimated in the reverse link can be used in the precoder at the base station transmitter to pre-equalize the signal transmitted in the forward link.

In the efficient FMT equalization scheme proposed in section 5.2 based on a fixed frequency domain DFE per subchannel, the overall response that we are going to try to equalize is known a priori since it is related only to the low pass prototype filter and not to the channel. Therefore, TH precoding is a good candidate to overcome the two problems just presented and it is straightforward to use. In Fig. 36 we propose how to use THP at the input of each subchannel in combination with the efficient implementation presented in section 5.2:

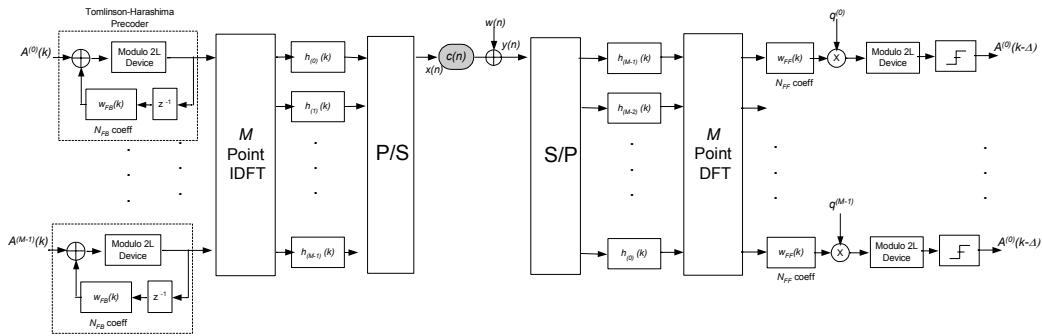


Fig. 36 Proposed FMT system with a fixed DFE equalizer per subchannel in the form of THP for the feedback section in cascade with a complex gain to compensate the amplitude and phase rotation of the multipath channel

In Appendix C we present the THP operation in detail and how it can be extended to get better results in FMT systems.

THP alone does not give any major advantage for of two reasons:

- Although it does not propagate errors, it is more sensitive to errors because of the bounded partition as shown in Appendix C [45][46].
- The PAPR increases and this is a major problem in OFDM. The increase is higher for low order constellations such as QPSK.

To solve the first problem, we can use other THP coding algorithms such as the flipped partition discussed in Appendix C [45][46]. In FMT subchannels with a high SNR, the flipped partition will not bring any advantage because the received symbol is unlikely to fall outside the bounded partition. However, in channels with a low SNR, there will be an improvement using this technique. With FMT operating in multipath channels we always meet the situation where some channels experience a low SNR (see section 5.2.5), hence, the flipped partition appears to be a good solution.

We also note that THP enables us to liberate the receiver of some of the computational complexity requirements of FMT by bringing the feedback section of the equalizer to the transmitter.

Also the combination of trellis coding with TH precoding has been a topic of recent research interest [48][49] and can be easily used with the proposed implementation.

5.4. Adaptive equalizers in FMT

In the previous sections, the equalizer coefficients are computed based on perfect knowledge of the channel. Therefore, prior to the computation of the coefficients using non-recursive equations, a channel estimation needs to be performed.

The approach to be used in this section will not employ explicit channel estimation but will instead use algorithms to adapt the equalizer coefficients based on received training symbols.

First, we will present two basic adaptive algorithms that can be used to adapt the coefficients of the Feedforward and Feedback sections of a DFE equalizer. Since all the coefficients need to be adapted, we have two major drawbacks:

- The convergence time is long and long training sequences will be needed.
- The complexity of the adaptive algorithms is related to the length of the adaptive equalizers which is high in our case.

Therefore, more efficient receiver architectures in terms of convergence time and computational complexity will be proposed.

5.4.1. Adaptive Decision Feedback Equalization

In this section, we will study adaptive DFEs that remove the ISI introduced by the channel and the prototype filter. Using the same configuration presented in section 5.1, all the coefficients in the feedforward and feedback section $\{w_{FF,i}, w_{FB,i}\}$ of the equalizer will need to be trained.

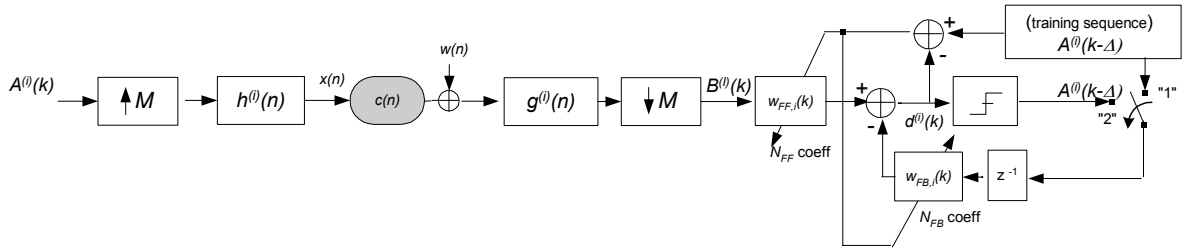


Fig. 37 Equivalent subchannel in FMT with adaptive persubchannel DFE

In Fig. 37 we show how the equivalent subchannel adaptive equalizer will be implemented. At the start of the training phase, the switch is in position “1” and known preamble (training) symbols are fed into the feedback filter. At the end of the training, the switch is moved to position “2”. In the same way, the coefficients of the feedforward and feedback filters are initially adjusted with the help of the training sequence. If we need further adaptation after the training sequence has finished (switch in position “2”), we can continue the adaptation with decision directed training.

The training sequence is the same as the input sequence but with a delay Δ . After some simulations, we have seen that the optimal delay is, in most of the cases, equal to:

$$\Delta = \gamma + N_{FF} - 3 \quad (72)$$

where γ is the delay introduced by the filter bank (equal to the value of the overlap) and N_{FF} is the length of the feedforward filter.

As in section 5.1, it is useful to define two vectors. The data in the tapped delay line:

$$\underline{x}^{(i)}(k) = [B^{(i)}(k), \dots, B^{(i)}(k - N_{FF} + 1), A^{(i)}(k - \Delta - 1), \dots, A^{(i)}(k - \Delta - N_{FB})]^T \quad (73)$$

And the vector $\underline{w}_{i,k}$ with the DFE coefficients of the i -th subchannel as:

$$\underline{w}_{i,k} = \left[w_{FF,i,k}^{* (0)}, \dots, w_{FF,i,k}^{* (N_{FF} - 1)}, -w_{FB,i,k}^{* (1)}, -w_{FB,i,k}^{* (2)}, \dots, -w_{FB,i,k}^{* (N_{FB})} \right]^T \quad (74)$$

where the subscript k denotes the filter coefficients computed at time k .

In this architecture, as in section 5.1, we will have a different set of coefficients for each of the subchannels and therefore, a different computation has to be performed.

Coefficient adjustment uses either the the least-mean squares (LMS) or recursive-least-squares (RLS) algorithm. The RLS algorithm converges faster than the LMS, although it has higher computational complexity and is sensitive to quantization errors [42]. We will now show how to use them from the point of view of our architecture.

In the following formulas describing the two algorithms, the subchannel index i is omitted for compactness.

The LMS algorithm

In Appendix B we have derived the Wiener-Hopf linear equations that give the solution of the DFE filter coefficients to minimize:

$$E\{|e(k)|^2\} = E\{|A(k - \Delta) - y(k)|^2\} \quad (75)$$

where $y(k)$ is the output of the DFE filter before the slicer.

For those equations, we needed the statistics of the channel and therefore, its definition. To do this, we first estimate the channel and then, in a non recursive fashion, we compute the optimal coefficients \underline{w}_0 of the filter as.

$$\begin{aligned} \underline{R}_{xx} \underline{w}_0 &= \underline{p} \\ \underline{w}_0 &= \underline{R}_{xx}^{-1} \underline{p} \end{aligned} \quad (76)$$

Where \underline{w}_0 is a vector containing the feedforward and feedback equalizer defined in Eq.(74). We note that in Eq (76) we need to compute the inverse of a large matrix to find the optimum coefficients. A simple method that avoids the inversion is to use the steepest descent [42] based on the surface defined by the mean square error in Eq. (75). However, for the steepest descent, we need the value of the gradient of the surface and the gradient depends on \underline{R}_{xx} and \underline{p} , which are unknown. To overcome this problem, estimates of the gradient vector are used instead of the true values. This is the basis of the LMS algorithm.

After some manipulation, the recursive LMS algorithm to update the filter coefficients is defined as [42]:

DFE filter output before the slicer	$y(k) = \underline{w}_k^H \underline{x}(k)$
Error signal:	$e(k) = A^{(i)}(k - \Delta) - \underline{w}_k^H \underline{x}(k)$
Tap weight adaptation	$\underline{w}_{k+1} = \underline{w}_k + \mu \underline{x}(k) e^*(k)$

It is common to start the iterative process with the initial guess $\underline{w}_{i,0} = (0)$

The step-size parameter is chosen as:

$$0 < \mu < \frac{2}{(N_{FF} + N_{FB})S_{\max}} \quad (77)$$

where S_{\max} is the maximum value of the power spectral density of the tap input $x(k)$.

The convergence time is affected by the eigenvalue ratio of the correlation matrix of the input data to the DFE. The larger the eigenvalue ratio, the slower the convergence.

Although the computational complexity of the LMS algorithm is not high, the convergence in terms of the number of training symbols is approximately 20 times the number of coefficients in the DFE filter ($N_{FF} + N_{FB}$). If we consider that we have a different DFE for each of the subchannels, this algorithm with the architecture presented is not appropriate for the wireless applications for which we would have to adapt the algorithm continuously.

The RLS algorithm

The RLS algorithm overcomes some practical limitations of the LMS filter by providing a faster rate of convergence that is insensitive to variations in the eigenvalue spread of the correlation matrix of the input signal. The price paid for these improvements is increased computational complexity.

Instead of minimizing the MMSE, the cost function that the RLS algorithm will minimize is:

$$\zeta(k) = \sum_{m=1}^k \lambda^{k-m} |e(m)|^2, \quad (78)$$

where $e(m)$ is the difference between the training sequence $A^{(i)}(m-\Delta)$ and the output $d^{(i)}(m)$ produced by the adaptive filter with coefficients \underline{w}_k where subscript k denotes the coefficients computed at iteration time k :

$$e(m) = A^{(i)}(m - \Delta) - \underline{w}_k^H \underline{x}(m) \quad (79)$$

We note that the tap weight vector computed at time k , \underline{w}_k , is constant for the whole summation in Eq. (78) and it is the one computed at time k . In Eq. (78) λ is a positive constant close to, but less than, unity. When $\lambda=1$, we have the ordinary method of least squares. The inverse $1-\lambda$ is a measure of the memory of the algorithm. The special case $\lambda=1$ corresponds to infinite memory.

Using the Matrix Inversion Lemma and some other techniques, the coefficients that minimize the cost function can be computed using the following algorithm [42]:

Initialization:

$$\begin{aligned} \underline{w}_{i,0} &= \underline{0} \\ \underline{P}(0) &= \delta^{-1} \underline{I} \end{aligned} \quad (80)$$

with δ a small positive constant for high SNR and large positive constant for low SNR.

For each time instant $k=1,2,\dots$ compute

$$\begin{aligned}
 \underline{\Pi}(k) &= \underline{P}(k-1)\underline{x}(k) \\
 \underline{K}(k) &= \frac{\underline{\Pi}(k)}{\lambda - \underline{x}^H(k)\underline{\Pi}(k)} \\
 \xi(k) &= A^{(i)}(k-\Delta) - \underline{w}_{i,k-1}^H \underline{x}(k) \\
 \underline{w}_{i,k} &= \underline{w}_{i,k-1} + \underline{K}(k)\xi^*(k) \\
 \underline{P}(k) &= \lambda^{-1} \underline{P}(k-1) - \lambda^{-1} \underline{K}(k)\underline{x}^H(k)\underline{P}(k-1)
 \end{aligned} \tag{81}$$

we can see, $\xi(k)$ as a tentative value of $e(k)$ before updating the DFE coefficients.

Note that the equalizer coefficients change with time by an amount equal to the error $\xi(k)$ multiplied by a Kalman gain vector $\underline{K}(k)$. Since $\underline{K}(k)$ has $N_{FF}+N_{FB}$ elements, each tap coefficient is controlled by one of the elements of $\underline{K}(k)$. This results in rapid convergence. In contrast, the LMS algorithm has only one variable (μ) for all the coefficients. The other factor which allows the RLS algorithm to converge much more quickly than LMS is that RLS uses a deterministic (non-statistical) error criterion. This means that it is no longer necessary to use a small step size to average-out the random data fluctuations (as with LMS).

The convergence time of the RLS algorithm is approximately $3(N_{FF}+N_{FB})$. Although this can be considered fast compared with other adaptive equalization algorithms, considering that we have M subchannels (M usually higher than 64), we still need a high number of training symbols before the algorithm converges. Moreover, the wireless channel is changing, therefore, we would need to train the equalizer for every new data burst sent.

The disadvantage is that RLS requires many more calculations, approximately $O((N_{FF}+N_{FB})^2)$ per sample and in FMT, the length of the feedforward and feedback is usually higher than the overlap γ . However, there are now a number of Fast RLS algorithms with $O(N_{FF}+N_{FB})$, for example ‘‘Fast Kalman’’, ‘‘FAEST’’ and ‘‘FTF’’ [42] with a computational complexity around $10(N_{FF}+N_{FB})$ multiplications per sample.

Summary-adaptive DFEs

An architecture based on the adaptive algorithm is shown in Fig. 38

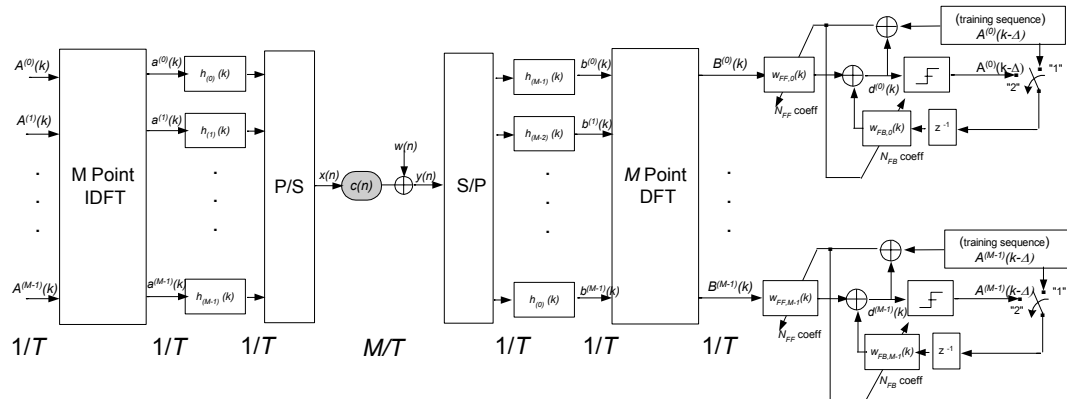


Fig. 38 FMT with adaptive per subchannel equalization

There are four major drawbacks in the implementation shown in Fig. 38:

- We need a long training sequence for equalizer convergence.
- The computational complexity is very high because it depends on the total number of coefficients in the DFE filter (usually high). In RLS, it grows much faster than in LMS
- If we want to use THP for the feedback section of the DFE, the receiver needs to know the feedback coefficients. Therefore, a reverse link is needed.
- As discussed in section 5.3, coding is in conflict with the DFE idea (for the case where we do not use THP).

5.4.2. Simulation results

In Fig. 39 and 40, we investigate the convergence of the RLS algorithm as a function of different length DFEs when used with the architecture of Fig. 38. The simulation environment is the one defined previously in section 5.2.5.

We see that although the convergence rate of the RLS is high, we still need a large number of training symbols. In addition, this training sequence needs to be applied to each of the subchannels M .

After some simulations, we have seen that increasing the number of DFE coefficients does not bring any clear improvement and the convergence time and computational complexity both increase.

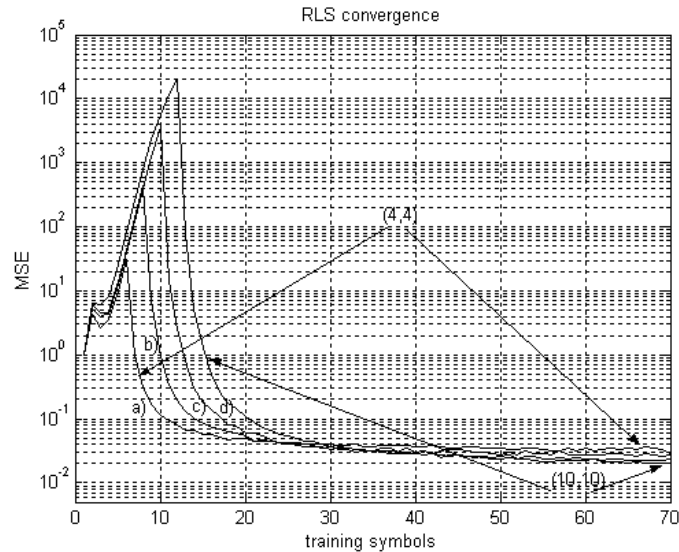


Fig. 39 Convergence rate (MSE of the tentative error in the RLS algorithm) for exponentially power decay Rayleigh channel, rms delay spread=60ns, $\gamma=10$, $\text{SNR}_{\text{channel}}=25\text{dB}$, $M=64$, sampling rate $M/T=50\text{ns}$, DFE equalizer with (N_{FF}, N_{FB}) : a) (4,4), b) (6,6), c) (8,8), d) (10,10)

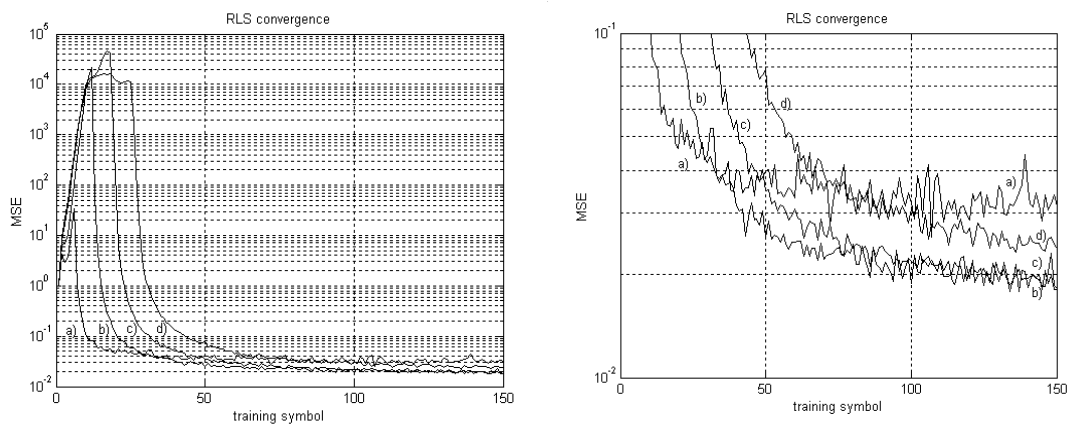


Fig. 40 Convergence rate (MSE of the tentative error in the RLS algorithm) for exponentially power decay Rayleigh channel, rms delay spread=60ns, $\gamma=10$, $\text{SNR}_{\text{channel}}=25\text{dB}$, $M=64$, sampling rate $M/T=50\text{ns}$, DFE equalizer with (N_{FF}, N_{FB}) : a) (4,4), b) (10,10), c) (16,16), d) (22,22)

Since we need to apply the algorithm to each of the subchannels, the total complexity and the number of training symbols is too high to be used in wireless channels which are variable in nature.

Similarly to the results presented in section 5.2.5, in Fig. 41 we compare the achievable bit rate of:

- OFDM with a cyclic prefix adjusted to suit to the RMS delay spread.
- FMT system perfectly equalized based on a perfect channel estimate with $(N_{FF}, N_{FB})=(10,10)$.
- FMT system with a fixed frequency domain DFE equalizer $(N_{FF}, N_{FB})=(10,10)$ and 1 tap equalizer given by the inverse of a perfect channel estimate.
- FMT system with $(N_{FF}, N_{FB})=(10,10)$ using the RLS algorithm to adapt the DFE equalizer coefficients.

In all the cases, the overlap γ is equal to 10.

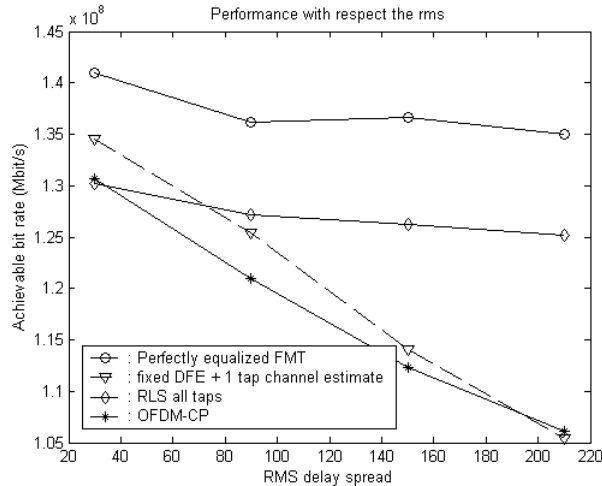


Fig. 41 Achievable bit rate for exponentially power decay Rayleigh channel, $\gamma=10$, $\text{SNR}_{\text{channel}}=25\text{dB}$, $M=64$, sampling rate $T/M=50\text{ns}$, 100 training symbols, DFE equalizer with $(N_{FF}, N_{FB})=(10,10)$

From Fig. 41 we can see that there is a gap between the achievable bit rate with the optimal coefficients (perfectly equalized FMT) and the ones trained with the RLS algorithm. Therefore, in addition to having a high computational complexity and a long convergence time, the equalizer coefficients are far from converging to the optimal value.

5.4.3. Proposed simplified adaptive algorithms

To simplify the receiver and the total amount of training symbols, we can take a similar approach to that employed in section 5.2.1 in which the equalization process is undertaken in two parts:

- A fixed DFE that compensates the ISI introduced by the prototype filter
- A complex gain based on a channel estimate that compensates the channel gain/phase rotation introduced by the dispersive channel as in OFDM systems.

In our solution instead of using a complex gain based on a channel estimate, we propose to make this gain adaptive by using one of the adaptive algorithms proposed in the previous section.

The problem with the adaptive DFEs investigated in the previous section is that they need long training sequences to converge because of the large number of filter coefficients. In our new proposal, the filter has only one tap therefore, convergence can be obtained with a very short training sequence. In addition, the computational complexity during the training process is proportional to the length of the filter which is also short.

In section 5.2.5, we showed via simulations that the assumption of flat fading for the subchannels did not hold for channels with a high RMS delay spread.

We remind ourselves here that one of the major advantages of FMT modulation over conventional OFDM modulation is that FMT does not need the use of the CP. This improvement will be greater in long delay spread situations where OFDM will require longer CPs. However, the one tap solution can only deal with a short delay spread.

In Fig. 42 we show the 20MHz frequency response of two channels with two different RMS delay spreads: 27ns and 200ns. We could consider the 27ns delay spread to model an indoor environment and the 200ns delay spread to model a short range outdoor environment. When using 64 subchannels with a delay spread of 27ns we can consider that the frequency response is flat for each subchannel. However, this assumption does not hold for the RMS delay spread of 200ns as shown in Fig. 42(b).

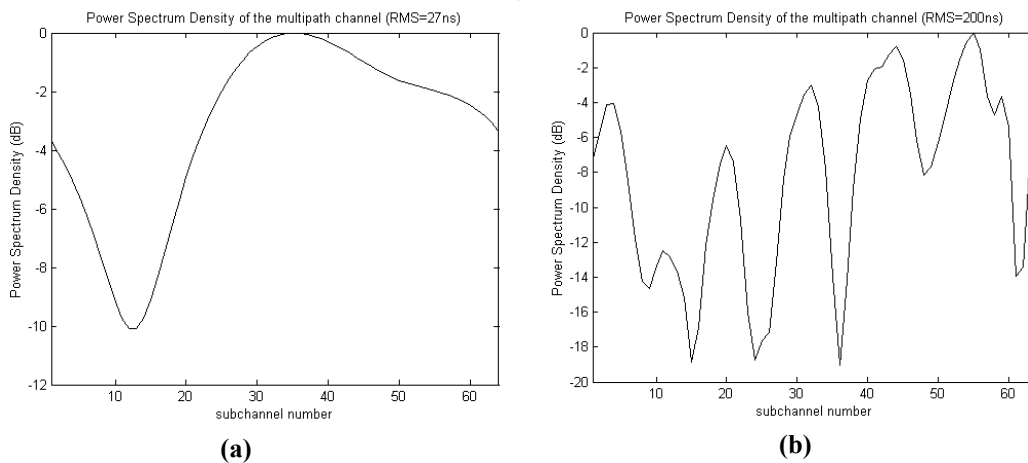


Fig. 42 Frequency response of two single realizations of a Rayleigh exponential power decay channel in a HIPERLAN/2 system with 64 subchannels (a) RMS delay spread equal to 27ns (b) RMS delay spread equal to 200 ns

5.4.4. Further improvement in outdoor environments

To improve the performance of our proposed 2 stage equalisation process, we can go one step further and instead of using 1 tap per subchannel, we can use a transversal adaptive filter with 1, 2, 3, ... Q taps, depending up on the coherence bandwidth of the channel. For moderately high delay spreads compared to the sampling rate, we still can assume that the frequency response of the channel will not vary much across the subchannel. Therefore, the size of the Q tap adaptive equalizer can be kept low (eg, 1, 2, 3 or 4 taps) thus minimising the complexity and the convergence time.

Based on the results, we will give some guidance for the number of coefficients that we need in the transversal filter depending up on the coherence bandwidth and subchannel separation.

Since the number of coefficients in the adaptive filter is going to be low, we can consider the use of the RLS algorithm to train the filter which has a complexity proportional to the square of its length.

The equivalent subchannel response will be the one shown in Fig. 43

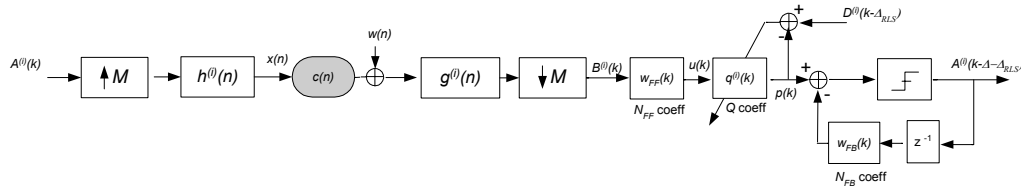


Fig. 43. Proposed FMT equalization with a fixed frequency domain DFE and an adaptive transversal equalizer with RLS update.

The cost function that the recursive algorithm will minimize is:

$$\zeta(k) = \sum_{m=1}^k \lambda^{k-m} |e(m)|^2, \quad (82)$$

where in this scheme, $e(m)$ is the difference between the training sequence $D^{(i)}(m-\Delta_{RLS})$ and the output $p(m)$ produced by the adaptive filter with coefficients $q^{(i)}(k)$ calculated at time k .

The training sequence $D^{(i)}(k)$ shown in Fig. 43 is computed as follows:

$$D^{(i)}(k) = w_{FF}(k) \otimes \left(\left(g^{(i)}(n) \otimes h^{(i)}(n) \right)_{\downarrow M} \right) \otimes A^{(i)}(k) \quad (83)$$

where $A^{(i)}(k)$ are the known training symbols and \otimes indicates convolution.

It is important to note that the adaptive filter must be placed after the feedforward filter. We remember that the feedforward removes the ISI due to precursors of the response of the filter bank. If we placed the adaptive filter before the feedforward filter, the ISI of the precursor of the first data symbols after the training sequence would affect the training algorithm and these symbols are unknown at the receiver.

In the case that the overlap value of the prototype is not sufficient so that ICI or the SNR due to AWGN cannot be neglected, the ICI from adjacent channels should be considered for as part of the training sequence. In this case, during training we should consider not just the per subchannel equivalent given in Fig. 43 but the whole filter bank implementation. However, when simulated in our system, no significant difference in the results was observed.

It is known that when using adaptive transversal equalizers to adapt to signals in which we do not have any previous knowledge about the response, the best performance is achieved by selecting a delay introduced by the adaptive equalizer filter Δ_{RLS} that matches the midpoint of the transversal equalizer [42]. Therefore, the overall delay will be the delay used when we compute the fixed DFE equalizer Δ , plus the delay of the adaptive equalizer Δ_{RLS} .

It is also important to note that with this implementation, the use of THP is straightforward since the feedback section is known in advance. If we use THP, the adaptive filter to compensate the effects of the multipath channel needs to be placed

before the modulo $2L$ operator. All the discussions in section 5.3 about precoding extensions are applicable to this implementation. This implementation with THP is shown in proposed in Fig. 44.

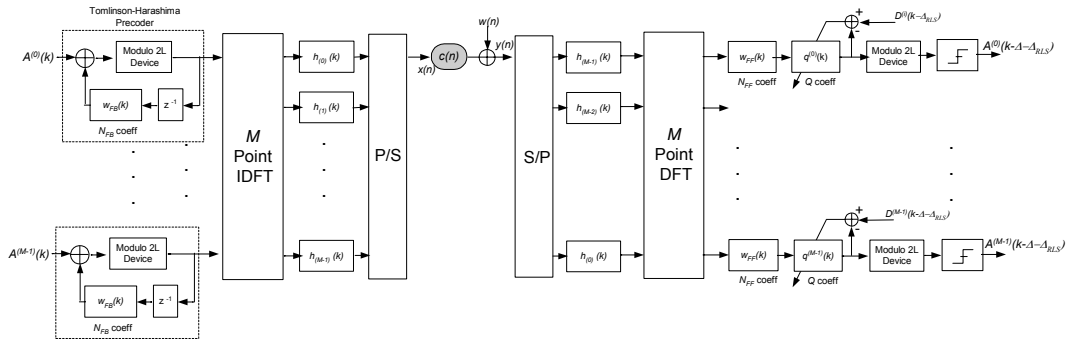


Fig. 44 Proposed FMT system with a fixed DFE equalization per subchannel in the form of THP for the feedback section in cascade with an adaptive equalizer to compensate the channel response

5.4.5. Simulation results

We consider the multicarrier systems operating at a frequency of 5.2GHz as in HIPERLAN/2 with the same conditions and parameters as used previously in section 5.2.5.

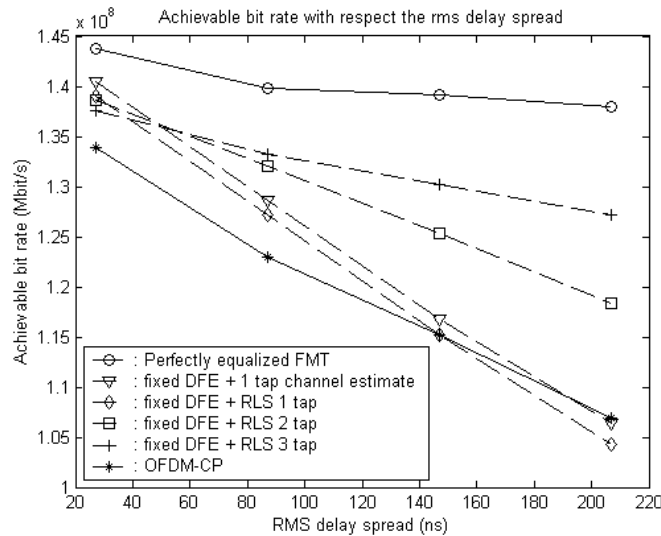


Fig. 45 Achievable bit rates (Mbit/s) for different FMT architectures in a multipath channel with rms in the range [27ns-210ns], $M=64$, $\gamma=10$, $(N_{FF}, N_{FB})=(18,18)$, $\text{SNR}_{\text{channel}}=25\text{dB}$

In Fig. 45 we compare 6 different FMT schemes:

- OFDM with a cyclic prefix adjusted to suit to the RMS delay spread.
- FMT system perfectly equalized based on ideal channel estimation.
- FMT system with a fixed DFE equalizer and 1 tap equalizer given by the inverse of the ideal channel estimate.
- 3 different FMT systems with a fixed DFE and a transversal filter with 1,2 or 3 taps trained with the RLS algorithm.

We see that for short RMS delay spread values, to use more taps (i.e. 2 or 3) in the adaptive filter does not bring any improvement and as we discussed in section 5.4, the use of more taps will require more training symbols and higher computational complexity. However, as the delay spread increases, it is worthwhile to use more taps and we see that the difference in the achievable bit rate between the FMT receiver with $Q=1$ and $Q=3$ taps is considerable.

As in section 5.2.5, we remember that we have been very conservative and the OFDM system used for the simulations was implemented with a CP length suited to the specific rms delay spread of the channel. In real systems, the delay spread cannot be known in advance and the system is designed for the longest rms delay that can be encountered in the intended environments. Therefore, FMT will give better performance compared to OFDM in a more realistic scenario.

5.4.6. Conclusions about the proposed scheme

We have seen that adaptive equalizers are an alternative and effective solution to equalization for FMT. However, the option of using a general adaptive filter as described in section 5.4.1 entails the use of a long training sequence and the computational complexity is very high. We have proposed a solution, similar to the one in section 5.2.1, in which we split the equalizer into a cascade of two filters: a fixed DFE to compensate the effect of the prototype and a short adaptive transversal equalizer to compensate the effect of the subchannel.

One of the main advantages of FMT modulation over conventional OFDM modulation is that FMT does not need the use of the CP. This improvement will be higher in outdoor environments where longer CPs are needed since channels have longer delay spreads. Therefore, it is interesting to find FMT architectures that can deal with long delay spread and still have a reduced computational complexity. Previous efficient equalization schemes [38] assume subchannel flatness to design an efficient receiver architecture that performs well in indoor environments. In this section, we have proposed an efficient receiver architecture that can deal with longer delay spread. This architecture is based on

- A fixed DFE that compensates the ISI introduced by the prototype filter where the feedback section of the equalizer can be taken to the transmitter in the form of a Tomlinson Harashima precoder. We have presented the advantages and disadvantages of using the Tomlinson Harashima precoder since this is an option (though not necessary) for our architecture.
- An adaptive transversal filter with a number of coefficients $Q=1, 2, 3, \dots$ that compensates for the effect of the channel. The advantage of using the RLS algorithm to initialise the adaptive filter is that the convergence time in terms of the number of training symbols is short compared to other adaptive algorithms as LMS and the complexity is proportional to Q^2 (also low).

The results have been shown in terms of achievable bit rates for the FMT architectures proposed and OFDM with CP using parameters similar to ones representative of the HIPERLAN/2 standard. It has been shown that our proposed receiver architecture is suitable for short range outdoor environments where delay spreads of up to 210ns are encountered.

We have seen that Tomlinson Harashima precoding with this implementation is straightforward to use since the feedback section of the DFE is known in advance because it is based on the prototype. As we discussed in the section 5.3, THP has the disadvantage of increasing the PAPR. Among the main advantages of THP are the elimination of error propagation and the possibility of combining it with channel coding (for example trellis coding). Some partition extensions can also be applied which will improve the performance in the subchannels with a low SNR.

Chapter 6. Conclusions, future improvements and usage

In this thesis, we have presented the theory of FMT modulation and detailed its limitations and advantages when used in wireless environments. We have seen, that at the expense of higher computational complexity we obtain a higher spectral efficiency than conventional OFDM.

The reason to introduce this modulation technique is to solve some of the problems that arise from classic multicarrier systems which employ overlapping subchannel spectra. Fortunately, in addition to solving these problems, FMT still benefits from the robustness inherent in multicarrier communications in the presence of ISI.

In contrast to other filter bank multicarrier systems such as DWMT in which the filter bank design is based on the PR condition, in FMT this constraint is relaxed to solve other problems caused by overlapping subchannel spectra. However this now forces the use of per-subchannel equalization at the receiver to overcome the induced ISI.

In section 4 we have introduced an efficient filter bank implementation and the low pass prototype filter. In this section we have identified two parameters for its design and have proposed known filter design techniques that give good results. We expect that other design techniques based on other constraints will arise as the FMT technique becomes more mature.

An important issue in FMT is the per-subchannel equalization process presented in section 5 which is required to remove the ISI remaining in the subchannel owing to the perfect reconstruction violation. Although the equalization schemes proposed in two previous FMT publications give good results they result in high computational complexity or poor performance in certain scenarios. In this thesis, we have presented and investigated the performance of some efficient (in terms of computational complexity) equalization schemes that give good trade-offs in terms of performance and complexity.

We have also shown how precoding can be used with the proposed equalization techniques and we have also presented some precoding extensions that are straightforward to use with FMT.

However, the major disadvantages encountered in FMT are:

- High complexity owing to the filter bank and equalization.
- High delay between transmission and reception. This delay will seriously limit any performance advantages from schemes which rely on rapid feedback between the transmitter and receiver, for example fast closed loop power control or loading algorithms.
- High peak to average power ratio although this problem is common to all multicarrier techniques.

Limitations of the research and future improvements

Since FMT is a new modulation scheme (only 5 publications concerning FMT in journals or conferences), the aim of the research conducted here is to present an overview of the technique and to present results and proposals concerning the complexity performance trade-offs available.

Future work will also study, in a quantitative fashion, the effects of real impairments, such as timing and frequency offsets and the resulting interference between subcarriers. We expect that these impairments will be easier to solve owing to the non overlapping spectrum of the subcarriers. However, since the CP is not used, different solutions to conventional OFDM will be needed.

Another possible area of research is that of multiple access. Multiple Access Filtered Multitone (MA-FMT) in the uplink is potentially attractive for future wireless access. The interesting thing about FMT is that since the ICI is negligible, it is a good option for spectrum management in which we assign different subcarriers to different users. In this way, we can allocate different users in different subchannels without need for frame synchronization among different users. In conventional OFDM, it is not possible to work asynchronously in the uplink due to the power leaking from each subcarrier into the others. In conventional MA-OFDM, windowing is necessary in order to reduce the power that leaks from some user bands into others.

Due to the good spectral characteristics, we think that FMT is a good proposal for:

- Multiple access in indoor environments such as wireless LAN (Wi-LAN).
- Broadband Fixed Wireless Access (BFWA) in which there is a long delay spread and the need for a long CP results in a loss of efficiency in conventional OFDM. In addition, since the transmitter and receiver are not mobile, the multipath channel is more static than other wireless systems (eg, mobile phone networks), therefore training sequences to initialize the equalizer do not need to be sent as often.

References

- [1] G. Cherubini, E. Eleftheriou, and S. Olcer, "Filtered Multitone modulation for VDSL," in Proc. IEEE Globecom'99, Rio de Janeiro, Brazil, Dec 1999, pp. 1139-1144.
- [2] G. Cherubini, E. Eleftheriou, S. Olcer and J.M. Cioffi, "Filter Bank Modulation techniques for very high speed digital subscriber lines," IEEE Communications Magazine, vol. 38, pp. 98-104, May 2000.
- [3] J.G. Proakis, Digital Communication, McGraw-Hill, 1995.
- [4] R.W. Chang, "High Speed Multichannel data Transmission with Bandlimited Orthogonal Signals", bell System Technology Journal, Vol. 45, pp. 1745-1796, 1966.
- [5] B.R. Saltzberg, "Performance of an Efficient Parallel Data Transmission Systems", IEEE Transactions of Communication Technology, Vol. 15, No. 6, pp. 805-811, Dec. 1967.
- [6] B. Hirosaki, "An Orthogonal Multiplexed QAM System Using the Discrete Fourier Transform", IEEE Transactions on Communications, vol. COM-29, No. 7, July 1981.
- [7] R. Van Nee, R. Prasad, OFDM for Wireless Multimedia Communications, Artech House Publishers, 2000.
- [8] John A.C. Bingham, "Multicarrier Modulation for Data Transmission: An idea whose time has come," IEEE Communications Magazine, pp. 22.12-11.17, June 1972.
- [9] IBM et al., "CAP/QAM, DMT and filter bank modulation techniques for VDSL", Contribution D.649, ITU-T Study Group 15, Geneva, Switzerland, June 21-July 2, 1999.
- [10] J. Aris, "Comparative RF Indoor channel soundings at 2,5 and 17GHz," Wireless Personal Communications, vol. 3, no. 4, pp. 353-363, 1996.
- [11] Nobles, P., and F. Halsall, "Delay Spread and Received Power Measurements within a Building at 2GHz, 5GHz, and 17GHz", IEE Tenth International Conference on Antennas and Propagation, Edinburgh, UK, April 14-17, 1997.
- [12] Hafesi, P., D. Wedge, M. Beach, M. Lawton, "Propagation Measurements at 5.2 GHz in Commercial and Domestic Environments," IEEE PIMRC'97, Helsinki, pp. 509-513, Sept. 1-4, 1997.
- [13] G. Janssen, P. Stigter, and R. Prasad, "Wideband indoor channel measurements and BER analysis of frequency selective multipath channels," IEEE Trans. Communications, vol. 44, pp. 1272-1287, October 1996.
- [14] V. Erceg, K. Hari, et al., "Channel models for fixed wireless applications", tech. Rep., IEEE 802.16 Broadband Wireless Access Working Group, January 2001.
- [15] Chayat, N., "Tentative Criteria for Comparison of Modulation Methods", IEEE P802.11-97/96.
- [16] Pahlavan, K. Allan Levesque, Wireless Information Networks, Wiley-Interscience; New York: J. Wiley & Sons, 1995.
- [17] A. Saleh and R. Valenzuela, "A statistical model for indoor multipath propagation," IEEE J. Select. Areas Commun., vol. 5, pp. 128-137, February 1987.
- [18] Weinstein, S.B., and P.M. Ebert, "Data Transmission by Frequency Division Multiplexing Using the Discrete Fourier Transform," IEEE Trans. Comm., Vol. COM-19, pp. 628-634, Oct. 1971.
- [19] S.D. Sandberg, and M.A. Tzannes, "Overlapped discrete multitone modulation for high speed copper wire communications," IEEE J. Select. Areas Commun., vol. 13, pp. 1571-1585, Dec. 1995.
- [20] Muller, S.H. and Huber, J.B. "OFDM with Reduced Peak to Average Power Ratio by Optimum Combination of Partial Transmit Sequences", IEE Electronics Letters, Vol. 33, No. 5, pp 368-369, February 1997.
- [21] P.P. Vaidyanathan, "Filter Banks in Digital Communications". IEEE Circuits and Systems Magazine, vol. 1, no. 2, second quarter 2001.
- [22] John A.C. Bingham, "ADSL, VDSL and Multicarrier Modulation," Wiley Series in Telecommunications and Signal Processing, 2000.
- [23] "Broadband Radio Access Networks (BRAN); HIPERLAN 2; Physical (PHY) Layer," ETSI TS 101 475 V1.1.1. (2001-12).
- [24] Zou, W. and Wu.Y (1995), "COFDM: An Overview", IEEE transactions on broadcasting, vol. 41, No 1, March, pp 1-8.
- [25] M. Faulkner and S. He, "The effect of filtering on the performance of OFDM systems" Proc. ACTS'98 Summit, Rhodes (Greece): 817-822, June 1998.
- [26] ETSI, "Radio Broadcasting Systems: Digital Audio Broadcasting to Mobile, Portable and Fixed Receivers," European Telecommunication Standard, ETS 300-401, Feb. 1995.

- [27] ETSI, "Digital Video Broadcasting: Framing Structure, Channel Coding, and Modulation for Digital Terrestrial Television," European Telecommunication Standard, EN 300-744, Aug. 1997.
- [28] R.G. Gallager, "Information Theory and Reliable Communications," Wiley, New York, 1968.
- [29] P.S. Chow, J.M. Cioffi, J.A.C. Bingham, "A Practical Discrete Multitone Transceiver Loading algorithm for Data Transmission over spectrally shaped channels", IEEE Trans. On Comm., Vol. 43, N.2, April 1995, pp 773-775.
- [30] A. Leke, J.M. Cioffi, "A Maximum Rate Loading Algorithm for Discrete Multitone Modulation System", IEEE Proc. of Globecom'96, London, England, November 1997, vol. 3, pp 1514-1518.
- [31] T. Keller, L. Hanzo, "Adaptive Multicarrier Modulation: A Convenient Framework for Time-Frequency Processing in Wireless Communications", Proceedings of the IEEE, Vol. 88, No. 5, May 2000.
- [32] R. Hasholzner, C. Drewes, J.S. Hammerschmidt, "The effects of phase noise on 26Mb/s OFDMA broadband radio in the local loop systems", in Proc Int. Zurich Seminar on Broadband Communications (IZS'98).
- [33] C. Muschallik, "Influence of RF Oscillators on an OFDM signal," IEEE Transactions on Consumer Electronics, vol. 41, no. 3, pp. 592-03, Aug. 1995.
- [34] P.P. Vaidyanathan, Multirate systems and filter banks, Englewood Cliffs, Prentice Hall, 1993.
- [35] H.S. Malvar, Signal Processing with Lapped Transforms, Artech House, Boston 1992.
- [36] Editors: A.N. Akansu, M.J. Medley, Wavelet, Subband and Block Transforms in Communications and Multimedia, Kluwer Academic Publishers, Boston, 1999.
- [37] A.V. Oppenheim and R.W. Schaffer and J.R. Buck, Discrete Time Signal Processing, second edition, Prentice-Hall, Inc. Upper Saddle River, NJ, 1999.
- [38] N. Benvenuto, S. Tomasin, L. Tomba "Receiver Architectures for FMT Broadband Wireless systems," IEEE 53rd VTC Spring, Rhodes Island (Greece), vol. 1, pp. 643-647, May 2001.
- [39] T.W. Parks and J.H. McClellan, "Chebyshev approximation for nonrecursive digital filters with linear phase", IEEE Trans. On Circuit Theory, 19: 189-94, March 1972.
- [40] N. Al Dhahir and J.M. Cioffi, "MMSE Decision Feedback Equalizers: Finite-Length Results," IEEE Transactions on Information Theory, vol. 41, pp. 961-975, July 1995.
- [41] J.M. Cioffi, G.P. Dudevoir, M.V. Eyuboglu and G.D. Forney, Jr., "MMSE Decision Feedback Equalizers and Coding-Part I: Equalization Results," IEEE Transactions on Communications, vol. 43, pp. 2582-2594, October 1995.
- [42] S Haykin, Adaptive Filter Theory, Prentice Hall, Fourth Edition, 2002.
- [43] M. Tomlinson, "New automatic equalizer employing modulo arithmetic", Electron. Lett., vol. 7, pp. 138-139, 1971
- [44] H. Harashima, H. Miyakawa, "Matched transmission technique for channels with intersymbol interference" IEEE Trans. Commun., vol. 20, pp. 774-780, 1972
- [45] Y.L. Chan and W. Zhuang, "Modified TH-precoding with constant amplitude for indoor wireless system using QPSK", in Vehicular Tech. Conf. (VTC'96), pp. 810-814, IEEE, 1996
- [46] Y.L. Chan and W. Zhuang, "Channel precoding for indoor radio communications using dimension partitioning", IEEE Trans. Communications, vol. 45, pp. 334-343, March 1997.
- [47] L.F. Wei, "Generalized square and hexagonal constellations for intersymbol interference channels with generalized Tomlinson Harashima precoders", IEEE Trans. Communications, vol. 42, pp. 2713-2721, September 1994.
- [48] A.K. Aman, R.L. Cupo, and N.A. Zervos, "Combined trellis coding and DFE through Tomlinson precoding," IEEE J. Select. Areas Commun., vol. 9, pp. 876-884, Aug. 1991.
- [49] M.V. Eyuboglu and G.D. Forney Jr., "Trellis precoding: combined coding, precoding and shaping for intersymbol interference channels," IEEE Trans. Inform. Theory, vol. 38, pp. 301-314, Mar. 1992.
- [50] E. A. Lee and D.G. Messerschmitt, "Digital Communication", Second edition.
- [51] R.D. Wesel, J.M. Cioffi, "Precoding and the MMSE-DFE", Proceedings of the 28th Asilomar Conference on Signals, Systems & Computers, 1995.
- [52] N. Benvenuto, S. Tomasin and L. Tomba, "Equalization methods in OFDM and FMT Systems for Broadband Communications," IEEE Trans. On Communications (to appear).

Appendix A: The Multipath Channel

When a communications signal is transmitted, the signal reaches the receiver not only via a direct line of sight (LOS) path but also via other paths, which are caused by reflection, diffraction and scattering. These phenomena are explained below:

- **Reflection** occurs when an electromagnetic wave encounters a smooth and large (compared to the wavelength of the signal) surface. The wave is then reflected from the surface.
- **Diffraction** occurs when a radio wave encounters a dense obstacle also with large dimensions compared to the propagated wavelength. As a result, secondary waves are formed behind the obstructing element making reception possible even if there is no direct LOS between the transmitter and the receiver.
- **Scattering** occurs when a propagated wave encounters an obstacle whose dimensions are comparable to its wavelength. In such a case, the energy is spread out (scattered) in all directions.

Therefore, the transmitted signal, which experiences the influence of reflection, refraction and scattering, reaches the receiver via many different paths. This phenomenon is called multipath propagation. Each replica of the signal arriving at the receiver has traveled over a different distance and thus has suffered from different amplitude attenuation, phase shift, and arrives with a different time delay. The receiver collects a superposition of all multipath signals, which can lead to signal reinforcement or to signal cancellation giving rise to the term multipath fading.

A multipath channel model can represent all these distortions. This channel model is then used to simulate the distortions encountered in similar wireless environments. The multipath channel model can be modeled as a linear filter with additive white Gaussian noise, as depicted in Fig. A.1. The channel is then fully described by its time variant impulse response $c(t, \tau)$ (where τ indicates the delay and t the time variation of the function) and the noise statistics. The impulse response of the physical linear dispersive fading channel is expressed as the sum of a (possibly infinite) number L of delayed Dirac pulses (delays $\tau_l(t)$) with time varying complex path weights $\alpha_l(t)e^{j\phi_l(t)}$.

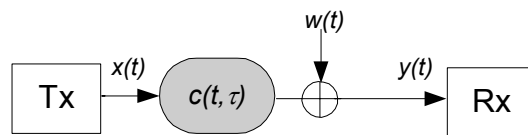


Fig. A.1 The channel model

$$c(t, \tau) = \sum_{l=0}^{L-1} \alpha_l(t) e^{j\phi_l(t)} \delta(t - \tau_l(t)) \quad (\text{A.1})$$

Normally, the delay of the first (shortest) ray is defined as $\tau_0 = 0$, since the absolute delay-times are not important.

Time variation of the channel is measured by the Doppler broadening and the Doppler shift of a spectral line. If we input to the channel a spectral line, we will get a signal at the output with a bandwidth B_d . The coherence time is the inverse of this bandwidth and is considered as the time interval over which the channel could be considered constant, $(\Delta t)_c = 1/B_d$.

Mobility in the channel is represented by t in Eq. (A.2). Analysis of this time varying filter model, however, is very difficult. Most propagation measurements have therefore assumed the channel to be stationary while collecting the impulse response profiles. The assumption of a stationary or quasistatic channel may be reasonable for indoor or short distance outdoor environments in which one does not expect a large degree of movement. For example, in an indoor environment, the velocity of the terminal is unlikely to exceed $v=1\text{m/s}$ and at an operating frequency of 17GHz this yields a channel coherence time of about 17 ms. This is about three orders of magnitude greater than the symbol period that we are going to consider in our FMT modulation schemes. For this reason, the tap gain process $\alpha_l(t)e^{j\phi_l(t)}$ varies very slowly relative to the information rate, and the Doppler effect, and therefore the time varying behaviour to a first approximation are negligible. In such cases, computation can be saved by assuming a quasi-static approach, where the taps are recomputed not at the simulation sampling rate, but a rate compatible with the Doppler spectrum.

In this way, the static channel model reduces to:

$$c(\tau) = \sum_{l=0}^{L-1} \alpha_l e^{j\phi_l} \delta(t - \tau_l) \quad (\text{A.2})$$

and the baseband received signal $y(t)$ to:

$$y(t) = \int_{-\infty}^{\infty} x(\tau) c(t - \tau) d\tau = \sum_{l=0}^{L-1} \alpha_l x(t - \tau_l) e^{j\phi_l} + w(t) \quad (\text{A.3})$$

We consider uncorrelated scattering which means that the attenuation and phase shift at different delays τ_l are independent.

The time variation of the value $\alpha_l(t)e^{j\phi_l(t)}$ has been shown experimentally and also argued theoretically to follow a zero mean complex value Gaussian distribution, therefore, $\alpha_l(t)$ follows a Rayleigh distribution [3]:

$$pdf(\alpha) = \frac{\alpha}{\sigma^2} e^{-\frac{\alpha^2}{2\sigma^2}} \quad , 0 \leq \alpha < \infty \quad (\text{A.4})$$

where σ is the variance of the underlying Gaussian process.

The conditions for this to be valid are that there are many statistically independent scatterers and no single scatter makes a dominant contribution. If there is one dominant contribution (usually a line of sight component), α has a Rice distributed pdf given by:

$$pdf(\alpha) = \frac{\alpha}{\sigma^2} e^{-\frac{\alpha^2 + A^2}{2\sigma^2}} \cdot I_0\left(\frac{\alpha A}{\sigma^2}\right) \quad , 0 \leq \alpha < \infty \quad (\text{A.5})$$

where $I_0(x)$ is the modified Bessel function of the first kind and zero order. Parameter A is the amplitude of the dominant component. The Rice parameter K_r is defined as $A^2/(2\sigma^2)$ and physically represents the ratio of the power received in the direct line of sight path, to the total power received via indirect scattered paths. Therefore, if there is no dominant propagation path, $K_r=0$ yielding the Rayleigh pdf.

If the amplitude is Rayleigh distributed, the phase shift is statistically independent of the amplitude distribution and is uniformly distributed between $[0,2\pi]$.

It is usual to consider that the variances σ in Eq. (A.5) and (A.6) associated with each tap coefficient decay according to some power delay profile [3]. The exponentially decaying profile is defined so that on average the strongest paths arrive earliest in time. However, there are some cases such as NLOS when weaker paths do precede the channel impulse response peak.

Effects of multipath propagation

The effect of multipath propagation on signal transmission can be analyzed in both the time and frequency domains.

Let us first concentrate on the effects observed in the time domain. Since multipath signals arrive at the receiver with different delays, the received symbols are spread in time. This may cause adjacent symbols to overlap and is known as inter-symbol interference (ISI). When the data are transmitted at a slow rate, the symbol duration is long compared to the delay spread caused by the channel, and the receiver can easily resolve the transmitted symbols. However, when the data symbols are transmitted at a high rate, the receiver is not able to resolve the adjacent symbols, because they overlap significantly. This is how multipath propagation spreads the signals in time making high bit rate transmission difficult to achieve.

The manifestation of the same effect in the frequency domain is the frequency selectivity of the channel. Due to the multipath propagation, the channel influences the transmitted signal and causes reinforcement at some frequencies and attenuation (deep fades) at others.

Although multipath propagation causes problems in signal reception, it should be noted that it also brings some advantages. For example, transmission is possible even if there is no direct path between the transmitter and the receiver.

Wideband Channel parameters

Some parameters that are often used to compare the severity of different multipath environments will now be presented. Measurements have shown that they do not vary greatly over the operating frequency range under consideration.

Maximum delay (τ_{\max})

The maximum delay spread is the delay to the last path having any “noticeable” amplitude. A “noticeable” amplitude is typically 20 or 30dB below the peak

amplitude. As we will show, this parameter influences the minimum cyclic prefix duration of the OFDM symbol. In indoor environments this value is around 200ns. In short range outdoor environments, it can go up to a few μs .

Root Mean Square (RMS) delay spread (τ_{RMS})

The RMS delay spread is a measure of how “spread” the delays are about the mean. It is defined as:

$$\tau_{RMS} = \sqrt{\overline{\tau^2} - (\overline{\tau})^2} \quad (\text{A.6})$$

where

$$\overline{\tau^n} = \frac{\sum_{i=0}^{L-1} \tau_i^n (\alpha_i)^2}{\sum_{i=0}^{L-1} (\alpha_i)^2} \quad \text{with } n=1 \text{ or } 2 \quad (\text{A.7})$$

τ_{RMS} is a good measurement of the multipath spread, and gives an indication of the severity of the ISI. Typical values of τ_{RMS} for indoor and short range outdoor channels are in the range of 20ns to 300ns [11][12]. Since this parameter will be related to the ISI introduced by the channel, it is usually given normalized to the symbol period T :

$$\tau_N = \frac{\tau_{RMS}}{T} \quad (\text{A.8})$$

Coherence Bandwidth (B_c)

The coherence bandwidth is the statistical average bandwidth of the radio channel over which signal propagation characteristics are correlated. B_c is defined as the value for which the complex autocorrelation function $|R(\Delta f)|$ of the channel frequency response $C(f)$ decreases by 3dB. Empirical values give:

$$B_c = \frac{1}{\lambda \tau_{RMS}} \quad (\text{A.9})$$

where λ depends on the impulse response and has values from 4-7 [13].

The definition is based on the complex autocorrelation function of the channel frequency response $H(f)$.

Two sinusoids with a frequency separation greater than B_c are affected differently by the channel [3]. If B_c is small in comparison with the bandwidth of the signal, we say that the channel is frequency selective. If B_c is higher than the bandwidth of the signal, we have flat fading and equalization of the channel is not necessary.

Modelling and simulation of the multipath channel

If we were to produce an exact channel model for a particular environment, we would need to know the attributes of every reflector in the environment at each moment in time. For instance, we would have to know the position of each reflector,

how much of the signal was reflected back to the receiver, and whether or not the reflector was moving. Obviously, it is not practical to have this kind of information for a given environment at each point in time. Therefore, channel models have been developed that emulate the typical or average behavior of a channel. However, “typical” or “average” will vary widely depending on the environment of the channel. For instance, the reflectors encountered in a delivery warehouse will be very different from those encountered in a small conference room in an office building. Thus, when simulating a particular environment, it is important to choose an accurate channel model.

There are many channel models described in the literature. They must be simple enough to allow an analytical computation of basic system performance and they must be very close to the physical reality. These requirements are contradictory, so models with different complexity and accuracy have been developed.

Besides the exponentially decaying Rayleigh Fading Channel described in section 2.1, here we present some other simple models that have become popular for wireless communications.

SUI Channels

The Stanford University Interim (SUI) channels comprise 6 models for 3 different terrain conditions. All of them are simulated using 3 taps, each having either a Rayleigh or Ricean amplitude distribution. The channel is assumed to be wide sense stationary uncorrelated scattering (WSSUS) [14].

Joint Standards Committee (JTC)

Joint Standards Committee (JTC) developed in 1994 a set of models that encompasses different scenarios. It was agreed upon in a standards committee and is therefore appropriate as a way to compare various systems' performance [16].

Saleh-Valenzuela

In the Saleh-Valenzuela Model, the channel impulse response is represented as a discrete time tapped delay line. The phase angles of individual rays are assumed to be statistically independent random variables with a uniform distribution over $[0, 2\pi)$. The rays arrive in clusters. They also have independent Rayleigh distributed amplitudes whose variances decay exponentially with cluster and ray delay. The clusters and the rays within a cluster form Poisson arrival processes that have different fixed rates [17].

Appendix B: Computation of the DFE coefficients

At the output of each of the subchannels, we will use a DFE equalizer as the one shown in Fig. 28. In the equalizer, the input $B^{(i)}(k)$, the desired output, $A^{(i)}(k)$ and the filter tap weights are all assumed to be complex variables. The estimated error $e^{(i)}(k)$ at the decision device is also complex and we may write:

$$e^{(i)}(k) = d^{(i)}(k) - y^{(i)}(k) \quad (\text{B.1})$$

where $d^{(i)}(k)$ is the output of the slicer and $y^{(i)}(k)$ the output of the DFE filtering operation.

The MMSE criterion to compute the DFE coefficients will minimize:

$$E\{|e^{(i)}(k)|^2\} = E\{|d^{(i)}(k) - y^{(i)}(k)|^2\} \quad (\text{B.2})$$

We consider a DFE with N_{FF} and N_{FB} coefficients. Let's indicate with $\{w_{FF,i}(k)\}$, $k=0,1,\dots,N_{FF}-1$, the feedforward taps of the i -th subchannel and the corresponding feedback filter with $\{w_{FB,i}(k)\}$, $k=1,2,\dots,N_{FB}$. Then we define two vectors containing the feedforward and feedback filters coefficients, respectively:

$$\underline{w}_{FF,i} = [w_{FF,i}(0), w_{FF,i}(1), w_{FF,i}(2), \dots, w_{FF,i}(N_{FF} - 1)] \quad (\text{B.3})$$

$$\underline{w}_{FB,i} = [w_{FB,i}(1), w_{FB,i}(2), w_{FB,i}(3), \dots, w_{FB,i}(N_{FB})] \quad (\text{B.4})$$

It is mathematically convenient to define an augmented response vector for the DFE as:

$$\underline{w}_i = [w_{FF,i}^*(0), w_{FF,i}^*(1), \dots, w_{FF,i}^*(N_{FF} - 1), -w_{FB,i}^*(1), -w_{FB,i}^*(2), \dots, -w_{FB,i}^*(N_{FB})]^T \quad (\text{B.5})$$

and the corresponding augmented DFE input vector $x^{(i)}(k)$ (data in the tapped delay line):

$$\underline{x}^{(i)}(k) = [B^{(i)}(k), B^{(i)}(k-1), \dots, B^{(i)}(k - N_{FF} + 1), d^{(i)}(k-1), d^{(i)}(k-2), \dots, d^{(i)}(k - N_{FB})]^T \quad (\text{B.6})$$

where $B^{(i)}(k)$ is the output of multirate filter bank:

$$B^{(i)}(k) = \sum_{n=0}^{N_{eq}-1} h_{overall}^{(i)}(n) A^{(i)}(k-n) + n_r^{(i)}(k) \quad (\text{B.7})$$

Therefore the output of the DFE operation is:

$$y^{(i)}(k) = \underline{w}_i^T \underline{x}^{(i)}(k) \quad (\text{B.8})$$

We now assume that the decisions are correct, $d^{(i)}(k) = A^{(i)}(k-\Delta)$ where Δ is a suitable delay between the FMT transmitter input and the DFE output. Thus, the data in the tapped delay line becomes:

$$\underline{x}^{(i)}(k) = [B^{(i)}(k), B^{(i)}(k-1), \dots, B^{(i)}(k - N_{FF} + 1), A^{(i)}(k - \Delta - 1), \dots, A^{(i)}(k - \Delta - N_{FB})]^T$$

$$(B.9)$$

The MMSE for the MMSE-DFE is [42]:

$$\sigma_{MMSE-DFE,i}^2 = \min_{w_{FB,i}, w_{FF,i}} E \left\{ \left| d^{(i)}(k) - y^{(i)}(k) \right|^2 \right\} \quad (B.10)$$

From Eq. (B.8),

$$e^{(i)}(k) = A^{(i)}(k - \Delta) - y^{(i)}(k) = A^{(i)}(k - \Delta) - \underline{w}_i^H \underline{x}^{(i)}(k) \quad (B.11)$$

$$\left| e^{(i)}(k) \right|^2 = e^{(i)}(k) e^{(i)*}(k) = \left\{ A^{(i)}(k - \Delta) - \underline{w}_i^H(k) \underline{x}^{(i)}(k) \right\} \left\{ A^{(i)*}(k - \Delta) - \underline{x}^{(i)H}(k) \underline{w}_i \right\} \quad (B.12)$$

When the filter taps are set to the optimal values, the **principle of orthogonality for the complex case** Error! Reference source not found. gives

$$E \{ e_0^{(i)*}(n) x^{(i)}(n - p) \} = 0, \text{ for } p=0, 1, \dots, N_{FF} + N_{FB} - 1 \quad (B.13)$$

Where $e_0^{(i)}$ is the optimum estimation error computed with the optimum Wiener-Hopf taps ($\underline{w}_{0,i}$):

$$e_0^{(i)}(k) = A^{(i)}(k - \Delta) - \underline{w}_{0,i}^H \underline{x}(k) \quad (B.14)$$

$$e_0^{(i)*}(k) = A^{(i)*}(k - \Delta) - \underline{x}^{(i)H}(k) \underline{w}_{0,i} \quad (B.15)$$

From Eq. (B.15), the orthogonality defined in Eq. (B.13) can be packed together as:

$$E \{ e_0^{(i)*}(k) \cdot \underline{x}^{(i)}(k) \} = E \left\{ \left[A^{(i)*}(k - \Delta) - \underline{x}^{(i)H}(k) \underline{w}_{0,i} \right] \underline{x}^{(i)}(k) \right\} = \underline{p}^{(i)} - \underline{R}_{xx}^{(i)} \underline{w}_{0,i} = [0, 0, \dots, 0]^T \quad (B.16)$$

where:

$$\underline{p}^{(i)} = E \{ A^{(i)*}(k - \Delta) \underline{x}^{(i)}(k) \} = E \left\{ \begin{array}{c} \left(\begin{array}{c} \text{Noverall}-1 \\ \left\{ \sum_{n=0}^{\text{Noverall}-1} h_{eq,i}(n) A^{(i)}(k - n) + n_r^{(i)}(k) \right\} A^{(i)*}(k - \Delta) \\ \text{Noverall}-1 \\ \left\{ \sum_{n=0}^{\text{Noverall}-1} h_{eq,i}(n) A^{(i)}(k - 1 - n) + n_r^{(i)}(k - 1) \right\} A^{(i)*}(k - \Delta) \\ \dots \\ \text{Noverall}-1 \\ \left\{ \sum_{n=0}^{\text{Noverall}-1} h_{eq,i}(n) A^{(i)}(k - N_{FF} + 1 - n) + n_r^{(i)}(k - N_{FF} + 1) \right\} A^{(i)*}(k - \Delta) \\ 0 \\ \dots \\ 0 \end{array} \right) \end{array} \right\} \quad (B.17)$$

$$\underline{p}^{(i)} = \begin{pmatrix} \sigma_{A^{(i)}}^2 h_{eq,i}(\Delta) \\ \sigma_{A^{(i)}}^2 h_{eq,i}(\Delta-1) \\ \dots \\ \sigma_{A^{(i)}}^2 h_{eq,i}(\Delta - N_{FF} + 1) \\ 0 \\ \dots \\ 0 \end{pmatrix}_{(N_{FF} + N_{FB}) \times 1} \quad (\text{B.18})$$

where we have applied:

- noise uncorrelated with the data
- data input, $A^{(i)}(k)$, are independent at different sampling times:

$$E\{A^{(i)}(k-i-t)A^{(i)}(k-j-p)\} = \sigma_{A^{(i)}}^2 \text{ when } i+t=j+p, \text{ and } 0 \text{ otherwise} \quad (\text{B.19})$$

$$E\{B^{(i)}(k-i)A^{(i)}(k-\Delta)\} = E\left\{\sum_{n=0}^{N_{eq}-1} h_{eq,i}(n)A^{(i)}(k-n-i) + n_r^{(i)}(k-i)\right\}A^{(i)}(k-\Delta) = h_{eq,i}(\Delta-i)\sigma_{A^{(i)}}^2 \quad (\text{B.20})$$

and the autocorrelation function $\underline{R}_{xx}(i)$ in Eq. (B.16) is defined as:

$$\underline{R}_{xx}(i) = E\{\underline{x}^{(i)}(k)\underline{x}^{(i)H}(k)\} \quad (\text{B.21})$$

and substituting Eq. (B.9) in Eq. (B.21) we obtain:

$$\underline{R}_{xx}(i) = E\left\{ \begin{pmatrix} B^{(i)}(k) \\ B^{(i)}(k-1) \\ \dots \\ B^{(i)}(k-N_{FF}+1) \\ A^{(i)}(k-\Delta-1) \\ \dots \\ A^{(i)}(k-\Delta-N_{FB}) \end{pmatrix} \begin{pmatrix} B^{(i)}(k) & \dots & B^{(i)}(k-N_{FF}+1) & A^{(i)}(k-\Delta-1) & \dots & A^{(i)}(k-D-N_{FB}) \end{pmatrix} \right\} \quad (\text{B.22})$$

Since the noise is uncorrelated with the data, we can represent the autocorrelation matrix R_{xx} as the addition of two matrices, one depending on the data and the other depending on the noise.

$$R_{xx} = R_{xxdata} + R_{xxnoise} \quad (\text{B.23})$$

We now divide the matrix \underline{R}_{xxdata} into 4 different matrix blocks:

$$\underline{A}_{N_{FF} \times N_{FF}}, \underline{B}_{N_{FB} \times N_{FB}}, \underline{C}_{N_{FB} \times N_{FF}}, \underline{D}_{N_{FF} \times N_{FB}} \quad (\text{B.24})$$

$$R_{xxdata} = \begin{pmatrix} \underline{A} & \underline{C} \\ \underline{D} & \underline{B} \end{pmatrix}_{(N_{FF} + N_{FB}) \times (N_{FF} + N_{FB})} \quad (\text{B.25})$$

Let's show how these block matrices are defined:

$$[A]_{i,l} = E\{B(k-i-l)B^*(k-l+1)\} = E\left\{\left(\sum_{t=0}^{N_{eq}-1} h_{eq}(t)A(k-i+1-t)\right)\left(\sum_{p=0}^{N_{eq}-1} h_{eq}(p)A(k-i+1-p)\right)^*\right\} \quad (\text{B.26})$$

$$[A]_{i,l} = \sigma_A^2 \sum_{t=0}^{N_{eq}-1} h_{eq}(t)h_{eq}^*(t+i-l) \quad i,l=1,2,\dots,N_{FF} \quad (\text{B.27})$$

$$[B]_{i,l} = \sigma_A^2 \delta(i-l) \quad , i,l=1,2,\dots,N_{FB} \quad (\text{B.28})$$

$$[C]_{i,l} = E\left\{B(k-i+1)A^*(k-D-j+1) = E\left\{\left(\sum_{t=0}^{N_{eq}-1} h_{eq}(t)A(k-i+1-t)\right)A^*(k-D-j+1)\right\}\right\} \quad (\text{B.29})$$

$$[C]_{i,l} = h_{eq}(D+j-i)\sigma_A^2 \quad , i=1,2,\dots,N_{FF}, l=1,2,\dots,N_{FB} \quad (\text{B.30})$$

$$[D]_{l,i} = [C]_{i,l}^* \quad l=1,2,\dots,N_{FB}, i=1,2,\dots,N_{FF} \quad (\text{B.31})$$

For $R_{xxnoise}$ we have:

$$R_{xxnoise} = E\left\{\begin{pmatrix} n_r(k) \\ n_r(k-1) \\ \dots \\ n_r(k-N_{FF}+1) \\ A(k-D-1) \\ \dots \\ A(k-D-1) \end{pmatrix} \begin{pmatrix} n_r^*(k) & \dots & n_r^*(k-N_{FF}+1) & A^*(k-D-1) & \dots & A^*(k-D-1) \end{pmatrix}\right\} \quad (\text{B.32})$$

Since the data is uncorrelated with the noise, the only elements nonzero will be a block matrix $E_{N_{FF} \times N_{FF}}$

$$R_{xxnoise} = \begin{pmatrix} \underline{E} & \underline{0} \\ \underline{0} & \underline{0} \end{pmatrix}_{(N_{FF}+N_{FB}) \times (N_{FF}+N_{FB})} \quad (\text{B.33})$$

where:

$$E\{n_r(k-l)n_r^*(k-j)\} = \sum_{n1=1}^{M\gamma} g^{(i)}(n_1) \cdot n(kM-n_1-l) \sum_{n2=1}^{M\gamma} g^{(i)*}(n_2) \cdot n^*(kM-n_2-j) \quad (\text{B.34})$$

And since the original noise samples are uncorrelated at different time instants:

$r_{xx}(i,j)$:

$$E\{n_r(k-l)n_r^*(k-j)\} = \sigma_n^2 \sum_{n1=1}^{M\gamma} g^{(i)}(n_1) \cdot g^{(i)*}(n_1+l-j) \quad (\text{B.35})$$

$$E\{n_r(k-l)n_r^*(k-j)\} = \sigma_n^2 \sum_{n_1=1}^{M\gamma-1} h(n_1-1)e^{j\frac{2\pi}{M}n_1i} \cdot h^*(n_1+l-j-1)e^{-j\frac{2\pi}{M}(n_1+l-j)i} \quad (\text{B.36})$$

$$E\{n_r(k-l)n_r^*(k-j)\} = \sigma_n^2 \sum_{n_1=1}^{M\gamma} h(n_1-1) \cdot h^*(n_1+l-j-1)e^{-j\frac{2\pi}{M}(l-j)i} \quad (\text{B.37})$$

Therefore, from Eq. (B.16) the Wiener–Hopf optimal coefficients are:

$$\underline{w}_{0,i} = \left(\underline{R}_{xx}^{(i)}\right)^{-1} \underline{p}^{(i)} \quad (\text{B.38})$$

It is important to remember how \underline{w}_i was defined in Eq. (B.5). For the tap weights that we need, we will take the complex conjugate (both Feedforward and Feedback taps) and for the Feedback coefficients, we will change the sign.

Appendix C: Precoding

Receiver architectures based on a DFE suffer from the following two problems:

- Error propagation as a result of an incorrect decision in the feedback section of a DFE producing additional errors that would not have occurred if the first decision had been correct.
- Coded modulation cannot be applied in a straightforward manner since DFE needs zero delay decisions for the feedback section which is irreconcilable with the basic idea of channel coding .

The second problem can be solved at the expense of receiver complexity, such as using parallel decision feedback decoding (PDFD) which puts the DFE function inside a Viterbi decoder. Due to its complexity, this approach is in conflict with desirable characteristics of wireless devices.

To overcome these problems, precoding at the transmitter using a Tomlinson Harashima Precoder (THP) [43][44] is a practical solution.

This technique is possible only when the transmitter knows the channel response. The idea of the precoding is to move the cancellation of the postcursor ISI to the transmitter, where the past transmitted symbols are known without the possibility of errors. This means that the postcursor ISI impulse response must be known precisely at the transmitter.

In TDD radio systems, forward and reverse channels are reciprocal during the time of two consecutive data frames. As a result, the channel information estimated in the reverse link can be used in the precoder at the base station transmitter to pre-equalize the signal transmitted in the forward link.

In the FMT efficient equalization scheme proposed in section 5.2 based on a fixed frequency domain DFE per subchannel, the overall response that we are going to try to equalize is known offline since it is related only to the low pass prototype filter and not to the channel. Therefore, TH precoding is a good candidate to overcome the two problems just presented.

However, moving the feedback filter to the transmitter can result in a significant power increase. To prevent most of this power increase, modulo arithmetic is employed in the THP to bound the level of the signal and guarantee the stability of the precoder. This form of THP is implemented at the input of each of the subchannels as shown in Fig. C.1

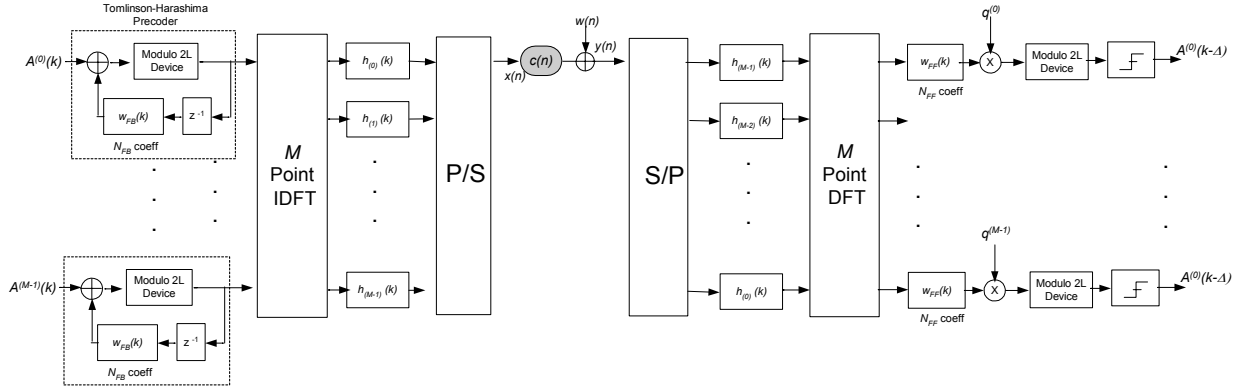


Fig. C.1 Proposed FMT system with a fixed DFE equalizer per subchannel in the form of THP for the feedback section in cascade with a complex gain to compensate the gain and phase rotation of the multipath channel

To show how the THP works we consider a conventional $L \times L$ QAM, where the modulo arithmetic operation (with parameter $2L$) is performed on both in phase and quadrature components of the signal. The cascade of the overall response due to the prototype (as defined in Eq. (66)) with the feedforward section of the DFE has a response $f(n)$, $n=0,1,\dots,N-1$.

In the case of $f(0)=1$, if the desired received sample at $t=kT+T$ is $A^{(i)}(k)$ at baseband, then the corresponding ISI is:

$$I(k) = \sum_{n=1}^{N-1} f(n)x(k-n) \quad (C.1)$$

where $x(i-k)$ is the previously transmitted signals at baseband. Then ISI free transmission can be achieved by transmitting:

$$x(k) = A^{(i)}(k) - I(k) \quad (C.2)$$

The persubchannel equalization using THP is shown in Fig. C.2 and describe here. The operation of the precoder is then to map the desired signal $A^{(i)}(k)$ to the transmitted signal $x(k)$, which can be described by the transfer function of the precoder:

$$\frac{X(z)}{A^{(i)}(z)} = \frac{1}{1+[F(z)-1]} = F^{-1}(z) \quad (C.3)$$

where:

$$F(z) = \sum_{n=0}^{N-1} f(n)z^{-n} \quad (C.4)$$

is the transfer function of the tx/rx filters based on the prototype and the feedforward. As long as $F(z)$ has all its zeros inside the unit circle of the complex z -plane, $F^{-1}(z)$ is stable and so is the precoder. However, if the channel is not minimum phase, the above condition is no longer valid and the precoder becomes unstable. The sequence $\{x(k)\}$ will tend to increase or diverge infinitely. In order to stabilize the precoder, TH

precoding uses a non linear modulo arithmetic operation. The precoder is basically an inverse filter $F^{-1}(z)$ of the transfer function $F(z)$, except that the output of the filter undergoes modulo arithmetic operation before being transmitted and being applied back to the feedback filter. That is, in order to achieve stability, the TH precoder sends (instead of $x(k)=A^{(i)}(k)-I(k)$):

$$x'(k) = \left[(A^{(i)}(k) - I(k)) \bmod 2L \right] = A^{(i)}(k) + 2Lv(k) - I(k) \quad (C.5)$$

for some complex integer $v(k)$ such that $|\text{Re}(x'(k))| < L$ and $|\text{Im}(x'(k))| < L$.

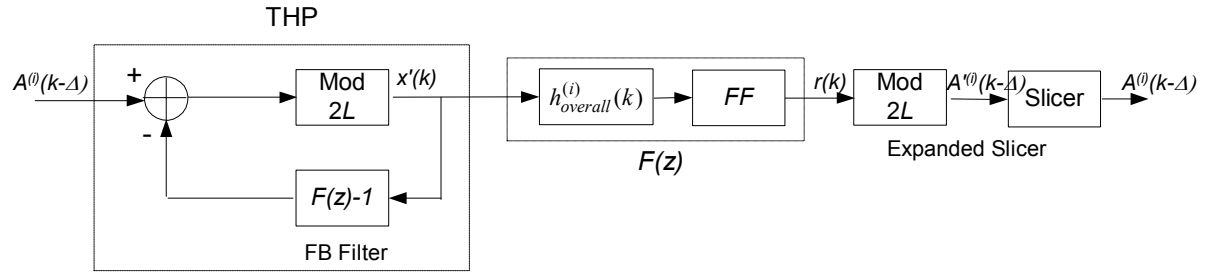


Fig. C.2 Equivalent subchannel response without considering the multipath channel

The corresponding z transform of the transmitted sequence $\{x(k)\}$ is:

$$X'(z) = A^{(i)}(z) + 2LV(z) - X'(z)[F(z) - 1] \quad (C.6)$$

$$X'(z) = \frac{[A^{(i)}(z) + 2LV(z)]}{F(z)} \quad (C.7)$$

where $A^{(i)}(z)$ and $V(z)$ are the z-transform of the sequence $\{A^{(i)}(k)\}$ and $\{v(k)\}$ respectively. The received sequence $\{r(k)\}$ in a noise free situation has the following z-transform:

$$R(z) = X'(z)F(z) = A^{(i)}(z) + 2LV(z) \quad (C.8)$$

which corresponds to $r(k) = A^{(i)}(k) + 2Lv[k]$. The desired signal $A^{(i)}(k)$ is recovered at the receiver by applying the same modulo operation to the received signal. Since $|\text{Re}(A^{(i)}(k))| < L$ and $|\text{Im}(A^{(i)}(k))| < L$, then $[r(k) \bmod 2L]$ must give $A^{(i)}(k)$.

We can see the operation of the TH precoding in the light of dimension partitioning as follows. The $L \times L$ QAM can be represented by its square signal constellation (centered at the origin with side length equal to $2L$) defined on a two dimensional Euclidian space. The desired signal $A^{(i)}(k)$, which is also the input signal of the precoder, can be represented by the corresponding point in the constellation. Because of the feedback path in the precoder, the input signal applied to the modulo $2L$ operator of the precoder is defined on the whole Euclidian space. Hence, the two dimensional Euclidian space is referred to as the signal space. The TH precoder has three functions:

1. **dimension partitioning:** the modulo $2L$ operator partitions the signal space into nonoverlapping square regions of side $2L$. Each of such regions is referred to as a partition. The partition centered at the origin is referred to as the base partition, over

which the QAM signal constellation is defined. All other partitions can be viewed as a replica of the base partition except that the centers of the partitions are shifted correspondingly. In other words, the desired signal $A^{(i)}(k)$ has a corresponding constellation point in each partition. The dimension partitioning corresponding to TH precoding is referred to as TH partitioning.

2. **selecting a shifted desired constellation point:** based on the ISI component $I(i)$, represented by a point in the signal space (called the ISI point), the precoder chooses the replica of the desired signal constellation point in such a partition that the selected point is closest to $I(i)$. The selected point, referred to as the shifted desired constellation point, represents the desired signal after the modulo $2L$ operation.

3.- **Precoding the transmitted signal:** the precoder calculates the difference between the shifted desired constellation point and the ISI point, and sends the difference as the precoded signal.

After the precoded signal travels along the frequency selective channel, the received signal is represented by the shifted desired constellation point in the signal space in the absence of additive white Gaussian noise. The decoder at the receiver (which is a modulo $2L$ operator) moves the shifted desired constellation point back to the base partition, and gives the desired signal as the output. An example of TH precoding is shown in Fig. C.3, where the desired signal $A^{(i)}(k)$ is represented by the constellation point \bullet in the base partition, and the replica of the constellation point in all the other partitions is also shown.

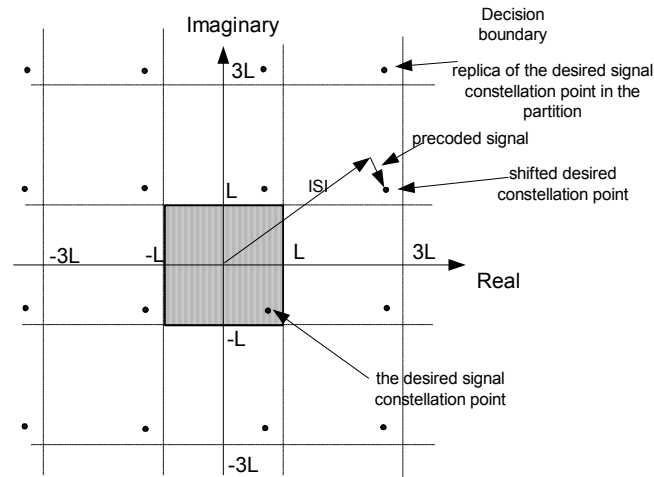


Fig. C.3 Dimension partitioning in TH precoding

The transmitted TH precoded signal is vulnerable to additive noise introduced by the wireless channel, due to the fact that TH partitioning reduces the decision regions for signal constellation points. A small noise component can shift the received signal from the correct decision region to an incorrect decision region and result in transmission error as shown in Fig. C.4.

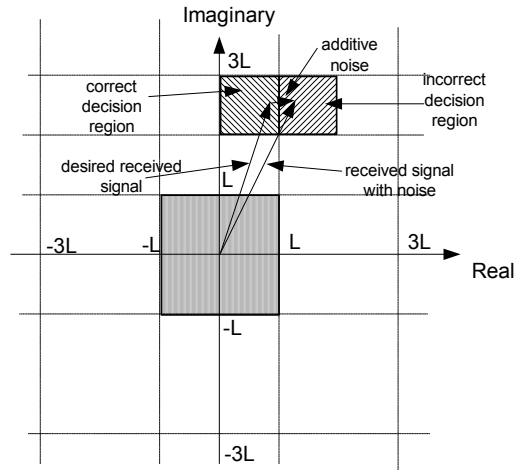


Fig. C.4 Signal shift due to noise in TH partitioning

We can develop a new precoding technique for the indoor wireless system, which can overcome the THP drawback that we have just mentioned.

The flipped partition

As we have said, the TH partitioning greatly reduces the signal decision region for each signal constellation point. As a result, transmission bit error rate due to AWGN and multipath is significantly increased. The problem can be mitigated to a certain degree if the adjacent regions in the adjacent partitions represent the same data symbol [45][46]. This can be achieved by flipping partitions (from TH partitioning) in such a way that regions representing the same data symbol in QPSK stick together to form a larger decision region. This result in the dimension partitioning of the signal space shown in Fig. C.5 which is referred to as flipped partitioning:

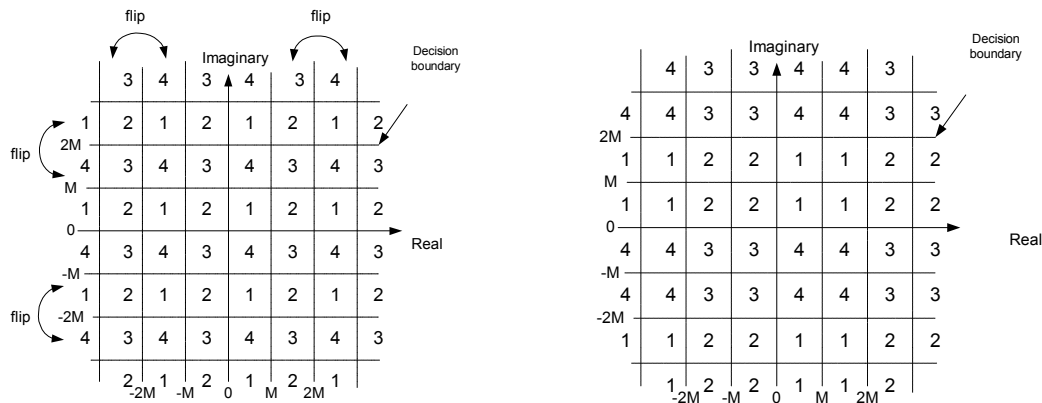


Fig. C.5 TH Precoded QPSK Decision Regions (a) original partition (“1”= $p/4$, “2”= $3p/4$, “3”= $5p/3$, “4”= $7p/4$) (b) Decision Flipped

A small amount of extra operations are required at transmitter and receiver in order to implement the mapping [46][45].

THP Conclusion

THP alone does not give any major advantage because of two reasons:

- Although it does not propagate errors, it is more sensitive to errors because of the bounded partition.
- The PAPR increases and this is a major problem in OFDM. The increase is higher in low order constellations such as QPSK.

However, it opens a possibility to other coding algorithms such as the flipped partition. In FMT subchannels with high SNR, the flipped partition will not bring any advantage because the received symbol is unlikely to fall outside of the bounded partition. However, in channels with low SNR, this will bring an improvement. Since in multipath channels with high RMS delay spread we always come into situation where some channels have a low SNR, then the use of flipped partition appears useful.

Although THP without any extension does not bring any improvement, we remember that it can be used in situations where we want to liberate the receiver of some of the computational complexity of FMT by bringing the feedback section of the equalizer to the transmitter.

On the other hand, the incorporation of trellis coding with TH precoding has been a topic of recent research interest [48][49] and can be easily used with the proposed implementation.